REFLECTED WAVE PROPAGATION IN A WEDGE

by

HIROSHI ISHII
B.Sc., Tohoku University, 1963
M.Sc., Tohoku University, 1965

A THESIS SUBMITTED IN PARTIAL FULFILMENT OF
THE REQUIREMENTS FOR THE DEGREE OF
DOCTOR OF PHILOSOPHY
in the Department
of
GEOPHYSICS

We accept this thesis as conforming to the

THE UNIVERSITY OF BRITISH COLUMBIA
September, 1969

In presenting this thesis in partial fulfilment of the requirements for an advanced degree at the University of British Columbia, I agree that the Library shall make it freely available for reference and Study. I further agree that permission for extensive copying of this thesis for scholarly purposes may be granted by the Head of my Department or by his representatives. It is understood that copying or publication of this thesis for financial gain shall not be allowed without my written permission.

Department of Geophysics

The University of British Columbia
Vancouver 8, Canada

Date 29th Sept. 1969

ABSTRACT

The behavior of elastic body waves in a dipping layer overlying an elastic medium has been theoretically investigated by a multiple reflection formulation.

Although the diffracted wave is not included in this formulation, its importance is studied by investigation of the amplitude discontinuities within the wedge.

For a plane SH wave incident at the base of the dipping layer perpendicular to strike, a series solution has been obtained. Numerical values of the amplitude, phase and phase velocity are calculated on the surface. For waves propagating in the up-dip direction the amplitude versus frequency curves for a constant depth to the interface change slowly with increasing dip for dip angles less than 20°. However for waves propagating in the down-dip direction the character of the amplitude curves change rapidly. In these cases, it is found that the diffracted wave plays an important role. In addition to satisfying the boundary conditions at the surface and the lower boundary of the wedge, the diffracted wave must also satisfy additional conditions along a dipping interface between the wedge boundaries due to the geometrical nature of the reflected wave solution. It is found that the phase velocities vary rapidly with both period of the wave and depth to the interface.

For incident plane P and SV waves, the complexity of the problem due to the converted waves does not allow the solution to be expressed in series form. However, a computational scheme has been developed which allows the

calculation of the disturbance due to the multiply reflected waves. For both incident P and SV waves, numerical values of displacements and displacement ratios are calculated on the surface. It is found that the displacement ratios for incident SV waves are much more sensitive to dip than are there for incident P waves. For incident P and SV waves propagating in the down-dip direction with a propagation direction $\alpha, \beta = 120°$, the amplitude ratio versus frequency curves for constant depth to interface do not have significant peaks for dip angles greater than 15°. The maximum discontinuities caused by the outgoing wave are also calculated to determine the role of the diffracted wave. As subsidiary problems the energy relations between waves at an interface between elastic media are determined in terms of propagation direction in a cylindrical system and the complex propagation direction is interpreted using the Rayleigh wave.

The final study is to determine by a reflected wave formulation the displacements due to periodic and impulsive line sources of SH waves in the wedge overlying an elastic medium. A formal solution is found by which the contributions due to head and reflected waves are determined by evaluation of the integrals by the method of steepest descent. Using ray paths, the contributions

of the integrals have been interpreted. The range of existence of head waves has been examined and the discontinuities associated with diffracted waves studied. In the case of a free or rigid lower boundary of the wedge, the dispersion relation has been determined.

TABLE OF CONTENTS

LIST OF FIGURES

LIST OF TABLES

ACKNOWLEDGEMENTS

I wish to express my sincere thanks to Dr. R. M. Ellis for his guidance and encouragement and for many hours of discussion during the course of the entire investigation.

Thanks are due to Drs. R. D. Russell and D. E. Smylie for reading the manuscript and Dr. G. K. C. Clarke for his comments on Chapter 4. I appreciate the constant interest and encouragement of Dr. Russell during my studies at the University of British Columbia.

Helpful discussions are acknowledged with my colleague Mr. O. G. Jensen, who also provided me with his program for plane waves incident on a horizontally layered system.

I would like to express my appreciation to Professor Akio Takagi, Chief, Akita Observatory, Tohoku University for granting educational leave and to Professor Ziro Suzuki who suggested studies at the University of British Columbia.

This manuscript was typed by Miss Judi Kalmakoff.

This study was supported by the National Research Council (Grant A-2617) to Dr. R. M. Ellis and the Defence Research Board of Canada (Grant 9511-76) to Drs. R. M. Ellis and R. D. Russell. A University of British Columbia Graduate Fellowship during the second year of this study is gratefully acknowledged.

CHAPTER 1

GENERAL INTRODUCTION

1.1 Preliminary Remarks

Elastic waves play very important roles in the determination of the crustal structure and the internal constitution of the earth. In the past decade new analysis techniques coupled with advances in instrumentation have lead to rapid expansion of our knowledge concerning the seismic properties of the earth. However, the analyses are restricted by the limited number of models which are available - mainly for horizontally layered structures. In earthquake seismology, surface waves have been particularly useful for interpretation as they yield an average structure over the propagation path and hence the horizontally layered formulation has proved to be adequate in most cases. However, body wave applications (e.g., Phinney (1964), Ellis and Basham (1968), Ibrahim (1969)) have only been moderately successful as body wave amplitudes depend on a localized region beneath the observation point which may be geologically complex as indicated by the reflection studies of Clowes et al (1968). Hence it is necessary and important to investigate the behavior of waves in a dipping layer to obtain an understanding of the more complex models.

1.2 Summary of Previous Studies

The interpretation of horizontally layered structures has been dominated by the theoretical studies of Haskell (1953, 1960, 1962). He considered an input wave at the base of a horizontally layered system and by applying the boundary conditions obtains propagator matrices which carry the displacements and stresses from one boundary to the next eventually obtaining a relation between the input wave at the lower boundary and the surface motion. For incident P and SV waves, the frequency domain input function may be eliminated by taking the ratio of the vertical and horizontal displacements. For incident P, the experimental V/H ratio versus frequency, and for incident SV, the experimental H/V ratio, can then be compared with theoretical Haskell ratios to determine crustal structure. Haskell's formulation is also applicable to surface wave studies.

Several studies for non-parallel boundaries have been done, mainly relating to surface waves. Hudson (1963), Nagumo (1961) and Sato (1963) dealt with SH waves in a wedge-shaped medium. Hudson studied SH waves from a line source in a wedge-shaped medium with a rigid lower surface. He obtained a solution composed of multiply reflected

and diffracted waves. Using this solution he investigated the effect of diffraction at the apex of the wedge by means of an approximate form of the diffracted pulse and found that the diffracted wave amplitude decreases as $1/\sqrt{r r_1}$ (where r and r_1 are the distances of the source and observation point from the vertex). Nagumo considered two dimensional elastic wave propagation in a liquid layer overlying a rigid bottom. He found that mode solutions exist. From the solution he investigated dispersion relations of the wave. Sato studied the diffraction problem of SH waves at an obtuse-angled corner due to incident plane SH pulse parallel to one of the free boundaries and calculated diffracted wave forms which he found diminished rapidly away from the vertex. Lapwood (1961), Kane and Spence (1963), Hudson and Knopoff (1964), McGarr and Alsop (1967) and others have studied Rayleigh wave transmission in a wedge-shaped medium. Lapwood investigated wave forms from a line pulse source on one of the free boundaries of a right angle, using integral transformation and approximation procedures. Kane and Spence (1963) and Hudson and Knopoff (1964) considered Rayleigh wave transmission on elastic wedges with free boundaries. The first authors employed an iteration procedure and the latter employed a Green's function technique in order to calculate transmission coefficients

of the Rayleigh wave. Using an approximate variational method, McGarr and Alsop (1967) computed the reflection and transmission coefficients for Rayleigh waves normally incident on vertical discontinuities. Conversely, there have only been a few studies (Fuchs (1966)) and Kane (1966)) on the effect of non-parallel boundaries for body waves; nevertheless body waves constitute an initial section of a seismogram which is very often used in analyses. Fuchs synthesized seismograms due to a primary P signal propagating along the median plane in a solid wedge with free boundaries, by taking a summation of reflected waves. He determined the dispersion of the body waves and particle motion. Kane employed a tree diagram which is obtained by reflecting the wedge rather than the rays and a vector which carries nine pieces of data. Thus, he calculated theoretical seismograms due to an input plane P pulse for the teleseismic response of an array of stations located on a uniformly dipping crust. In this way he demonstrated the signal distortion effects of the geometry. However the amplitude characteristics which are used for interpretation of crustal structure were not investigated nor was the diffracted wave.

1.2 Scope of This Thesis

The objective of this thesis is to extend the theory of body wave propagation in a dipping structure using a reflected wave formulation. Although the forms of the diffracted waves are not investigated, determination of the amplitude discontinuities due to the reflected wave within the wedge indicates its importance.

First, in Chapter 2, a plane SH wave incident at the base of a dipping layer is considered as in this case no converted waves are present. A solution by multiple reflection is obtained and the amplitude characteristics and phase velocity calculated on the surface in terms of depth to the interface, period of the wave, and dip angle. The discontinuities which result from the last reflection and which are related to diffracted waves are determined. This development in Chapter 2 serves as a guide for solving the more difficult problems of Chapters 3 and 4.

In Chapter 3, the corresponding problem is studied for incident P and SV waves. The complexity does not allow a series solution to be obtained; however, a computational scheme is developed which allows the calculation of the displacement and phase velocities. As subsidiary problems, the energy relations between waves at a boundary are given in terms of the propagation direction and the complex propagation direction interpreted.

In Chapter 4, propagation of SH waves from a periodic and impulsive line source in a dipping layer overlying an elastic medium is investigated using a reflected wave formulation. The contributions due to head and reflected waves are determined by evaluating the integrals by the method of steepest descent and a

comparison made with a horizontally layered case through the case of numerical examples. The range of existence of head waves is determined and the discontinuities associated with diffracted waves studied.

The study is summarized and suggestions made for further investigations in the final chapter.

The theory for multiply reflected waves as developed in this thesis could serve as a useful starting point for the study of diffraction. Techniques such as the geometrical theory of diffraction as developed by Keller (1962) appear to be applicable; however, they may not be practical due to the complexity introduced. In this theory for small wavelengths, Keller uses diffraction laws similar to laws of reflection and refraction which are derived from Fermat's principle. Away from the diffracting surfaces, he is able to use diffracted rays just like ordinary rays. By the use of the reflected wave solution and such a diffracted wave procedure, it may be possible to obtain a more satisfactory description of elastic waves in a wedge.

CHAPTER 2

MULTIPLE REFLECTION OF PLANE SH WAVES BY A DIPPING LAYER

2.1 Introduction

The calculation of the amplitude characteristics of waves propagating in horizontally layered media has been greatly simplified by the matrix formulation of Haskell (1953, 1960, 1962). The application of this formulation has proved to be a powerful method for determining the crust and upper mantle structure using surface waves. However, body wave applications have only been moderately successful. Even though for surface waves the regional structure may conform closely enough to the layered theory to allow a successful interpretation, the body wave amplitudes may not be useful for interpretation as they depend only on a localized area beneath the station which may be geologically complex. It is, therefore, important to study the effect of dipping boundaries on the characteristics observed at the surface. Fernandez and Careaga (1968) have suggested that a model of this type may be required to explain body wave observations at La Paz.

As an initial study of body waves interacting with a wedge overlying an elastic medium, all waves internally reflected between the free surface and the dipping layer due to a plane SH wave incident on the wedge perpendicular to the direction of strike will be considered. The objective

is to calculate the amplitude characteristics in terms of distance from the vertex, depth from the surface, and the period of the wave. On the basis of the results of previous workers, it is expected that the multiply reflected waves will play the most important role in a seismogram at observation points distant from the vertex and will be explicitly investigated in this study. For the diffracted wave, the boundary conditions are expressed and calculations made to indicate its importance in particular situations.

This simple case in which there is no coupling between wave types serves as a guide for solving the more difficult problems of incident P and SV waves as well as being of interest in its own right. Further, as surface wave, refracted wave and reflected wave components are obtained by evaluating the contribution of poles, branch points and saddle points respectively in terms of multiple reflection, the solution of the present problem is an important step leading to the solution of these more complex problems.

2.2 Wave Equation and Fundamental Solution

In this problem with a dipping boundary it is found convenient to choose a cylindrical coordinate system (r, θ, z) related to a cartesian system (x, y, z) as

shown in Figure 2-1. For a plane SH wave propagating in the x-y plane, the motion is independent of z and the displacement has only a z-component. Assuming a time variation of the form $e^{i\omega t}$, the equation of motion

$$\nabla^2 u = \frac{1}{c_b^2}\frac{\partial^2 u}{\partial t^2} \tag{2.1}$$

becomes in cylindrical coordinates

$$\left(\frac{\partial^2}{\partial r^2} + \frac{1}{r}\frac{\partial}{\partial r} + \frac{1}{r^2}\frac{\partial^2}{\partial \theta^2} + k_b^2\right) u = 0 \tag{2.2}$$

where $k_b = \omega / c_b$

We choose as the fundamental solution of this equation $A \cdot e^{ik_b r\cos(\theta-\alpha)}$ which is a plane wave of amplitude A propagating in the α direction.

The only non-zero component of stress is

$$P_{z\theta} = \mu \frac{\partial u}{\partial \theta} \tag{2.3}$$

2.3 Reflection and Refraction Coefficients

We now consider two elastic media divided by $\theta = \theta_d$ with waves from medium (2) incident on the interface (Figure 2-2). The solutions in media (1) and (2) can be written as

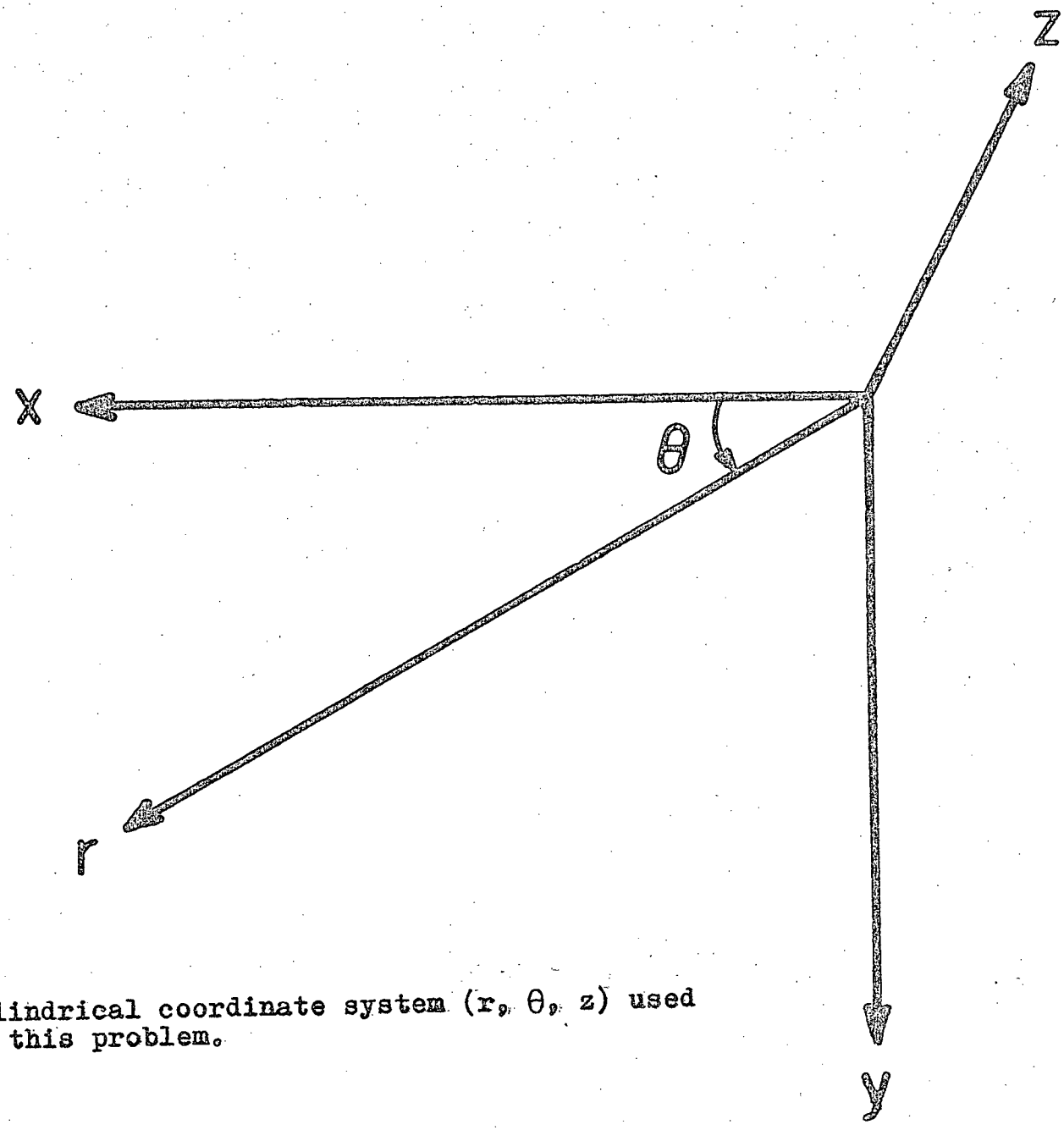

Fig. 2-1. Cylindrical coordinate system (r, θ, z) used in this problem.

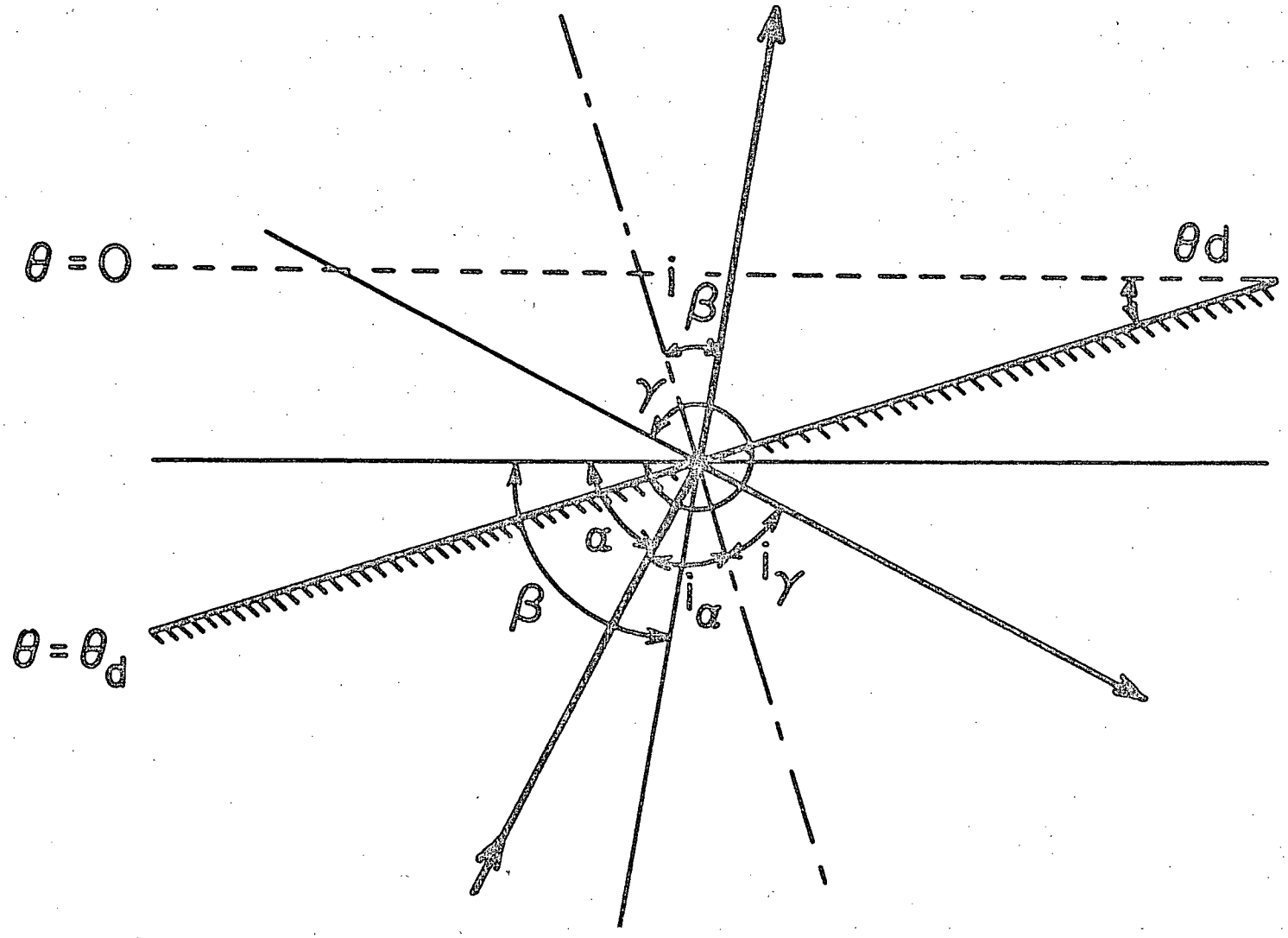

Fig. 2-2. Reflection and refraction at a boundary inclined at an arbitrary angle θ_d .

$$u_1 = A_{rf} \cdot e^{ik_{b1} r \cos(\theta-\beta)}$$

$$u_2 = A_i \cdot e^{ik_{b2} r \cos(\theta-\alpha)} + A_{rl} e^{ik_{b2} r \cos(\theta-\gamma)} \qquad (2.4)$$

The boundary conditions at the interface require continuity in displacement and stress. At $\theta = \theta_d$ we can therefore write

$$u_1 = u_2$$

$$(P_{z\theta})_1 = (P_{z\theta})_2 \qquad (2.5)$$

The condition of equality of phase at $\theta = \theta_d$ leads to

$$k_{b1}\cos(\theta_d-\beta) = k_{b2}\cos(\theta_d-\alpha) = k_{b2}\cos(\theta_d-\gamma) \qquad (2.6)$$

Using (2.3) and substituting (2.4) into (2.5), we obtain

$$\frac{A_{rl}}{A_i} = \frac{\delta \sin(\theta_d-\alpha) - \Delta \sin(\theta_d-\beta)}{\Delta \sin(\theta_d-\beta) - \delta \sin(\theta_d-\gamma)}$$

$$\frac{A_{rf}}{A_i} = \frac{\delta \sin(\theta_d-\alpha) - \delta \sin(\theta_d-\gamma)}{\Delta \sin(\theta_d-\beta) - \delta \sin(\theta_d-\gamma)} \qquad (2.7)$$

where $\Delta = C_{b2}/C_{b1}$ and $\delta = \mu_2/\mu_1$.

Using (2.6) and the geometric relationships between the angles α, β, γ and the angles $i_\alpha, i_\beta, i_\gamma$ (Figure 2-2), we have

$$\gamma = 2\theta_d + 2\pi - \alpha$$
$$\beta = \theta_d + \frac{\pi}{2} - \sin^{-1}\left(\frac{1}{\Delta}\cos(\theta_d - \alpha)\right) \tag{2.8}$$

and

$$\sin(\theta_d - \gamma) = -\sin(\theta_d - \alpha)$$
$$\sin(\theta_d - \beta) = -\sqrt{1 - (1/\Delta^2)\cos^2(\theta_d - \alpha)} \tag{2.9}$$

with $\theta_d < \alpha < \theta_d + \pi$

Finally, substituting (2.9) into (2.7) we obtain

$$\frac{A_{rl}}{A_i} = \frac{\sin(\theta_d - \alpha) + (1/\delta)\sqrt{\Delta^2 - \cos^2(\theta_d - \alpha)}}{\sin(\theta_d - \alpha) - (1/\delta)\sqrt{\Delta^2 - \cos^2(\theta_d - \alpha)}}$$
$$\frac{A_{rs}}{A_i} = \frac{2\sin(\theta_d - \alpha)}{\sin(\theta_d - \alpha) - (1/\delta)\sqrt{\Delta^2 - \cos^2(\theta_d - \alpha)}} \tag{2.10}$$

Thus, we have been able to denote the reflection and refraction coefficients in terms of the initial propagation direction, the dip angle, and the elastic constants.

In the case where the waves are incident on the boundary from medium (1), the same process yields the following equations:

$$\frac{A_{rl}}{A_i} = \frac{\Delta\sin(\theta_d - \alpha) - \delta\sqrt{1 - \Delta^2\cos^2(\theta_d - \alpha)}}{\Delta\sin(\theta_d - \alpha) + \delta\sqrt{1 - \Delta^2\cos^2(\theta_d - \alpha)}}$$
$$\frac{A_{rs}}{A_i} = \frac{2\Delta\sin(\theta_d - \alpha)}{\Delta\sin(\theta_d - \alpha) + \delta\sqrt{1 - \Delta^2\cos^2(\theta_d - \alpha)}} \tag{2.11}$$

and

$$\gamma = 2\theta_d + 2\pi - \alpha$$
$$\beta = \theta_d + \frac{3}{2}\pi + \sin^{-1}\left(\Delta \cos(\theta_d - \alpha)\right) \tag{2.12}$$

with $\theta_d + \pi < \alpha < \theta_d + 2\pi$

If $\Delta^2 \cos^2(\theta_d - \alpha) > 1$ then $\sqrt{1 - \Delta^2 \cos^2(\theta_d - \alpha)}$ must be replaced by $-i\sqrt{\Delta^2 \cos^2(\theta_d - \alpha) - 1}$ for the solution to remain finite at infinity.

For waves incident on the free surface, we have

$$A_{r\ell} = A_i$$
$$\gamma = 2\pi - \alpha \tag{2.13}$$

with $0 < \alpha < \pi$

2.4 Multiple Reflection Solution for a Wedge

Consider a wave $A_i \cdot e^{ik_{b2} r \cos(\theta - \alpha)}$ incident on the boundary $\theta = \theta_d$ from medium (2) (Figure 2-3) and assume a resulting reflected wave ψ_1'' and refracted wave ψ_1 of the forms

$$\psi_1'' = A_1'' \cdot A_i \cdot e^{ik_{b2} r \cos(\theta - \gamma_1)}$$
$$\psi_1 = A_1 \cdot A_i \cdot e^{ik_{b1} r \cos(\theta - \beta_1)}$$

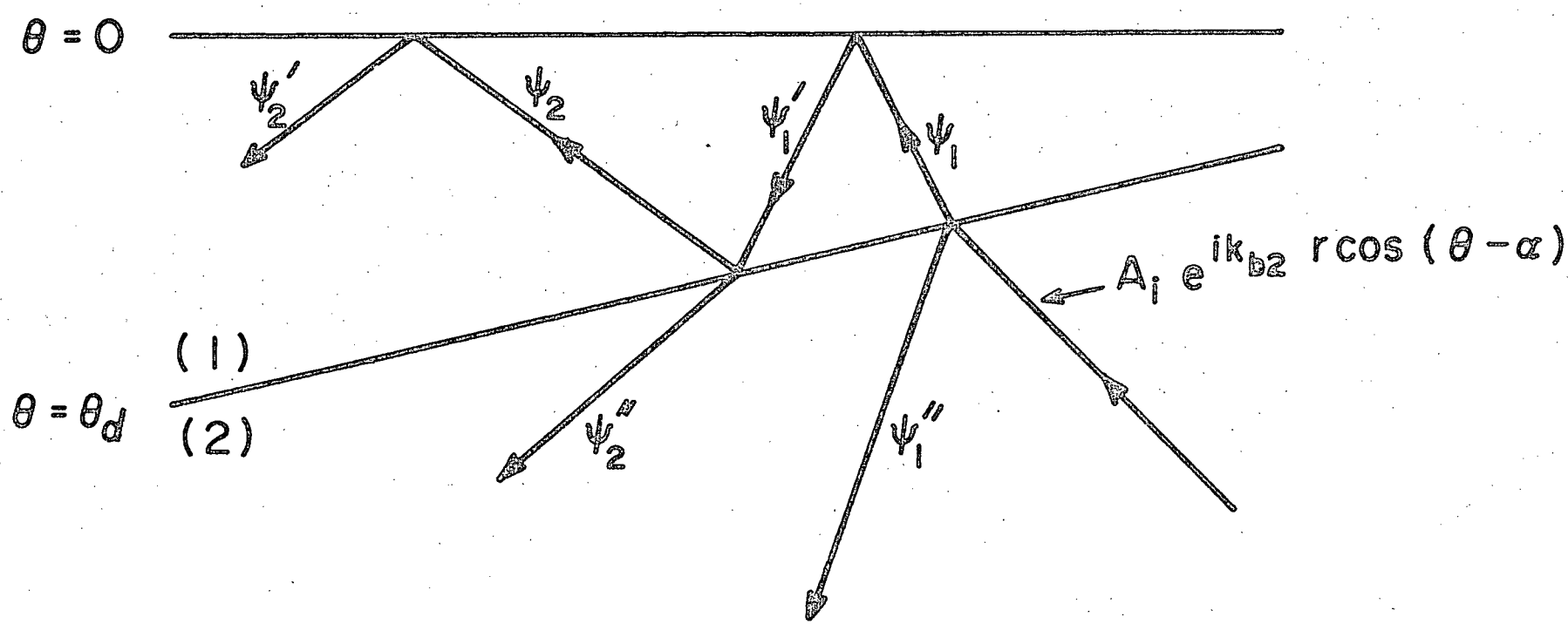

Fig. 2-3. Multiple reflection and refraction for a wedge-shaped medium with a wave incident with propagation direction α.

Using equations (2.8) and (2.10), the boundary conditions are satisfied for

$$A_1'' = \frac{\sin(\theta_d-\alpha)+(1/\delta)\sqrt{\Delta^2-\cos^2(\theta_d-\alpha)}}{\sin(\theta_d-\alpha)-(1/\delta)\sqrt{\Delta^2-\cos^2(\theta_d-\alpha)}}$$

$$\gamma_1 = 2\theta_d + 2\pi - \alpha \qquad (2.14)$$

and

$$A_1 = \frac{2\sin(\theta_d-\alpha)}{\sin(\theta_d-\alpha)-(1/\delta)\sqrt{\Delta^2-\cos^2(\theta_d-\alpha)}}$$

$$\beta_1 = \theta_d + \frac{\pi}{2} - \sin^{-1}\left(\frac{1}{\Delta}\cos(\theta_d-\alpha)\right) \qquad (2.15)$$

To satisfy the boundary condition at $\theta = 0$, we assume a reflected wave

$$\psi_1' = A_1 \cdot A_i \cdot e^{ik_{b1}r\cos(\theta-\gamma_1')}$$

By equation (2.13), the boundary condition is satisfied provided that

$$\gamma_1' = 2\pi - \beta_1$$

To satisfy the boundary conditions at $\theta = \theta_d$, we must assume the reflected and refracted waves

$$\psi_2 = A_2 \cdot A_1 \cdot A_i \cdot e^{ik_{b1}r\cos(\theta-\gamma_2)}$$

$$\psi_2'' = A_2'' \cdot A_1 \cdot A_i \cdot e^{ik_{b2}r\cos(\theta-\beta_2)}$$

which satisfy the boundary conditions for

$$A_2 = \frac{\Delta \sin(\theta_d - \gamma_1') - \delta\sqrt{1-\Delta^2\cos^2(\theta_d-\gamma_1')}}{\Delta \sin(\theta_d - \gamma_1') + \delta\sqrt{1-\Delta^2\cos^2(\theta_d-\gamma_1')}} \qquad (2.16)$$

$$\gamma_2 = 2\theta_d + 2\pi - \gamma_1'$$

and

$$A_2'' = \frac{2\Delta \sin(\theta_d - \gamma_1')}{\Delta \sin(\theta_d - \gamma_1') + \delta\sqrt{1-\Delta^2\cos^2(\theta_d-\gamma_1')}} \qquad (2.17)$$

$$\beta_2 = \theta_d + \frac{3}{2}\pi + \sin^{-1}(\Delta\cos(\theta_d - \gamma_1'))$$

using equations (2.11) and (2.12).

These steps are then repeated. However, it is not an infinite process for it terminates whenever $\pi < \gamma_n < \pi + \theta_d$ or $\pi < \gamma_n' < \pi + \theta_d$ for in these cases the wave propagates down the wedge without further collision with the boundaries. The last term of the series in medium 1 is of the form

$$A_i\left(\prod_{n=1}^{L} A_n\right) e^{ik_{b1}r\cos(\theta-\phi_n)}$$

where $L = n_{max}$

This gives rise to a discontinuity in the displacement,

$$A_i\left(\prod_{n=1}^{L} A_n\right) e^{-ik_{b1}r}$$

at $\theta = \phi_n - \pi$. Therefore, the solution for the diffracted waves must be of a form that will give continuity of displacement and stress at $\theta = \phi_n - \pi$ as well as satisfying the boundary conditions at $\theta = 0$ and $\theta = \theta_d$. As we shall see in the next section, the discontinuity at $\theta = \phi_n - \pi$ is in most cases small indicating that the multiple reflection solution usually dominates the seismogram. Further, Sato (1963) has shown that the amplitude of the diffracted wave decreases rapidly away from the region of the ray theory discontinuity and hence will be small at surface points distant from the vertex. We then write

$$M_1 = A_i \sum_{m=1}^{L'} \left(\prod_{n=1}^{m} A_n\right) e^{ik_{b1} r \cos(\theta - \gamma_m)}$$

$$M_1' = A_i \sum_{m=1}^{L'} \left(\prod_{n=1}^{m} A_n\right) e^{ik_{b1} r \cos(\theta - \gamma_{m'})} \qquad (2.18)$$

and

$$N_1 = A_i \sum_{m=1}^{L} \left(\prod_{n=1}^{m} A_n\right) e^{ik_{b1} r \cos(\theta - \gamma_m)}$$

$$N_1' = A_i \sum_{m=1}^{L} \left(\prod_{n=1}^{m} A_n\right) e^{ik_{b1} r \cos(\theta - \gamma_{m'})} \qquad (2.19)$$

where

$$A_n = \frac{\Delta \sin(\theta_d - \gamma'_{n-1}) - \delta\sqrt{1-\Delta^2\cos^2(\theta_d-\gamma'_{n-1})}}{\Delta \sin(\theta_d - \gamma'_{n-1}) + \delta\sqrt{1-\Delta^2\cos^2(\theta_d-\gamma'_{n-1})}} \qquad (2.20)$$

$$n \geqq 2$$

$$A_1 = \frac{2\sin(\theta_d-\alpha)}{\sin(\theta_d-\alpha) - (1/\delta)\sqrt{\Delta^2-\cos^2(\theta_d-\alpha)}} \qquad (2.21)$$

$$\gamma_m = 2\theta_d(m-1) + \beta_1 \qquad (2.22)$$

$$\gamma'_m = 2\pi - \gamma_m$$

$$\beta_1 = \theta_d + \frac{\pi}{2} - \sin^{-1}\left(\frac{1}{\Delta}\cos(\theta_d-\alpha)\right) \qquad (2.23)$$

$$L = m_{max} \qquad (2.24)$$

$$L' = m_{max} - 1$$

The solution can then be written in one of two forms depending on whether the last reflection is from $\theta = 0$ or $\theta = \theta_d$. In the first case we have

$$u_1 = N_1 + N'_1 \quad \text{for} \quad 0 \leqq \theta \leqq \gamma'_L - \pi$$
$$u_1 = N_1 + M'_1 \quad \text{for} \quad \gamma'_L - \pi \leqq \theta \leqq \theta_d \qquad (2.25)$$

with

$$\pi \leqq \gamma'_L \leqq \pi + \theta_d$$

and in the second case we have

$$\begin{aligned} \mathcal{U}_1 &= M_1 + M_1' \qquad \text{for } 0 \leqq \theta \leqq \gamma_L - \pi \\ \mathcal{U}_1 &= N_1 + M_1' \qquad \text{for } \gamma_L - \pi \leqq \theta \leqq \theta_d \end{aligned} \tag{2.26}$$

with $\pi \leqq \gamma_L \leqq \pi + \theta_d$

The amplitude A, the phase $\textcircled{H}$, and the phase velocity C_v (in the direction θ = constant) may be written as:

$$A = \sqrt{Re(\mathcal{U}_1)^2 + Im(\mathcal{U}_1)^2} \tag{2.27}$$

$$\textcircled{H} = \tan^{-1}\left(Im(\mathcal{U}_1) / Re(\mathcal{U}_1) \right) \tag{2.28}$$

$$C_v = -\omega \Big/ \left(\frac{Re(\mathcal{U}_1)\frac{d\,Im(\mathcal{U}_1)}{dr} - Im(\mathcal{U}_1)\frac{d\,Re(\mathcal{U}_1)}{dr}}{Re(\mathcal{U}_1)^2 + Im(\mathcal{U}_1)^2} \right) \tag{2.29}$$

2.5 Numerical Computation and Discussion

For the numerical computations, the values chosen for the parameters were $\mu_2/\mu_1 = 1.882$ and $C_{b2}/C_{b1} = 1.265$ which correspond to the crust - upper mantle model used by Haskell (1960).

2.5.1 Amplitude Discontinuity at $\theta = \phi_n - \pi$

As discussed in the previous section, the last reflection, which does not collide with a boundary, gives rise to a displacement discontinuity and corresponding to

this a δ -function in the stress at $\theta = \phi_n - \pi$. The magnitude of the displacement discontinuity versus dip angle is shown in Figure 2-4 for various angles of incidence as applicable to teleseismic waves. In the case where the magnitude is small the reflected wave solution adequately describes the physical problem. However, if the discontinuity is large, then a diffracted wave with a large amplitude in the region of $\theta = \phi_n - \pi$ is required to provide continuity in displacement and stress.

We see that for the incident wave propagating in the up-dip direction ($\alpha < 90^\circ$), the discontinuity is small for dip angles less than 15°. However, for incident waves propagating in the down-dip direction ($\alpha > 90^\circ$) the displacement discontinuity is large for some ranges of small dip angles. In these cases the diffracted wave is important because the internally reflected wave propagates out of the wedge after a small number of reflections. However, for surface points distant from the vertex, it is expected that the reflected wave amplitude will give a good approximation in most regions to the true amplitude as the discontinuity surface becomes distant from the free surface.

It should also be pointed out that in addition to the discontinuity within the wedge, discontinuities are

generated by the vertex on reflection of the incoming wave and each refraction into medium (2). In the reflected wave theory these appear as displacement and stress discontinuities radiating from the vertex. The effect of these will not normally be large on the surface of the wedge except close to the vertex as the amplitude decreases rather rapidly with distance and the wave will be partially reflected at the lower boundary of the wedge. However in any study of diffracted waves their relative importance should be investigated.

2.5.2 Surface Amplitude Characteristics

One effect of interest is the effect of a variation of dip angle on the amplitude characteristics at the surface for a constant depth to the boundary and fixed

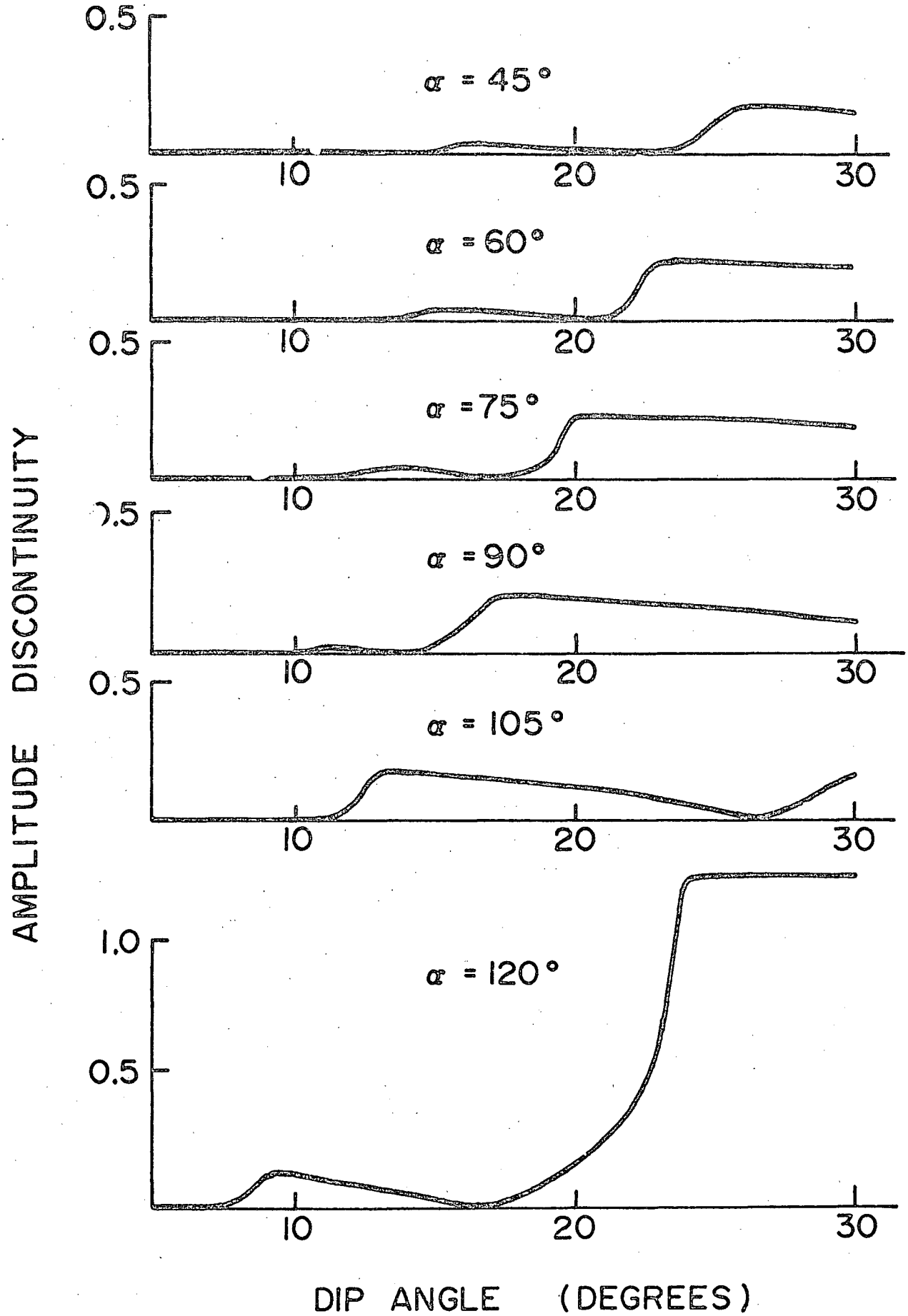

Fig. 2-4. Displacement discontinuity along the edge of outgoing reflected wave for unit amplitude incident waves with propagation direction α.

propagation direction. In Figures 2-5a and 2-5b the amplitude surfaces are plotted for the parameters dip angle and $\sigma = 2\sqrt{3}\pi H/C_{b1}T$ (H is depth to the boundary) for α = 60° and 120°. For fixed H and C_{b1} these are then amplitude surfaces for varying dip angle and period.

For an incident wave with propagation direction α = 60°, we see that the amplitude characteristics change slowly with increasing dip angle except in the range near 25°. However, for an incident wave with α = 120° the amplitude characteristics change rather rapidly with frequency over the range of dip angles considered. The curves 2-5a and 2-5b are typical of the characteristics for incident waves propagating in the up-dip and down-dip direction respectively. One of the reasons for this is indicated in Figure 2-4. For a propagation direction α = 60°, the amplitude discontinuity is small at $\theta = \phi_n - \pi$ for $\theta_d < 21°$ but for a propagation direction α = 120°, the discontinuity is significant over most of the range of dip angles considered. This indicates that in these regions of rapid changes of the amplitude characteristics, the multiple reflection solution as presented here does not fully describe the physical situation but that the diffracted wave is likely to play an important role. From a physical viewpoint, this larger diffracted wave for waves propagating in the down-dip direction arises as the wave

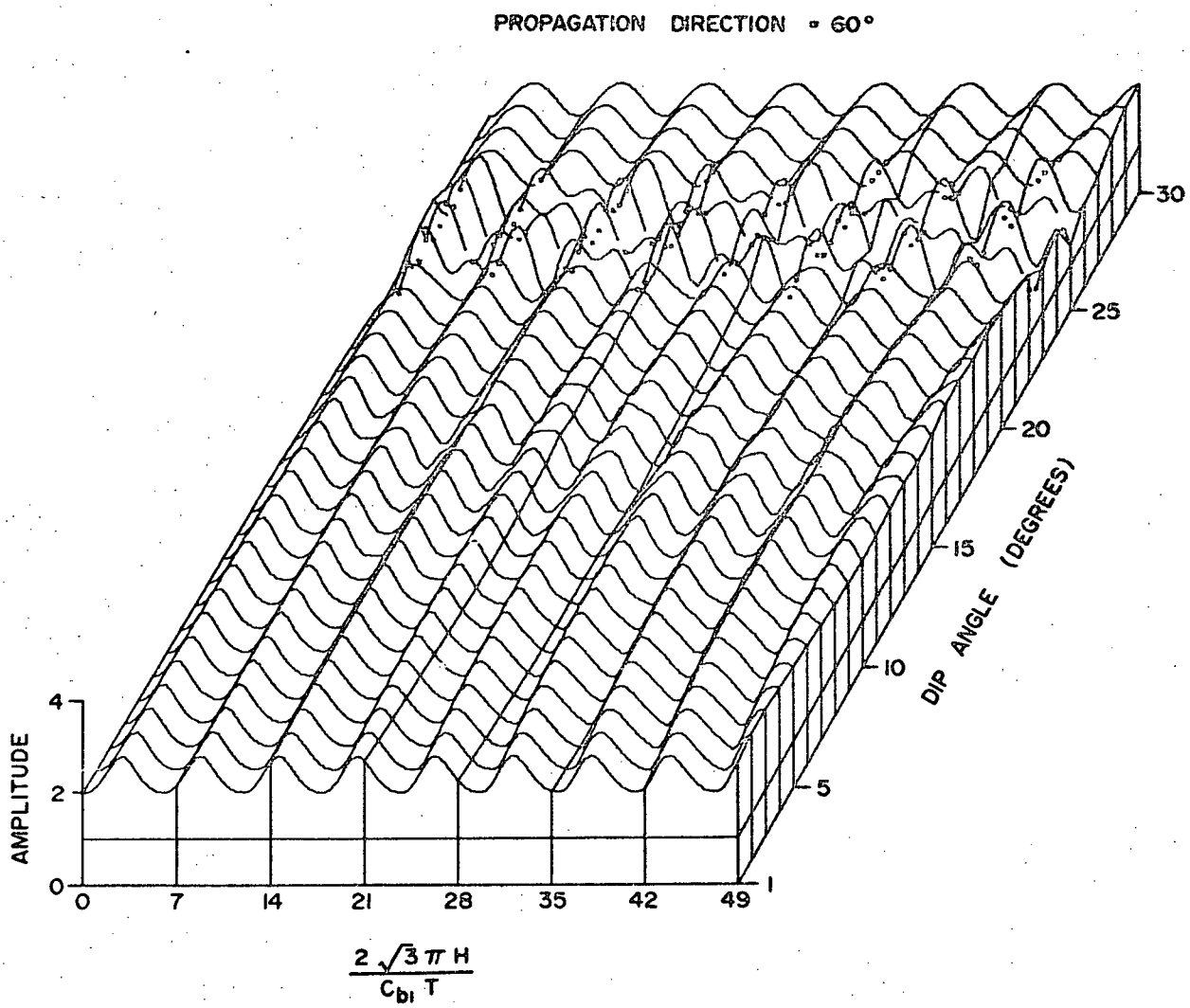

Fig. 2-5a. Amplitude surface for the parameters dip angle and $\sigma = 2\sqrt{3}\pi CH/C_{bl}T$ for an incident wave with propagation direction $\alpha = 60°$.

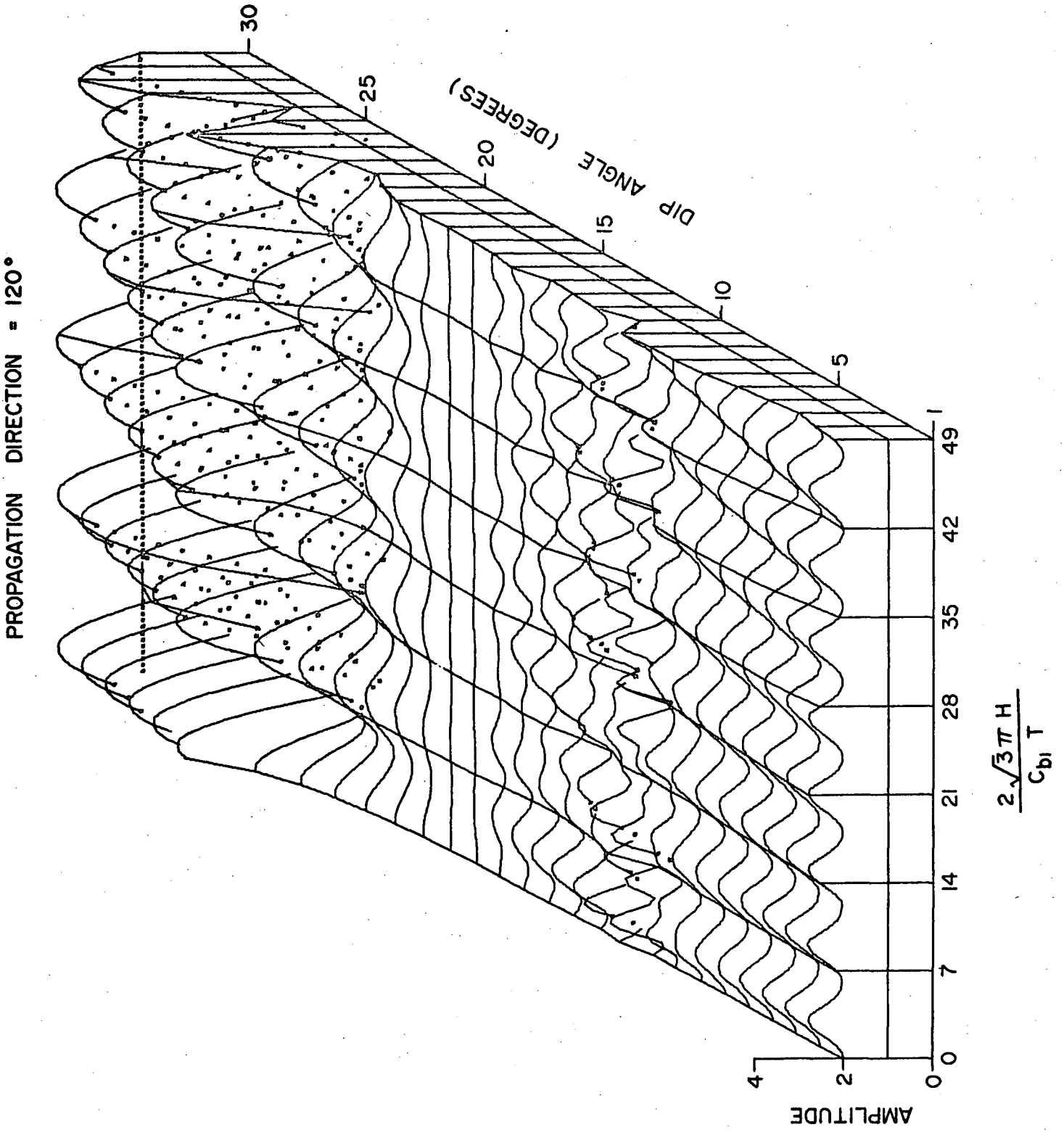

Fig. 2-5b. Amplitude surface for the parameters dip angle and $\delta = 2\sqrt{3}\pi H/C_{b1}T$ for an incident wave with propagation direction $\alpha = 120°$.

only collides with the boundary a very few times before it propagates out of the wedge and hence this wave, which leads to the diffracted wave, is still of significant amplitude. Hence we see that except for large dip angles and waves with large incident angles propagating in the down-dip direction the reflected wave solution adequately describes the physical problem.

Also of interest are the amplitude surfaces for the parameters δ and propagation direction for a constant dip angle. These are shown in Figures 2-6a and 2-6b for dip angles of 0° and 10°. These two graphs are similar in the range of propagation direction 45° to 90° in that for increasing propagation direction this amplitude versus δ curves oscillate more rapidly. It should be noted that the curve for a dip angle of 10° and propagation direction α = 45° has one additional oscillation between δ = 0 and δ = 49 as compared to the curve with no dip. For propagation directions greater than 110° the amplitude curves change rapidly with increasing angle. Again it should be noted from Figure 2-4 that we expect the diffracted wave to play a significant role for this range of propagation directions.

Finally, the amplitude surfaces for the parameters $\tau = \frac{2\pi r}{c_{b1} T}$ and dip angle (Figure 2-7) are considered. The

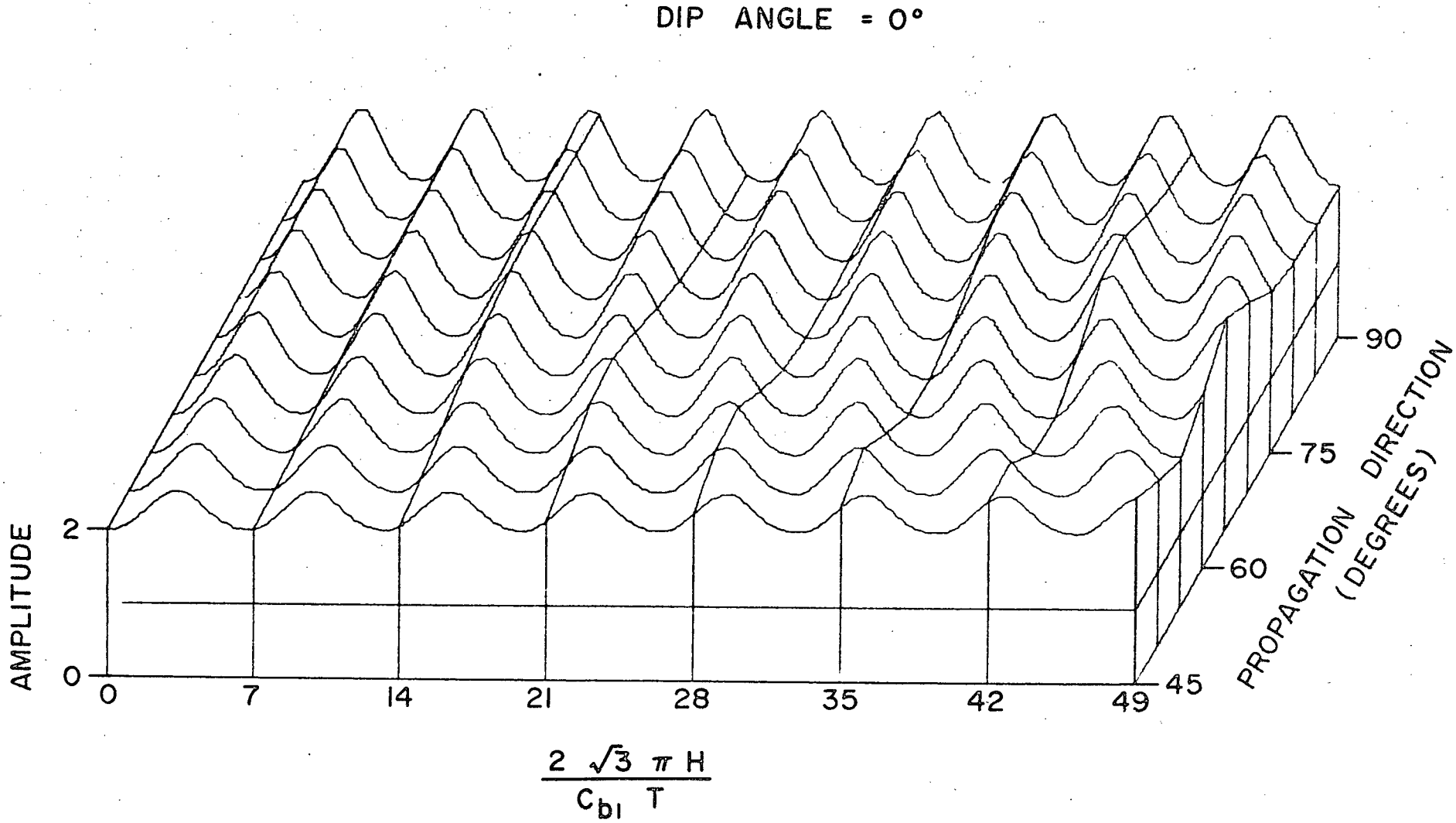

Fig. 2-6a. Amplitude surface for the parameters propagation direction α and $\delta = 2\sqrt{3}\pi H/C_{b1}T$ for a horizontal boundary.

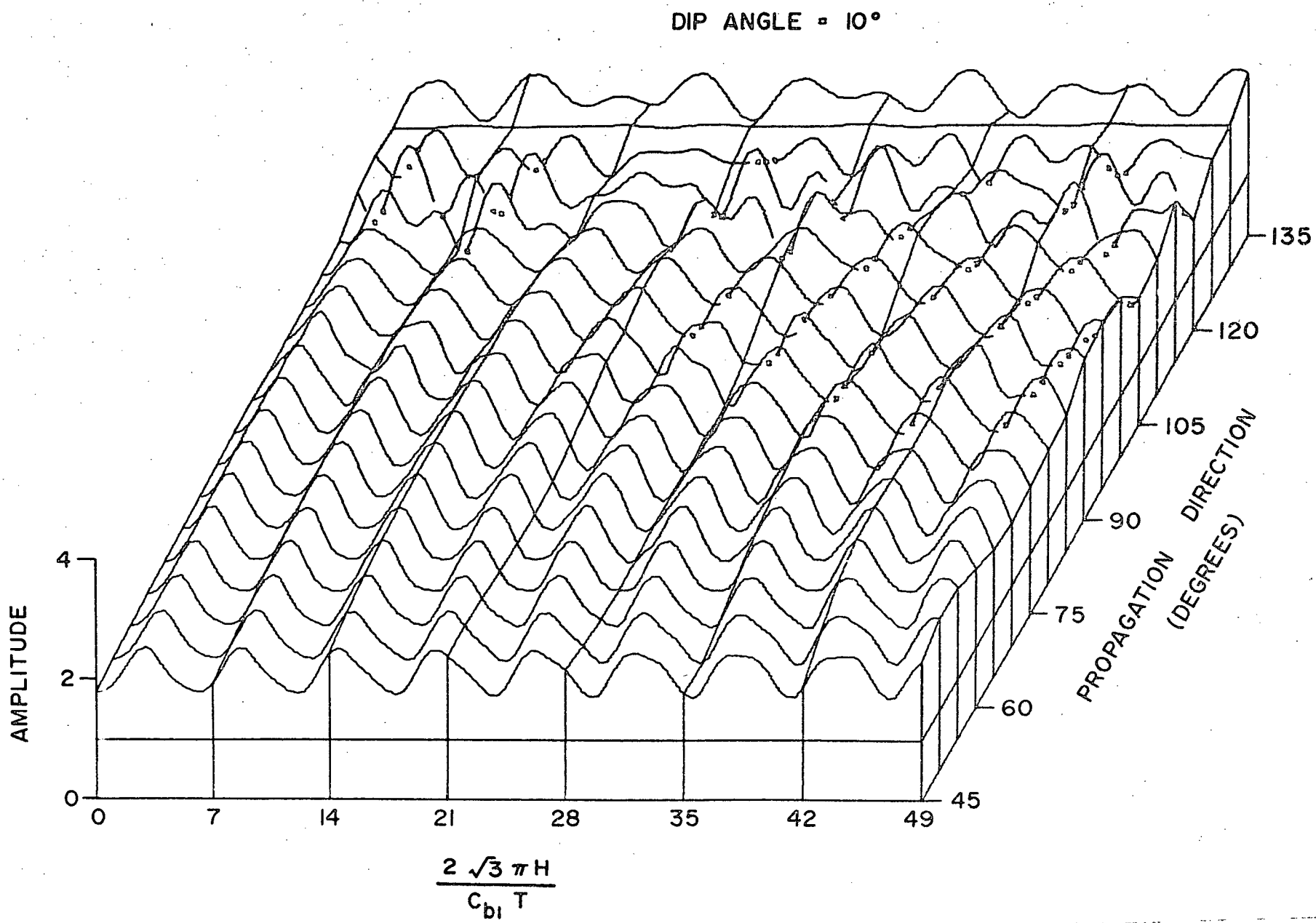

Fig. 2-6b. Amplitude surface for the parameters propagation direction α and $\delta = 2\sqrt{3}\pi H/C_{b1}T$ for a dip angle $\theta_d = 10°$.

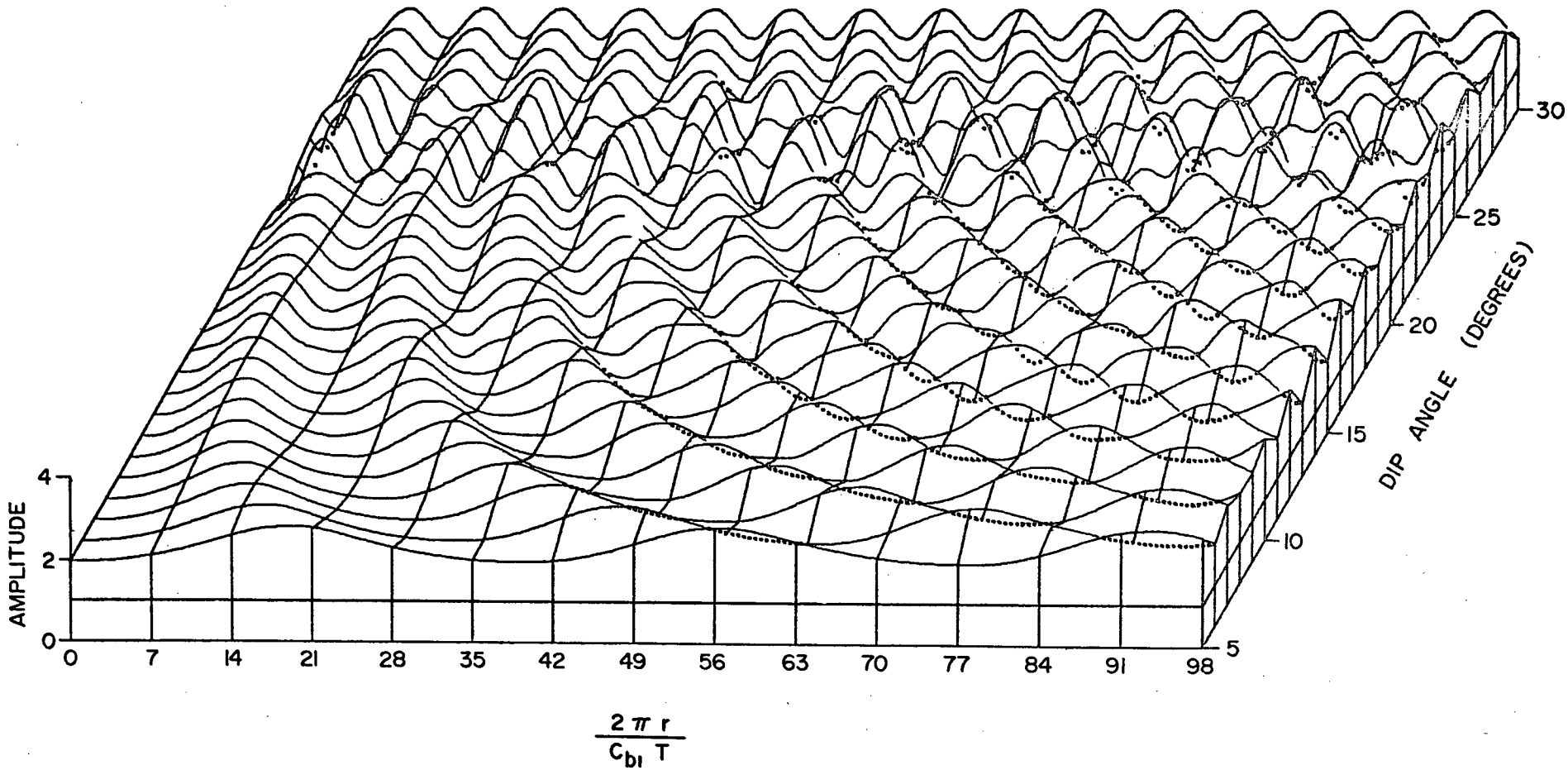

Fig. 2-7. Amplitude surface for the parameters dip angle and $\tau = 2\pi\gamma/c_{b1}T$ for an incident wave with propagation direction $\alpha = 60°$.

major feature of these curves is the increase in the rate of oscillation for the amplitude versus τ curves as the dip angle increases. Hence for a constant distance from the vertex the spectral character of a seismogram is expected to change rapidly with a changing dip angle.

2.5.3 Phase Velocity at the Free Surface

In Figure 2-8, the phase velocity curves are plotted for a dip angle of 10° for various propagation directions α. These differ markedly from the phase velocity for the horizontally layered case (thin lines) as dispersion is present which depends on both the period of the wave and depth to boundary. The amplitude of the phase velocity oscillations increases with increasing propagation angle until an angle is reached which corresponds to vertical incidence for the horizontally layered case. Beyond this angle the oscillations then decrease. Clearly, measurements of phase velocity on a wedge-shaped medium will deviate markedly from the horizontally layered case due to variations with both period of the wave and depth to the interface.

An explanation of the large variations in the phase velocity which occur for incident waves in the up-dip direction is as follows. In this case waves propagate toward the vertex and then have their direction reversed and propagate out of the wedge. For small incident angles (α = 75°), the amplitudes upon reversal of direction will still be large resulting in a significant contribution to the phase velocity with little change in the transfer function compared to the horizontally layered situation.

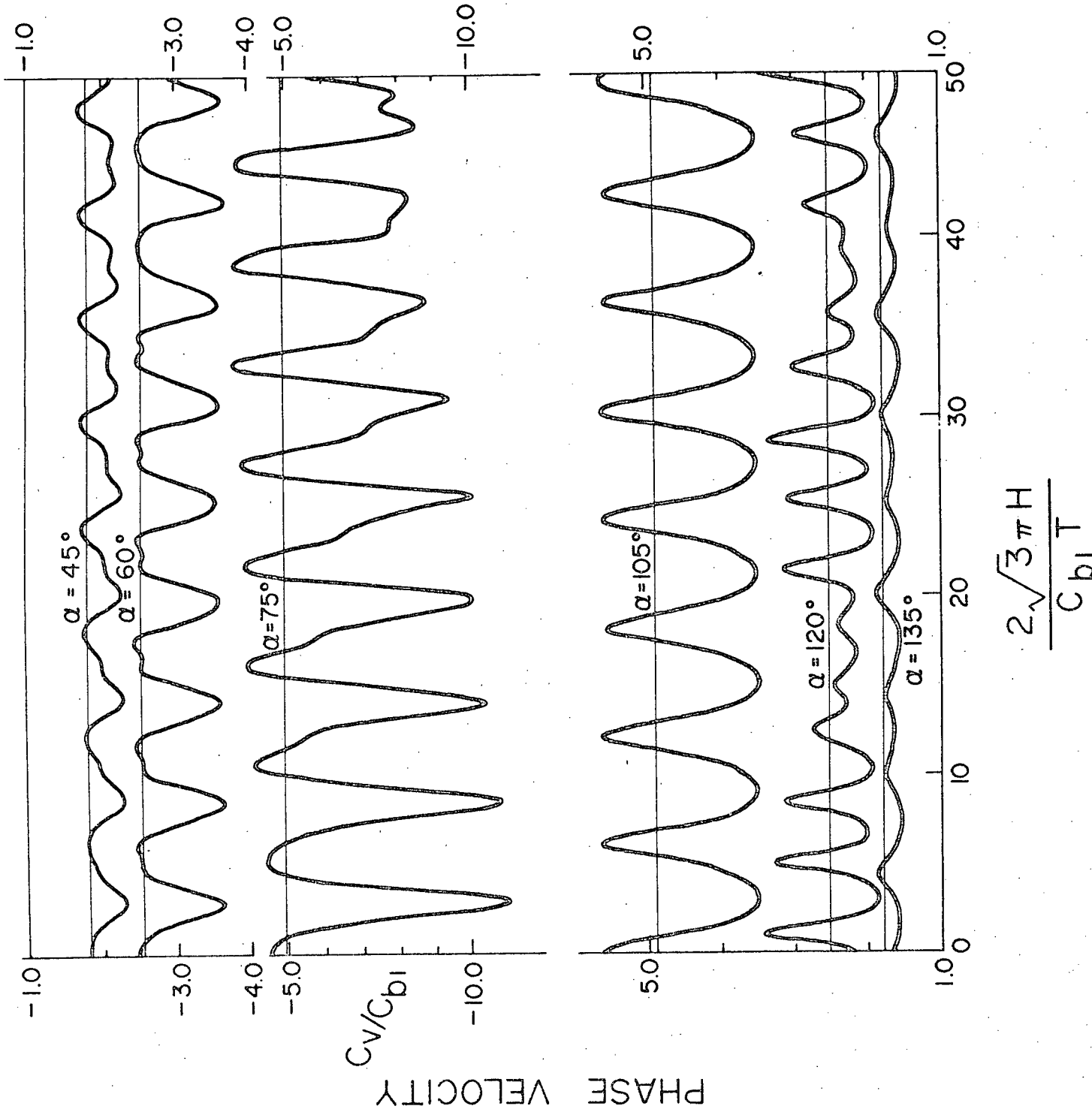

Fig. 2-8. Phase velocity C_v/C_{b1} curves versus $\delta = 2\sqrt{3}\pi H/C_{b1}T$ for a dip angle of 10° and propagation direction α . The thin horizontal lines are the phase velocities for the horizontally layered case.

CHAPTER 3

MULTIPLE REFLECTION OF PLANE P AND SV WAVES BY A DIPPING LAYER

3.1 Introduction

In the previous chapter the problem of a plane SH waves incident at the base of a dipping layer was considered. A solution by multiple reflection for waves incident at any angle perpendicular to strike has been obtained for the amplitude, phase and phase velocity. In this chapter the case of incident P and SV waves is considered. Experimental investigators who use displacement characteristics to interpret crustal structure (e.g., Phinney, 1964) have been limited in their calculations to horizontally layered structures. Consequently, the present analysis will expand the number of models available for interpretation purposes.

3.2 Equations of Motion and Boundary Conditions

In this problem, it is again convenient to choose a cylindrical co-ordinate system (r, θ, z) related to a cartesian system (x, y, z) as shown in Figure 2-1. For plane P and SV waves propagating in the x-y plane, the motion is independent of z and the displacement has only r and θ components. The equations of motion in cylindrical coordinates are:

$$\rho \frac{\partial^2 u_r}{\partial t^2} = (\lambda + 2\mu) \frac{\partial \Theta}{\partial r} - \frac{2\mu}{r} \frac{\partial \tilde{\omega}_z}{\partial \theta} \tag{3.1}$$

$$\rho \frac{\partial^2 u_\theta}{\partial t^2} = (\lambda + 2\mu) \frac{1}{r} \frac{\partial \Theta}{\partial \theta} + 2\mu \frac{\partial \tilde{\omega}_z}{\partial r} \tag{3.2}$$

where:

$$\Theta = \frac{1}{r} \frac{\partial}{\partial r} (r u_r) + \frac{1}{r} \frac{\partial u_\theta}{\partial \theta} \tag{3.3}$$

$$2\tilde{\omega}_z = \frac{1}{r} \frac{\partial}{\partial r} (r u_\theta) - \frac{1}{r} \frac{\partial u_r}{\partial \theta} \tag{3.4}$$

and ρ is density; λ and μ, Lamé's constants; u_r and u_θ, displacements in the r and θ directions. The stress components are expressed by

$$\widehat{\theta\theta} = \lambda \Theta + 2\mu \left(\frac{1}{r} \frac{\partial u_\theta}{\partial \theta} + \frac{u_r}{r} \right) \tag{3.5}$$

$$\widehat{r\theta} = \mu \left(\frac{\partial u_\theta}{\partial r} - \frac{u_\theta}{r} + \frac{1}{r} \frac{\partial u_r}{\partial \theta} \right) \tag{3.6}$$

Using equations (3.3) and (3.4) in the equations of motion, we obtain

$$\rho \frac{\partial^2 \Theta}{\partial t^2} = (\lambda + 2\mu) \left(\frac{\partial^2 \Theta}{\partial r^2} + \frac{1}{r} \frac{\partial \Theta}{\partial r} + \frac{1}{r^2} \frac{\partial^2 \Theta}{\partial \theta^2} \right) \tag{3.7}$$

$$\rho \frac{\partial^2 \tilde{\omega}_z}{\partial t^2} = \mu \left(\frac{\partial^2 \tilde{\omega}_z}{\partial r^2} + \frac{1}{r} \frac{\partial \tilde{\omega}_z}{\partial r} + \frac{1}{r^2} \frac{\partial^2 \tilde{\omega}_z}{\partial \theta^2} \right) \tag{3.8}$$

and in the stress relations, we obtain

$$\widehat{\theta\theta} = \rho C_a^2 \Theta - 2\rho C_b^2 \frac{\partial u_r}{\partial r} \tag{3.9}$$

$$\widehat{r\theta} = 2\rho C_b^2 \left(\frac{\partial u_\theta}{\partial r} - \tilde{\omega}_z \right) \tag{3.10}$$

where $C_a = \sqrt{\frac{\lambda+2\mu}{\rho}}$ and $C_b = \sqrt{\frac{\mu}{\rho}}$, the P and S wave velocities respectively. Assuming a time variation of the form $e^{i\omega t}$, equations (3.1), (3.2), (3.7) and (3.8) become

$$u_r = -\frac{1}{k_a^2}\frac{\partial \Theta}{\partial r} + \frac{2}{k_b^2}\left(\frac{1}{r}\frac{\partial \tilde{\omega}_z}{\partial \theta}\right) \tag{3.11}$$

$$u_\theta = -\frac{1}{k_a^2}\left(\frac{1}{r}\frac{\partial \Theta}{\partial \theta}\right) - \frac{2}{k_b^2}\frac{\partial \tilde{\omega}_z}{\partial r} \tag{3.12}$$

$$\nabla^2 \Theta + k_a^2 \Theta = 0 \tag{3.13}$$

$$\nabla^2 \tilde{\omega}_z + k_b^2 \tilde{\omega}_z = 0 \tag{3.14}$$

where $k_a = \frac{\omega}{C_a}$, $k_b = \frac{\omega}{C_b}$ and $\nabla^2 = \frac{\partial^2}{\partial r^2} + \frac{1}{r}\frac{\partial}{\partial r} + \frac{1}{r^2}\frac{\partial^2}{\partial \theta^2}$

Substituting (3.11) and (3.12) into (3.9) and (3.10), we have

$$\widehat{\theta\theta} = \rho C_a^2 \Theta + 2\rho C_b^2 \left\{ \frac{1}{k_a^2}\frac{\partial^2 \Theta}{\partial r^2} - \frac{2}{k_b^2}\frac{\partial}{\partial r}\left(\frac{1}{r}\frac{\partial \tilde{\omega}_z}{\partial \theta}\right) \right\} \tag{3.15}$$

$$\widehat{r\theta} = -2\rho C_b^2 \left\{ \frac{1}{k_a^2}\frac{\partial}{\partial r}\left(\frac{1}{r}\frac{\partial \Theta}{\partial \theta}\right) + \frac{2}{k_b^2}\frac{\partial^2 \tilde{\omega}_z}{\partial r^2} + \tilde{\omega}_z \right\} \tag{3.16}$$

We choose as the fundamental solution of equations (3.13) and (3.14), $E\cdot e^{ik_a r\cos(\theta-\alpha)}$ and $F\cdot e^{ik_b r\cos(\theta-\beta)}$, plane waves propagating in the α and β directions respectively. Substituting the fundamental solutions into (3.11), (3.12), (3.15) and (3.16) we have the following expressions for displacements and stresses:

$$u_r = -\frac{i}{k_a} E\cos(\theta-\alpha) e^{ik_a r\cos(\theta-\alpha)} - \frac{2i}{k_b} F\sin(\theta-\beta) e^{ik_b r\cos(\theta-\beta)} \tag{3.17}$$

$$u_\theta = \frac{i}{k_a} E\sin(\theta-\alpha) e^{ik_a r\cos(\theta-\alpha)} - \frac{2i}{k_b} F\cos(\theta-\beta) e^{ik_b r\cos(\theta-\beta)} \tag{3.18}$$

$$\widehat{\theta\theta} = \rho\{C_a^2 - 2C_b^2\cos^2(\theta-\alpha)\} E\, e^{ik_a r\cos(\theta-\alpha)} - 4\rho C_b^2 F\cos(\theta-\beta)\sin(\theta-\beta) e^{ik_b r\cos(\theta-\beta)} \tag{3.19}$$

$$\widehat{r\theta} = -2\rho C_b^2 \{E\cos(\theta-\alpha)\sin(\theta-\alpha) e^{ik_a r\cos(\theta-\alpha)} + (1-2\cos^2(\theta-\beta)) F e^{ik_b r\cos(\theta-\beta)}\} \tag{3.20}$$

3.3 Reflection and Refraction Coefficients

In this section the reflection and refraction coefficients in terms of the initial propagation direction and the elastic constants will be considered. First consider two elastic media separated by $\theta = \theta_d$ with waves from medium (2) incident on the interface (Figure 3-1). The solutions of the equations of motion, (3.13) and (3.14), in media (1) and (2) can be written as

$$
\begin{aligned}
\Theta_1 &= A_{rf}\, e^{ik_{a1} r\cos(\theta-\alpha_{rf})} \\
\tilde{\omega}_{z1} &= B_{rf}\, e^{ik_{b1} r\cos(\theta-\beta_{rf})} \\
\Theta_2 &= C_{in}\, e^{ik_{a2} r\cos(\theta-\alpha)} + C_{rl}\, e^{ik_{a2} r\cos(\theta-\alpha_{rl})} \\
\tilde{\omega}_{z2} &= D_{in}\, e^{ik_{b2} r\cos(\theta-\beta)} + D_{rl}\, e^{ik_{b2} r\cos(\theta-\beta_{rl})}
\end{aligned}
\tag{3.21}
$$

where

$$
k_{ai} = \frac{\omega}{c_{ai}}, \quad k_{bi} = \frac{\omega}{c_{bi}}
$$

$$
c_{ai} = \sqrt{\frac{\lambda_i + 2\mu_i}{\rho_i}}, \quad c_{bi} = \sqrt{\frac{\mu_i}{\rho_i}} \qquad \text{for } i = 1, 2
$$

The boundary conditions at $\theta = \theta_d$ are

$$
\begin{aligned}
u_{r1} &= u_{r2} \\
u_{\theta 1} &= u_{\theta 2} \\
\widehat{\theta\theta}_1 &= \widehat{\theta\theta}_2 \\
\widehat{r\theta}_1 &= \widehat{r\theta}_2
\end{aligned}
\tag{3.22}
$$

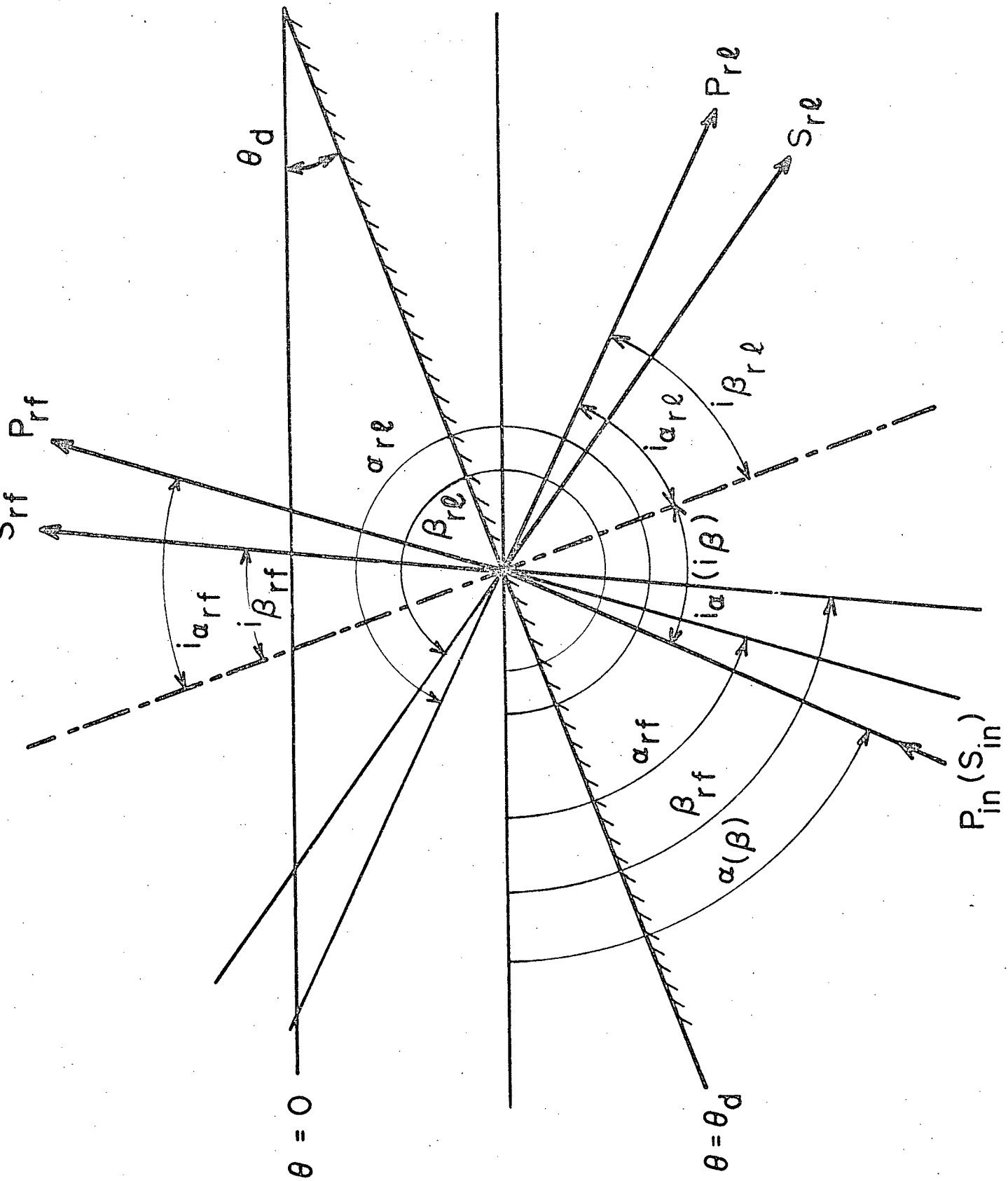

Fig. 3-1. Reflection and refraction of waves at a boundary inclined at an arbitrary angle θ_d with the nomenclature for angles between rays and the horizontal and boundary surfaces indicated.

For a solution of the form (3.21), the displacements and stresses in medium (1) and medium (2) are from expressions (3.17) to (3.21)

$$
\begin{aligned}
u_{r1} &= -i\frac{1}{k_{a1}} A_{rf}\cos(\theta-\alpha_{rf})e^{ik_{a1}r\cos(\theta-\alpha_{rf})} \\
&\quad -i\frac{2}{k_{b1}} B_{rf}\sin(\theta-\beta_{rf})e^{ik_{b1}r\cos(\theta-\beta_{rf})} \\
u_{r2} &= -i\frac{1}{k_{a2}} C_{in}\cos(\theta-\alpha)e^{ik_{a2}r\cos(\theta-\alpha)} \\
&\quad -i\frac{1}{k_{a2}} C_{r\ell}\cos(\theta-\alpha_{r\ell})e^{ik_{a2}r\cos(\theta-\alpha_{r\ell})} \\
&\quad -i\frac{2}{k_{b2}} D_{in}\sin(\theta-\beta)e^{ik_{b2}r\cos(\theta-\beta)} \\
&\quad -i\frac{2}{k_{b2}} D_{r\ell}\sin(\theta-\beta_{r\ell})e^{ik_{b2}r\cos(\theta-\beta_{r\ell})} \\
u_{\theta 1} &= i\frac{1}{k_{a1}} A_{rf}\sin(\theta-\alpha_{rf})e^{ik_{a1}r\cos(\theta-\alpha_{rf})} \\
&\quad -i\frac{2}{k_{b1}} B_{rf}\cos(\theta-\beta_{rf})e^{ik_{b1}r\cos(\theta-\beta_{rf})} \\
u_{\theta 2} &= i\frac{1}{k_{a2}} C_{in}\sin(\theta-\alpha)e^{ik_{a2}r\cos(\theta-\alpha)} \\
&\quad +i\frac{1}{k_{a2}} C_{r\ell}\sin(\theta-\alpha_{r\ell})e^{ik_{a2}r\cos(\theta-\alpha_{r\ell})} \\
&\quad -i\frac{2}{k_{b2}} D_{in}\cos(\theta-\beta)e^{ik_{b2}r\cos(\theta-\beta)} \\
&\quad -i\frac{2}{k_{b2}} D_{r\ell}\cos(\theta-\beta_{r\ell})e^{ik_{b2}r\cos(\theta-\beta_{r\ell})}
\end{aligned}
\tag{3.23}
$$

$$\widehat{\theta\theta}_1 = \rho_1\{C_{a1}^2 - 2C_{b1}^2\cos^2(\theta-\alpha_{rf})\}A_{rf}e^{ik_{a1}r\cos(\theta-\alpha_{rf})}$$
$$-4\rho_1 C_{b1}^2\cos(\theta-\beta_{rf})\sin(\theta-\beta_{rf})B_{rf}e^{ik_{b1}r\cos(\theta-\beta_{rf})}$$

$$\widehat{\theta\theta}_2 = \rho_2\{C_{a2}^2 - 2C_{b2}^2\cos^2(\theta-\alpha)\}C_{in}e^{ik_{a2}r\cos(\theta-\alpha)}$$
$$+\rho_2\{C_{a2}^2 - 2C_{b2}^2\cos^2(\theta-\alpha_{rl})\}C_{rl}e^{ik_{a2}r\cos(\theta-\alpha_{rl})}$$
$$-4\rho_2 C_{b2}^2\cos(\theta-\beta)\sin(\theta-\beta)D_{in}e^{ik_{b2}r\cos(\theta-\beta)}$$
$$-4\rho_2 C_{b2}^2\cos(\theta-\beta_{rl})\sin(\theta-\beta_{rl})D_{rl}e^{ik_{b2}r\cos(\theta-\beta_{rl})} \qquad (3.24)$$

$$-\frac{1}{2\rho_1 C_{b1}^2}\widehat{r\theta}_1 = \cos(\theta-\alpha_{rf})\sin(\theta-\alpha_{rf})A_{rf}e^{ik_{a1}r\cos(\theta-\alpha_{rf})}$$
$$+\{1-2\cos^2(\theta-\beta_{rf})\}B_{rf}e^{ik_{b1}r\cos(\theta-\beta_{rf})}$$

$$-\frac{1}{2\rho_2 C_{b2}^2}\widehat{r\theta}_2 = \cos(\theta-\alpha)\sin(\theta-\alpha)C_{in}e^{ik_{a2}r\cos(\theta-\alpha)}$$
$$+\cos(\theta-\alpha_{rl})\sin(\theta-\alpha_{rl})C_{rl}e^{ik_{a2}r\cos(\theta-\alpha_{rl})}$$
$$+\{1-2\cos^2(\theta-\beta)\}D_{in}e^{ik_{b2}r\cos(\theta-\beta)}$$
$$+\{1-2\cos^2(\theta-\beta_{rl})\}D_{rl}e^{ik_{b2}r\cos(\theta-\beta_{rl})}$$

Application of the boundary conditions (3.22) leads immediately to the equality of phase which for incident P or SV waves yields respectively

$$\left.\begin{matrix} k_{a2}\cos(\theta_d-\alpha) \\ \text{or} \\ k_{b2}\cos(\theta_d-\beta)\end{matrix}\right\} = k_{a2}\cos(\theta_d-\alpha_{rl}) = k_{b2}\cos(\theta_d-\beta_{rl}) \qquad (3.25)$$
$$= k_{a1}\cos(\theta_d-\alpha_{rf}) = k_{b1}\cos(\theta_d-\beta_{rf})$$

which is Snell's Law expressed in a cosine form.

The boundary conditions (3.22) then yield the following equations

$$\begin{pmatrix} \cos(\theta_d-\alpha_{rf}) & 2\nu_{b1}\sin(\theta_d-\beta_{rf}) & -\nu_{a2}\cos(\theta_d-\alpha_{rl}) & -2\nu_{b2}\sin(\theta_d-\beta_{rl}) \\ \sin(\theta_d-\alpha_{rf}) & -2\nu_{b1}\cos(\theta_d-\beta_{rf}) & -\nu_{a2}\sin(\theta_d-\alpha_{rl}) & 2\nu_{b2}\cos(\theta_d-\beta_{rl}) \\ 1-2\nu_{b1}^2\cos^2(\theta_d-\alpha_{rf}) & -4\nu_{b1}^2\cos(\theta_d-\beta_{rf})\times\sin(\theta_d-\beta_{rf}) & -\delta\{\nu_{a2}^2-2\nu_{b2}^2\cos(\theta_d-\alpha_{rl})\} & 4\delta\nu_{b2}^2\cos(\theta_d-\beta_{rl})\times\sin(\theta_d-\beta_{rl}) \\ P\cos(\theta_d-\alpha_{rf})\times\sin(\theta_d-\alpha_{rf}) & P\{1-2\cos^2(\theta_d-\beta_{rf})\} & -\cos(\theta_d-\alpha_{rl})\times\sin(\theta_d-\alpha_{rl}) & 2\cos^2(\theta_d-\beta_{rl})-1 \end{pmatrix}$$

$$\times\begin{pmatrix} A_{rf} \\ B_{rf} \\ C_{rl} \\ D_{rl} \end{pmatrix} = \begin{pmatrix} \nu_{a2}\cos(\theta_d-\alpha) & 2\nu_{b2}\sin(\theta_d-\beta) \\ \nu_{a2}\sin(\theta_d-\alpha) & -2\nu_{b2}\cos(\theta_d-\beta) \\ \delta\{\nu_{a2}^2-2\nu_{b2}^2\cos^2(\theta_d-\alpha)\} & -4\delta\nu_{b2}^2\cos(\theta_d-\beta)\times\sin(\theta_d-\beta) \\ \cos(\theta_d-\alpha)\sin(\theta_d-\alpha) & 1-2\cos^2(\theta_d-\beta) \end{pmatrix}\times\begin{pmatrix} C_{in} \\ D_{in} \end{pmatrix} \qquad (3.26)$$

where $P=\left(\frac{\nu_{b1}}{\nu_{b2}}\right)^2/\delta$, $\delta=\rho_2/\rho_1$, $\nu_{a2}=C_{a2}/C_{a1}$, $\nu_{b1}=C_{b1}/C_{a1}$, and $\nu_{b2}=C_{b2}/C_{a1}$.

To solve equations (3.26) in the case of either an incident P or SV wave, the angles $\alpha_{r\ell}$, $\beta_{r\ell}$, α_{rs} and β_{rs} must be determined in terms of the incident and boundary angles. For a P wave incident from medium (2), the following geometric relationships are evident from Figure 3-1.

$$\begin{aligned}
\alpha &= \theta_d + \tfrac{1}{2}\pi - i_\alpha \\
\alpha_{r\ell} &= \theta_d + \tfrac{3}{2}\pi + i_{\alpha_{r\ell}} \\
\beta_{r\ell} &= \theta_d + \tfrac{3}{2}\pi + i_{\beta_{r\ell}} \\
\alpha_{rs} &= \theta_d + \tfrac{1}{2}\pi - i_{\alpha_{rs}} \\
\beta_{rs} &= \theta_d + \tfrac{1}{2}\pi - i_{\beta_{rs}}
\end{aligned} \tag{3.27}$$

for $\theta_d < \alpha \leq \theta_d + \frac{\pi}{2}$. Using (3.25) we then obtain

$$\begin{aligned}
\alpha_{r\ell} &= \theta_d + \tfrac{3}{2}\pi + \sin^{-1}\{\cos(\theta_d - \alpha)\} = 2\theta_d + 2\pi - \alpha \\
\beta_{r\ell} &= \theta_d + \tfrac{3}{2}\pi + \sin^{-1}\{(C_{b2}/C_{a2})\cos(\theta_d - \alpha)\} \\
\alpha_{rs} &= \theta_d + \tfrac{1}{2}\pi - \sin^{-1}\{(C_{a1}/C_{a2})\cos(\theta_d - \alpha)\} \\
\beta_{rs} &= \theta_d + \tfrac{1}{2}\pi - \sin^{-1}\{(C_{b1}/C_{a2})\cos(\theta_d - \alpha)\}
\end{aligned} \tag{3.28}$$

where the principal value of the inverse sine is taken in each case. It is easily verified that (3.28) also holds for $\theta_d + \frac{\pi}{2} \leq \alpha < \theta_d + \pi$. For incident SV waves, we find

$$\begin{aligned}
\alpha_{r\ell} &= \theta_d + \tfrac{3}{2}\pi + \sin^{-1}\{(C_{a2}/C_{b2})\cos(\theta_d - \beta)\} \\
\beta_{r\ell} &= \theta_d + \tfrac{3}{2}\pi + \sin^{-1}\{\cos(\theta_d - \beta)\} = 2\theta_d + 2\pi - \beta
\end{aligned} \tag{3.29}$$

$$\alpha_{rf} = \theta_d + \frac{1}{2}\pi - \sin^{-1}\{(C_{a1}/C_{b2})\cos(\theta_d - \beta)\}$$
$$\beta_{rf} = \theta_d + \frac{1}{2}\pi - \sin^{-1}\{(C_{b1}/C_{b2})\cos(\theta_d - \beta)\} \qquad (3.29)$$

Hence, by setting $D_{in} = 0$ in (3.26) and substitution of (3.28), the reflection and refraction coefficients for an incident P wave can be determined. Similarly, by setting $C_{in} = 0$ and the use of (3.29) allows us to determine the reflection and refraction coefficients for an incident SV wave.

For P waves incident on the boundary from medium (1) we determine the following expressions for the angles.

$$\alpha_{rl} = \theta_d + \frac{1}{2}\pi - \sin^{-1}\{\cos(\theta_d - \alpha)\} = 2\theta_d + 2\pi - \alpha$$
$$\beta_{rl} = \theta_d + \frac{1}{2}\pi - \sin^{-1}\{(C_{b1}/C_{a1})\cos(\theta_d - \alpha)\}$$
$$\alpha_{rf} = \theta_d + \frac{3}{2}\pi + \sin^{-1}\{(C_{a2}/C_{a1})\cos(\theta_d - \alpha)\} \qquad (3.30)$$
$$\beta_{rf} = \theta_d + \frac{3}{2}\pi + \sin^{-1}\{(C_{b2}/C_{a1})\cos(\theta_d - \alpha)\}$$

and for S waves

$$\alpha_{rl} = \theta_d + \frac{1}{2}\pi - \sin^{-1}\{(C_{a1}/C_{b1})\cos(\theta_d - \beta)\}$$
$$\beta_{rl} = \theta_d + \frac{1}{2}\pi - \sin^{-1}\{\cos(\theta_d - \beta)\} = 2\theta_d + 2\pi - \beta$$
$$\alpha_{rf} = \theta_d + \frac{3}{2}\pi + \sin^{-1}\{(C_{a2}/C_{b1})\cos(\theta_d - \beta)\} \qquad (3.31)$$
$$\beta_{rf} = \theta_d + \frac{3}{2}\pi + \sin^{-1}\{(C_{b2}/C_{b1})\cos(\theta_d - \beta)\}$$

Equations (3.26) may then be used to determine the reflection and refraction coefficients for waves incident from medium (1) by the use of (3.30) and (3.31) and the following substitutions:

$\rho_1 \to \rho_2$, $\rho_2 \to \rho_1$, $C_{a1} \to C_{a2}$, $C_{a2} \to C_{a1}$, $C_{b1} \to C_{b2}$, and $C_{b2} \to C_{b1}$. It should be noted that A_{rs} and B_{rs} are in this case amplitudes in medium (2) and C_{rl} and D_{rl} amplitudes in medium (1).

Finally, we consider waves incident on the free surface $\theta = 0$ (Figure 3-2). The solutions of (3.13) and (3.14) in medium (1) can be written as

$$\Theta_1 = A_{in} e^{ik_{a1} r \cos(\theta-\alpha)} + A_{rl} e^{ik_{a1} r \cos(\theta-\alpha_{rl})}$$
$$\tilde{\omega}_{z1} = B_{in} e^{ik_{b1} r \cos(\theta-\beta)} + B_{rl} e^{ik_{b1} r \cos(\theta-\beta_{rl})} \qquad (3.32)$$

Following the same procedure as before we find the equations between the amplitude coefficients to be

$$\begin{bmatrix} 1-2\nu_{b1}^2\cos^2\alpha_{rl} & 4\nu_{b1}^2\cos\beta_{rl}\sin\beta_{rl} \\ -\cos\alpha_{rl}\sin\alpha_{rl} & 1-2\cos^2\beta_{rl} \end{bmatrix} \cdot \begin{bmatrix} A_{rl} \\ B_{rl} \end{bmatrix} =$$
$$\begin{bmatrix} 2\nu_{b1}^2\cos^2\alpha-1 & -4\nu_{b1}^2\cos\beta\sin\beta \\ \cos\alpha\sin\alpha & 2\cos^2\beta-1 \end{bmatrix} \cdot \begin{bmatrix} A_{in} \\ B_{in} \end{bmatrix} \qquad (3.33)$$

For P wave incidence the following relations are seen to hold

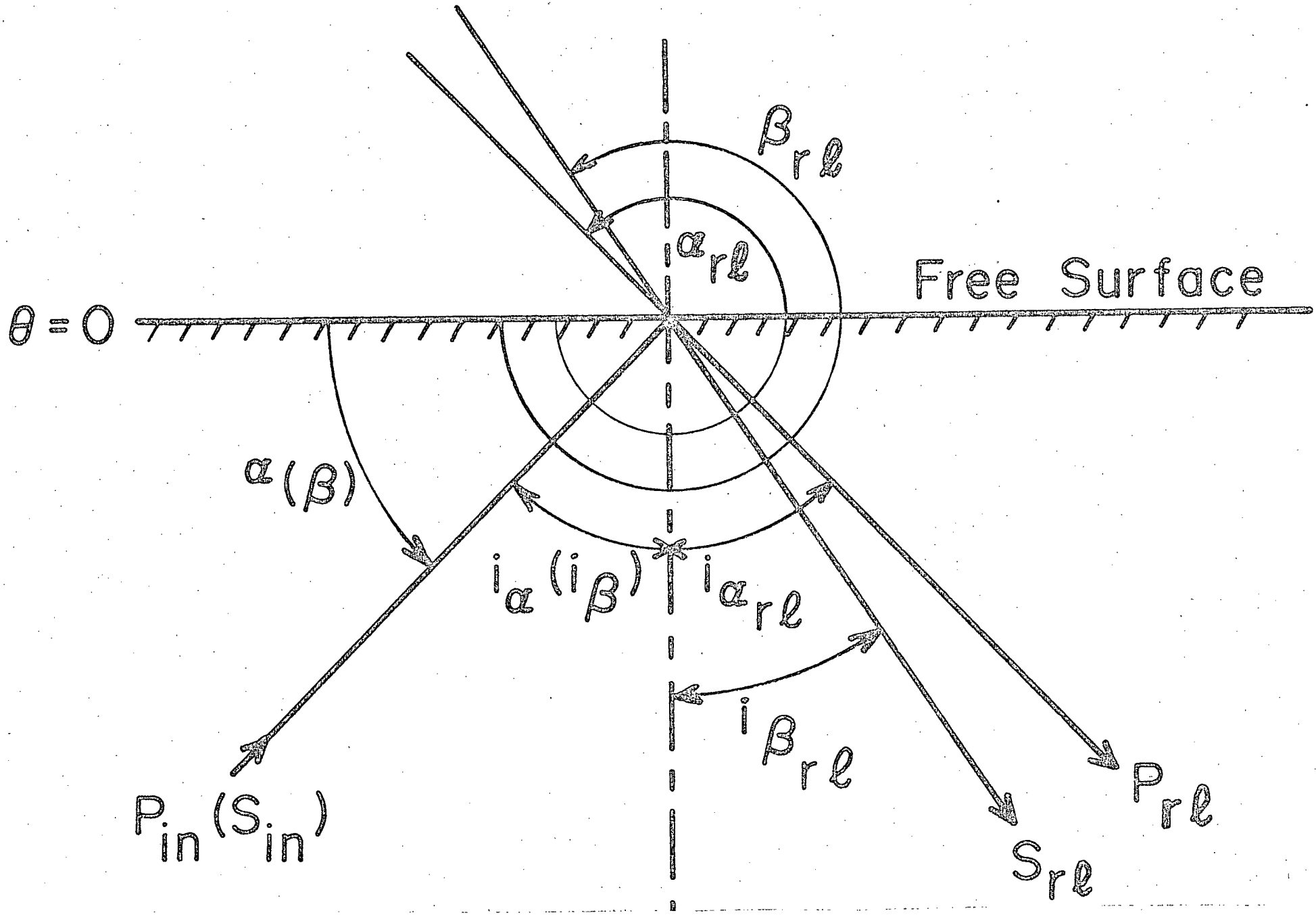

Fig. 3-2. Reflection of waves at a free surface with nomenclature for angles between rays and the free surface indicated.

$$\cos\alpha_{rl} = \cos\alpha$$
$$\cos\beta_{rl} = (C_{b1}/C_{a1})\cos\alpha$$
$$\sin\alpha = \sqrt{1-\cos^2\alpha}$$
$$\sin\alpha_{rl} = -\sqrt{1-\cos^2\alpha} \qquad (3.34)$$
$$\sin\beta_{rl} = -\sqrt{1-(C_{b1}/C_{a1})^2\cos^2\alpha}$$
$$\alpha_{rl} = \frac{3}{2}\pi + \sin^{-1}\{\cos\alpha\} = 2\pi - \alpha$$
$$\beta_{rl} = \frac{3}{2}\pi + \sin^{-1}\{(C_{b1}/C_{a1})\cos\alpha\}$$

and for an incident SV wave

$$\cos\alpha_{rl} = (C_{a1}/C_{b1})\cos\beta$$
$$\cos\beta_{rl} = \cos\beta$$
$$\sin\beta = \sqrt{1-\cos^2\beta}$$
$$\sin\alpha_{rl} = -\sqrt{1-(C_{a1}/C_{b1})^2\cos^2\beta} \qquad (3.35)$$
$$\sin\beta_{rl} = -\sqrt{1-\cos^2\beta}$$
$$\alpha_{rl} = \frac{3}{2}\pi + \sin^{-1}\{(C_{a1}/C_{b1})\cos\beta\}$$
$$\beta_{rl} = \frac{3}{2}\pi + \sin^{-1}\{\cos\beta\} = 2\pi - \beta$$

Using (3.34) and (3.35) in (3.33), we obtain for incident P waves

$$A_{rl} = \frac{4\nu_{b1}^3\cos^2\alpha\sin\alpha\sqrt{1-\nu_{b1}^2\cos^2\alpha} - (1-2\nu_{b1}^2\cos^2\alpha)^2}{4\nu_{b1}^3\cos^2\alpha\sin\alpha\sqrt{1-\nu_{b1}^2\cos^2\alpha} + (1-2\nu_{b1}^2\cos^2\alpha)^2} A_{in}$$

$$B_{rl} = \frac{2\cos\alpha\sin\alpha(1-2\nu_{b1}^2\cos^2\alpha)}{4\nu_{b1}^3\cos^2\alpha\sin\alpha\sqrt{1-\nu_{b1}^2\cos^2\alpha} + (1-2\nu_{b1}^2\cos^2\alpha)^2} A_{in} \qquad (3.36)$$

and for incident S waves

$$A_{re} = \frac{-8\nu_{b1}^2 \cos\beta \sin\beta (1-2\cos^2\beta)}{4\cos^2\beta \sin\beta \sqrt{\nu_{b1}^2 - \cos^2\beta} + (1-2\cos^2\beta)^2} B_{in}$$

$$B_{re} = \frac{4\cos^2\beta \sin\beta \sqrt{\nu_{b1}^2 - \cos^2\beta} - (1-2\cos^2\beta)^2}{4\cos^2\beta \sin\beta \sqrt{\nu_{b1}^2 - \cos^2\beta} + (1-2\cos^2\beta)^2} B_{in} \qquad (3.37)$$

In expressions (3.36) and (3.37), it should be noted that when the argument A in a square root is negative, then $\sqrt{A}$ must be replaced by $-i\sqrt{A}$ for the solution to remain finite at infinity. As a check on the amplitude coefficients in this form, the energy flux equations have been derived in Appendix I.

3.4 Computation of Displacement in the Case of a Dipping Layer

To determine the amplitude at any point in a wedge we must sum the complex amplitudes of all waves which arrive. From (3.23) we see that this requires the calculation of the amplitude coefficient and propagation direction for each wave. In the process of computation, complex angles have been employed in order that the cases for total reflection and incident angles greater than the critical angle are automatically involved in results. In Appendix II, investigation of a Rayleigh wave written in terms of complex angles

shows that the real part of the angle indicates the propagation direction and the imaginary part gives the decrease of amplitude.

As a P and S wave arise from the initial refraction and from each reflection from the free surface and the boundary between media, the rays increase in number as 2^{n+1} where n is the order of reflection. The reflection process is terminated whenever the propagation direction is between π and $\pi+\theta_d$ for in that case the wave propagates out of the wedge. For computation purposes a further artificial termination was introduced by neglecting all waves whose amplitude was less than $\varepsilon=10^{-4}$ (the displacement amplitudes are normalized by the displacement amplitudes which the incident wave would have on the free surface in the absence of the boundary).

For computational purposes, it is important to note that the amplitudes and propagation direction for a wavefront is the same at all points. Hence, if the amplitudes (M) and propagation directions (m) are determined for all waves reverberating in the wedge, then the total amplitude of motion at any point may easily be calculated. Further, as the M and m of reflected waves depend directly on M and m of the input wave, it is important at the initial refraction and each reflection to store M and m for waves which may generate further waves. The rather

complex computation scheme used can best be understood by examination of the flow chart (Figure 3-3). M and m for the refracted waves are first calculated and stored in vectors in order that they later can be used to calculate the amplitude and phase at any point in the wedge. As the P wave is to be followed through the wedge, the amplitude and propagation direction of the S wave (M_S and m_S) are also temporarily stored in a vector which will later be used to investigate waves due to S wave conversion. M and m are then calculated and stored for the ray which propagates through the system as P (at the same time storing M_S and m_S in the subsidiary vector) until P either propagates out of the system or the amplitude is less than ε . The waves generated by the S wave of this order and higher order waves they may generate are then examined (with attention again first focussed on the P), then those generated by the next lowest order until finally the refracted S and its resulting waves are examined. Upon completion of this calculation the vertical and horizontal displacement and the vertical-horizontal displacement ratio may then be calculated for different σ .

In these computation the values chosen for the parameters were $C_{b1}/C_{a1} = 0.5784$, $C_{a2}/C_{a1} = 1.267$ $C_{b2}/C_{a1} = 0.7319$ and $\rho_2/\rho_1 = 1.175$ which correspond to crust-upper mantle model employed by Haskell (1962).

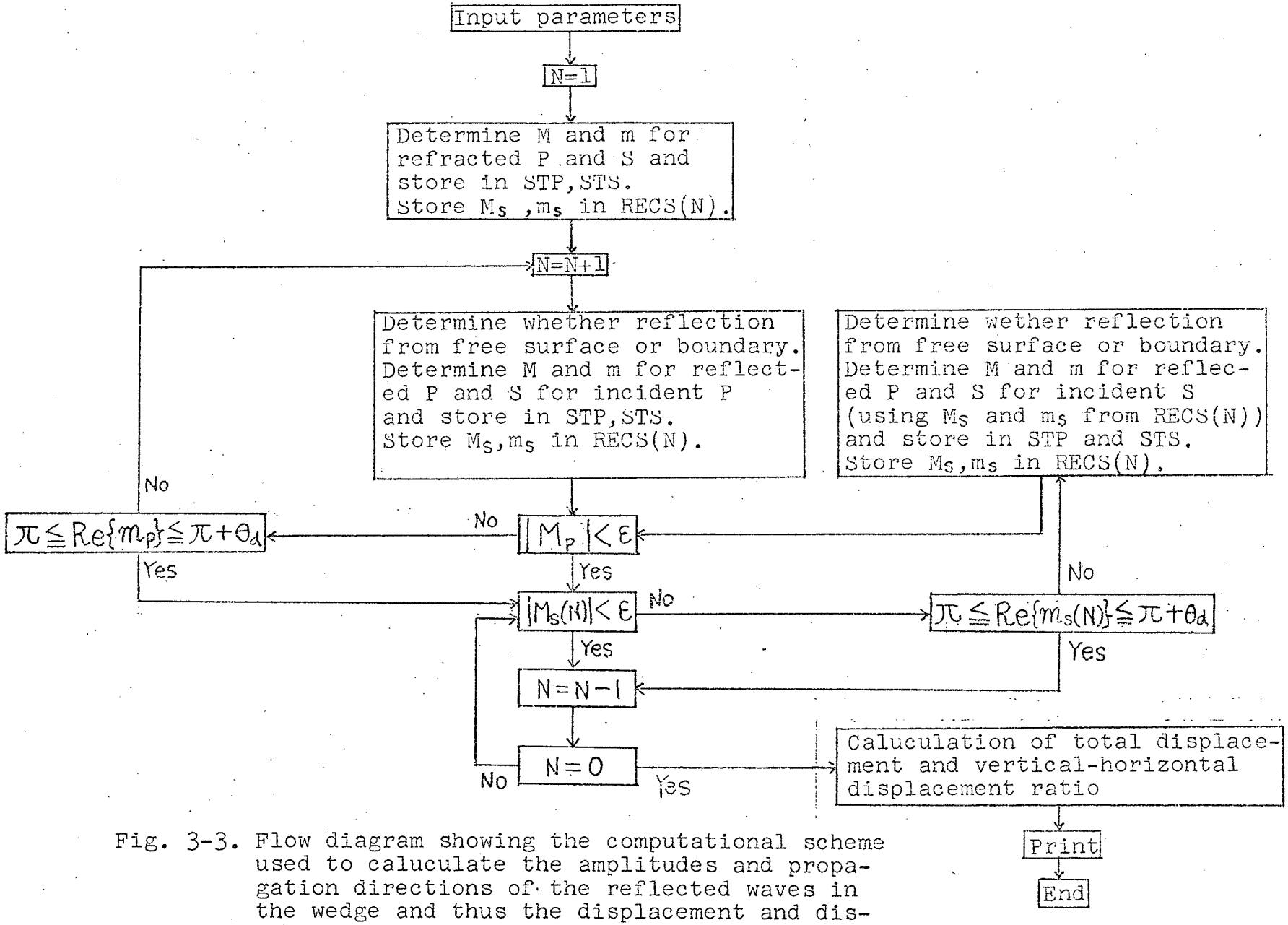

Fig. 3-3. Flow diagram showing the computational scheme used to caluculate the amplitudes and propagation directions of the reflected waves in the wedge and thus the displacement and displacement ratio at any point. Notation is given in Table 1.

Table 1. Notation used in Figure 3-3.

STP(K,2) - complex storage matrix for P amplitudes and propagation directions
STS(K,2) - complex storage matrix for S amplitudes and propagation directions
RECS(L,2) - complex matrix to temporarily retain S amplitudes and propagation directions of S rays which may generate further significant amplitudes
N-1 - no. of reflections a wave has undergone
M - amplitude
m - complex propagation direction
Subscripts p and s indicate P and S wave types

3.5 Displacement Discontinuities

As discussed in the previous chapter, the last reflection which does not collide with boundaries gives rise to a diffracted wave which in the reflected wave solution appears as a displacement discontinuity. When the displacement discontinuity is small, only a small diffracted wave is required to provide continuity in displacement and stress and hence the reflected wave solution adequately describes the physical problem. Large discontinuities will require large diffracted waves; however, at large distances from the vertex the solution is still expected to be adequate as diffracted waves decrease rapidly with distance.

For incident P waves the magnitude of the maximum discontinuity of both the radial component from the last P wave and the tangential component from the exiting S wave is shown in Figure 3-4 for incident waves with propagation directions α = 60° and 120°. Several points should be noted. The discontinuity in the case of down-dip propagation is much larger than for the up-dip direction. This is expected since fewer reverberations occur before the wave propagates out of the wedge. The discontinuity from P waves is relatively large in comparison to that for S waves and rapid changes in the amplitude result as the maximum discontinuity is associated with different exiting waves for different dip angles. The particularly rapid decreases observed result when an SV wave generating an exiting reflected P wave reaches the critical angle. The maximum P wave discontinuity at the next calculated point (calculation interval = 0.25°) is then due to another wave which may be of much lower amplitude.

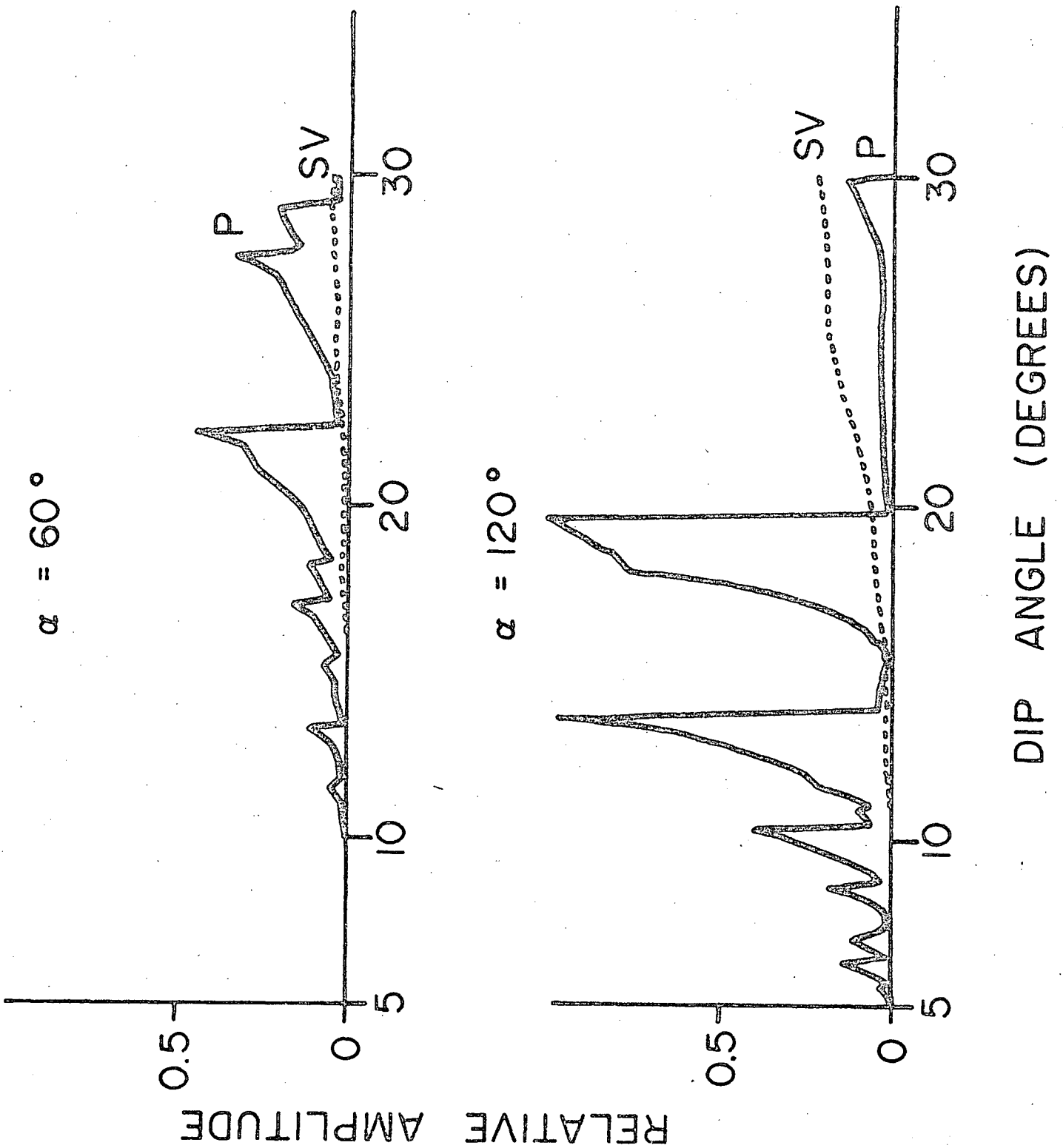

Fig. 3-4. Maximum displacement discontinuity of the radial component from the exiting P waves and tangential component from the exiting SV waves for an incident P wave with propagation directions $\alpha=60°$ and $\alpha=120°$.

For an incident SV wave (Figure 3-5), the displacement discontinuities are negligible for dip angles less than 21° for an incident wave with $\beta = 60°$ indicating that this solution very closely approximates the complete solution. Again the discontinuity is larger for the incident wave propagating in the down-dip direction.

However in the case for $\beta = 120°$ the large discontinuity for the outgoing P wave is for large dip angles rather than the smaller dip angles ($\theta_d < 20°$) as found for the incident P wave case. The physical reason for this is not clear.

As discussed in Chapter 2, discontinuities exist in medium (2) due to the reflection of the incident wave and refraction of waves back into the lower medium. Except close to the vertex, the amplitudes of the resulting diffracted waves are expected to be small.

3.6 Surface Displacements and Displacement Ratios

3.6.1 Incident P

Horizontal and vertical displacements are plotted versus the parameters $\sigma = 2\sqrt{3}\,\pi H/C_{a1}T$. (H is depth to the interface) and illustrated in Figure 3-6. For an

initial propagation direction of 60° the vertical component changes very slowly with increasing dip angle. The horizontal displacement changes rather more rapidly; however the major changes in character occur for $\theta_d > 20°$ where from Figure 3-4, we see that the role of the diffracted ray becomes important. For α = 120°, a more rapid change in character of both the vertical and horizontal surfaces

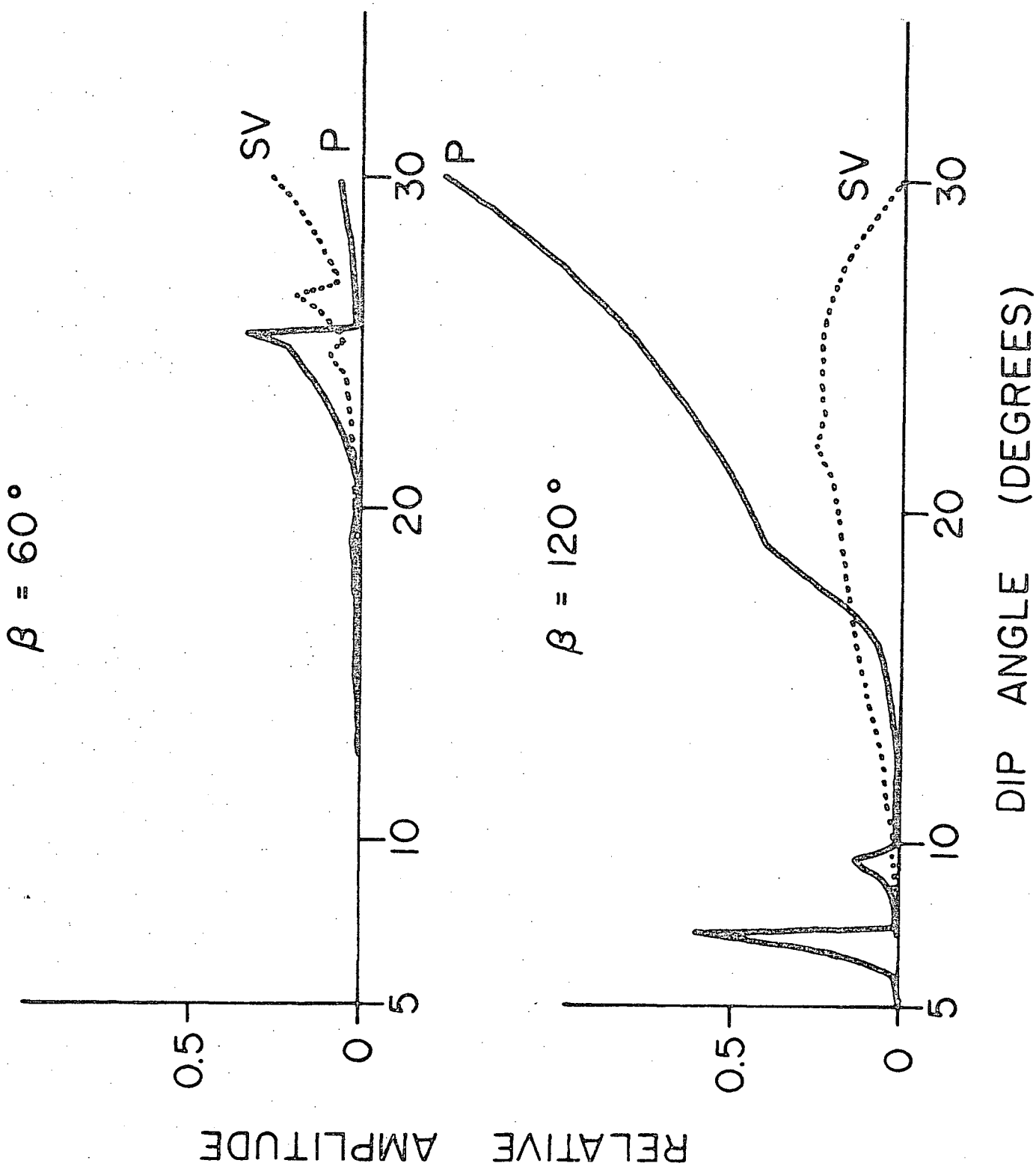

Fig. 3-5. Maximum displacement discontinuity of the radial component from the exiting P waves and tangential component from the exiting SV waves for an incident SV wave with propagation directions $\beta=60°$ and $\beta=120°$.

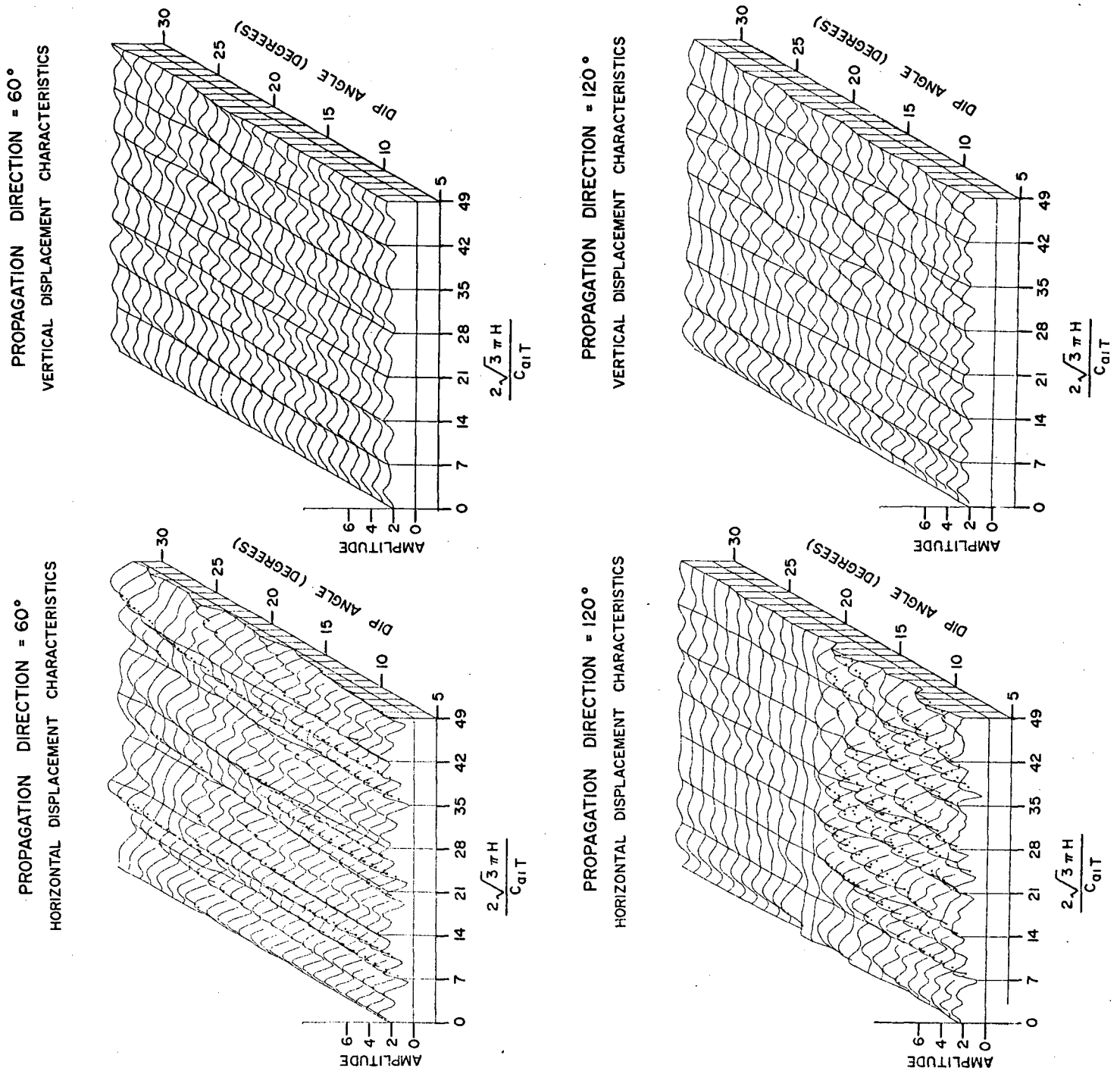

Fig. 3-6. Horizontal and vertical displacements versus the parameter $\delta = 2\sqrt{3}\pi H/C_{\alpha 1}T$ for incident P waves with propagation directions $\alpha = 60°$ and $\alpha = 120°$ for the range of dip angles $5° \leqq \theta_d \leqq 30°$.

is evident with increasing dip angle. This is particularly true in the horizontal where for $\theta_d > 17°$ the surface is rather featureless. However it should be noted that the discontinuity curves in this case indicated that the diffracted wave may be important over most of the range of dip angles.

The displacement ratios V/H which are of interest in practical analysis are shown in Figure 3-7. For the initial propagation direction $\alpha = 60°$, the ratios are very similar for dip angles less than 10°. For dip angles greater than 10°, the peaks move to larger values of δ and increase markedly in amplitude. For $\alpha = 120°$, the ratios change much more rapidly even at small dip angles with the peaks moving to increasing δ again. However in this case the amplitude decreases until for $\theta_d \geqq 20°$ the V/H ratio is almost constant for variable δ .

3.6.2 Incident SV

From Figure 3-8, it is seen that the displacement surfaces exhibit significant character. One particular feature is that for dip angles greater than 18°, the period of the variation of horizontal displacement becomes short and the corresponding amplitude small for $\beta = 60°$. It should be noted that this change occurs before diffracted waves become

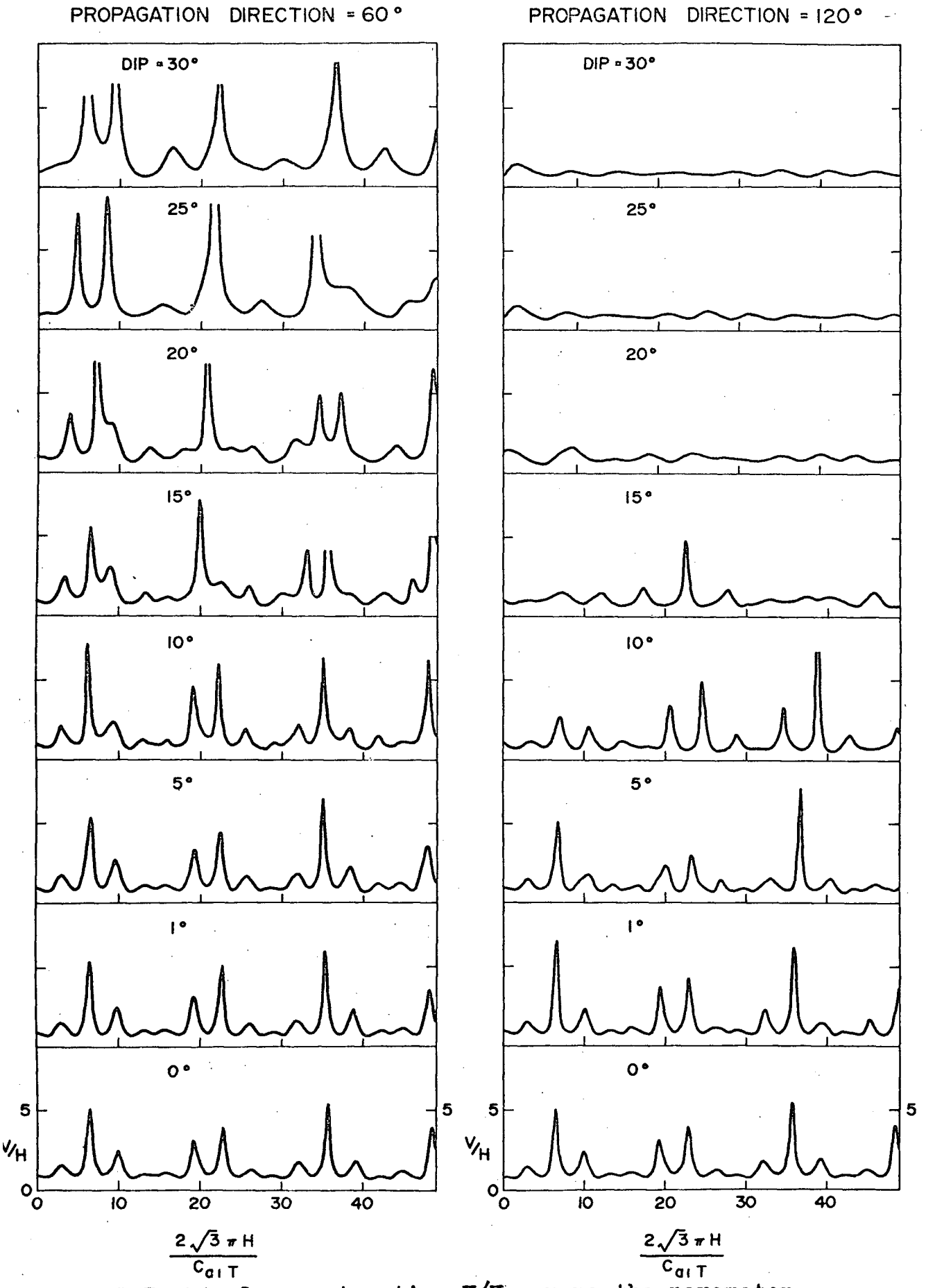

Fig. 3-7. Displacement ratios V/H versus the parameter $\sigma = 2\sqrt{3}\pi H/C_{a1}T$ for incident P waves with propagation directions $\alpha = 60°$ and $\alpha = 120°$ for the range of dip angles $5° \leqq \theta_d \leqq 30°$.

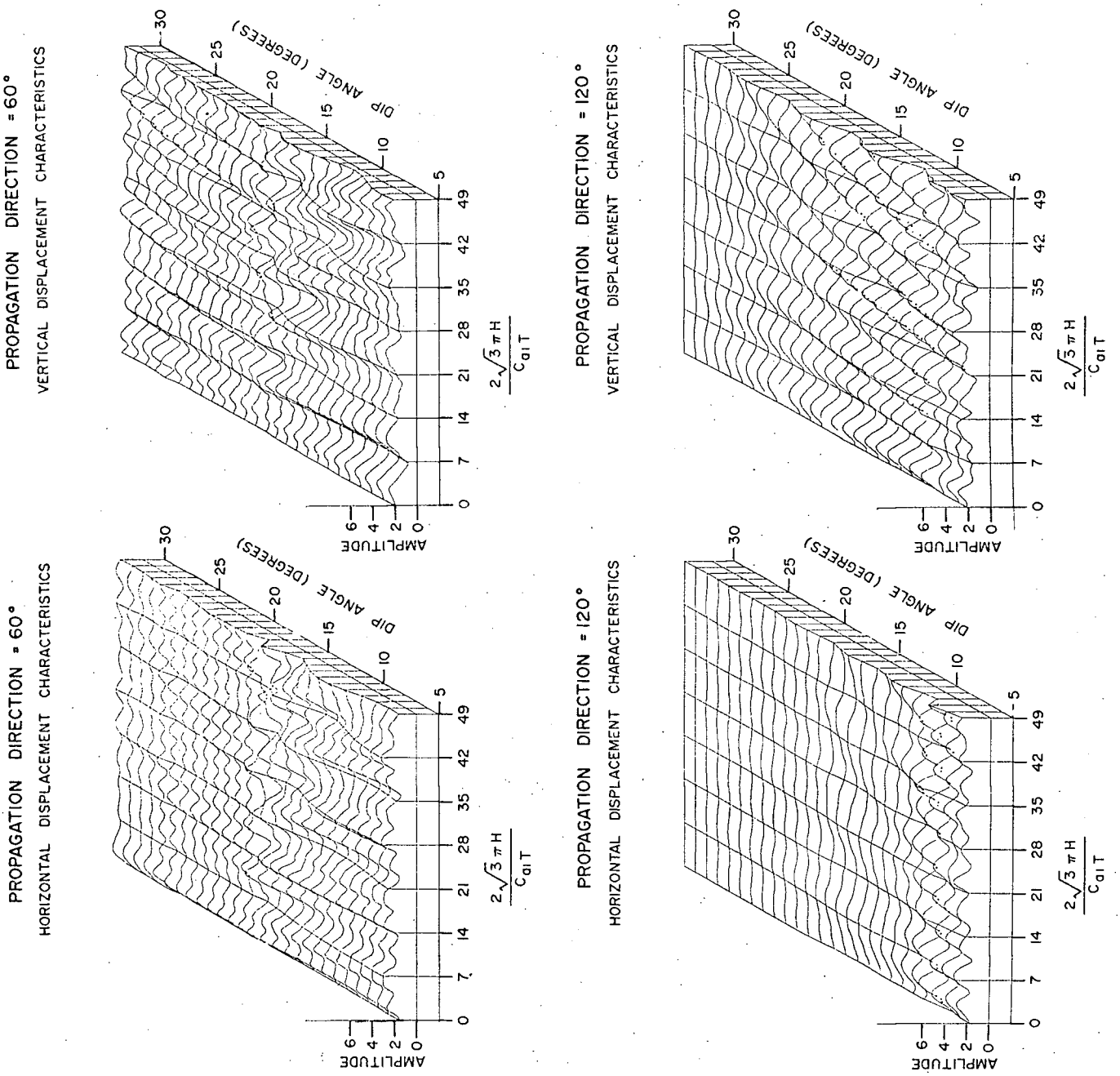

Fig. 3-8. Horizontal and vertical displacements versus the parameter $\delta = 2\sqrt{3}\pi H/C_{a1}T$ for incident SV waves with propagation directions $\beta = 60°$ and $\beta = 120°$ for the range of dip angles $5° \leqq \theta_d \leqq 30°$.

significant. For β = 120° the horizontal displacement oscillations become very small for dip angles greater than 10° while the vertical displacement oscillations more slowly decrease in amplitude with increasing dip angle and at the same time the period of the variation lengthens.

The above features are most evident in the displacement ratio curves H/V (Figure 3-9). For even small dip angles marked differences from the horizontally layered curves are evident. At the larger dip angles for propagation direction β = 60° we see the rapid oscillations due to the horizontal component and for β=120° the ratio becomes featureless.

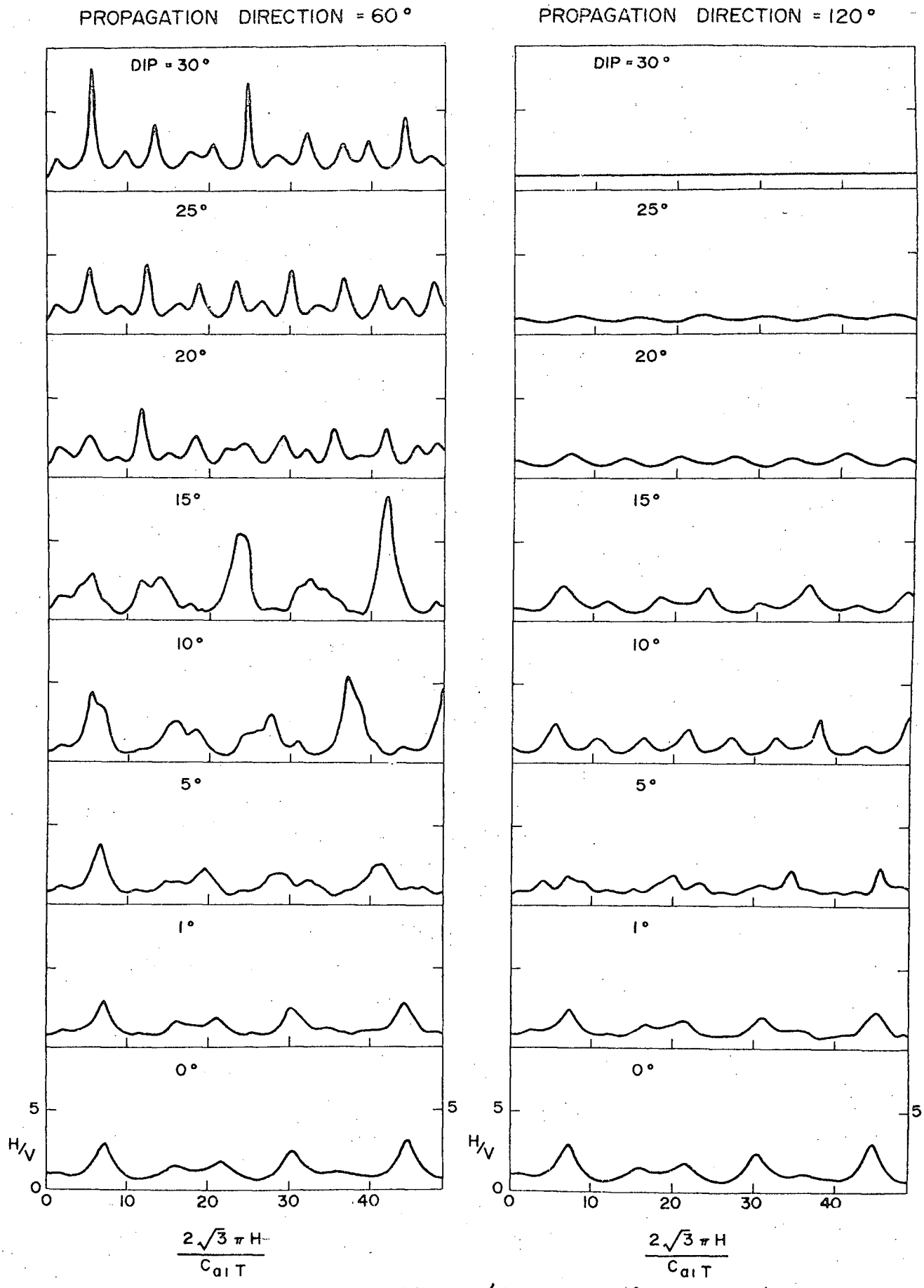

Fig. 3-9. Displacement ratios H/V versus the parameter $\delta = 2\sqrt{3}\pi\upsilon H/C_{a1}T$ for incident SV waves with propagation directions $\beta = 60°$ and $\beta = 120°$ for the range of dip angles $5° \leqq \theta_d \leqq 30°$.

CHAPTER 4

HEAD AND REFLECTED WAVES FROM AN SH LINE SOURCE IN A DIPPING LAYER OVERLYING AN ELASTIC MEDIUM

4.1 Introduction

A number of workers (e.g., Lapwood (1961), Hudson (1963), and Hudson and Knopoff (1964)) have investigated the propagation of surface and diffracted waves in wedge-shaped media. Hudson (1963) pointed out that the solution in the case of a rigid lower boundary could be divided into two parts - the multiply reflected and diffracted wave solutions. However, the early part of the seismogram consisting of head and multiply reflected waves which are often used in interpretation has not been well studied for a dipping layer overlying an elastic medium. In the present chapter the author will establish one method of solution and will theoretically investigate the problem for an SH line source in an elastic wedge overlying an elastic medium.

In Chapter 2, a solution for the problem of multiple reflection of plane SH waves by a dipping layer has been found. By integration of a solution of this type, the disturbance due to a line source is sought which does not include the diffracted wave term. However, for a transient input, an observation point distant from the vertex receives the reflected and refracted waves earlier than the diffracted

waves which result from collisions with the vertex. Therefore the present solution should apply to the composition of the initial section of the seismogram. The formal solution is evaluated by the steepest descent technique as recommended by Honda and Nakamura (1954) for evaluation of branch line integrals and as applied by Emura (1960) and others. In this way the wave forms and the ranges of existence of the head waves are determined for various dip angles for comparison with the case of a horizontal layer. For all computations the following elastic parameters corresponding to those of Haskell (1960) are used in the S wave velocity in the upper layer C_{b1} = 3.64 km/sec, the velocity ratio $\Delta = C_{b2}/C_{b1} = 1.27$, and the rigidity ratio $\delta = \mu_2/\mu_1 = 1.88$.

As surface waves are obtained from the contributions of poles, the surface wave problem reduces to finding poles of the finite series expression of our solution. Further, the discontinuities in displacement associated with the diffracted waves have been found and hence this problem is separated from the determination of the solution due to other waves. The solution of the present problem is therefore an important step for the consideration of surface and diffracted waves.

4.2 Equation of Motion and Boundary Conditions

The propagation of SH waves through a system con-

sisting of an elastic medium of rigidity μ_1 , density ρ_1 , and a dip angle $\theta_1+\theta_2$, overlying an elastic medium of rigidity μ_2 and density ρ_2 (Figure 4-1) will be considered. The free surface is $\theta=-\theta_1$ and the boundary between the elastic media is $\theta=\theta_2$. A cartesian system (x , y , z) is related to the cylindrical coordinates (r , θ , z) by the standard relationships $x=r\cos\theta$, $y=r\sin\theta$, and $z=z$. The motion is generated by a line source (S) of SH waves located at (d , 0) in the cylindrical coordinate system.

For the above problem, the motion is independent of z , and the displacement has only a z-component. Then, assuming a time variation of the form $e^{i\omega t}$, the equation of motion

$$\nabla^2 u_i = \frac{1}{c_{bi}^2}\frac{\partial^2 u_i}{\partial t^2} \qquad i=1,2 \tag{4.1}$$

becomes in cylindrical coordinates

$$\left(\frac{\partial^2}{\partial r^2}+\frac{1}{r}\frac{\partial}{\partial r}+\frac{1}{r^2}\frac{\partial^2}{\partial\theta^2}+k_{bi}^2\right)u_i=0 \qquad i=1,2 \tag{4.2}$$

where $c_{bi}=\sqrt{\mu_i/\rho_i}$ is the velocity of the S waves and $k_{bi}=\omega/c_{bi}$.

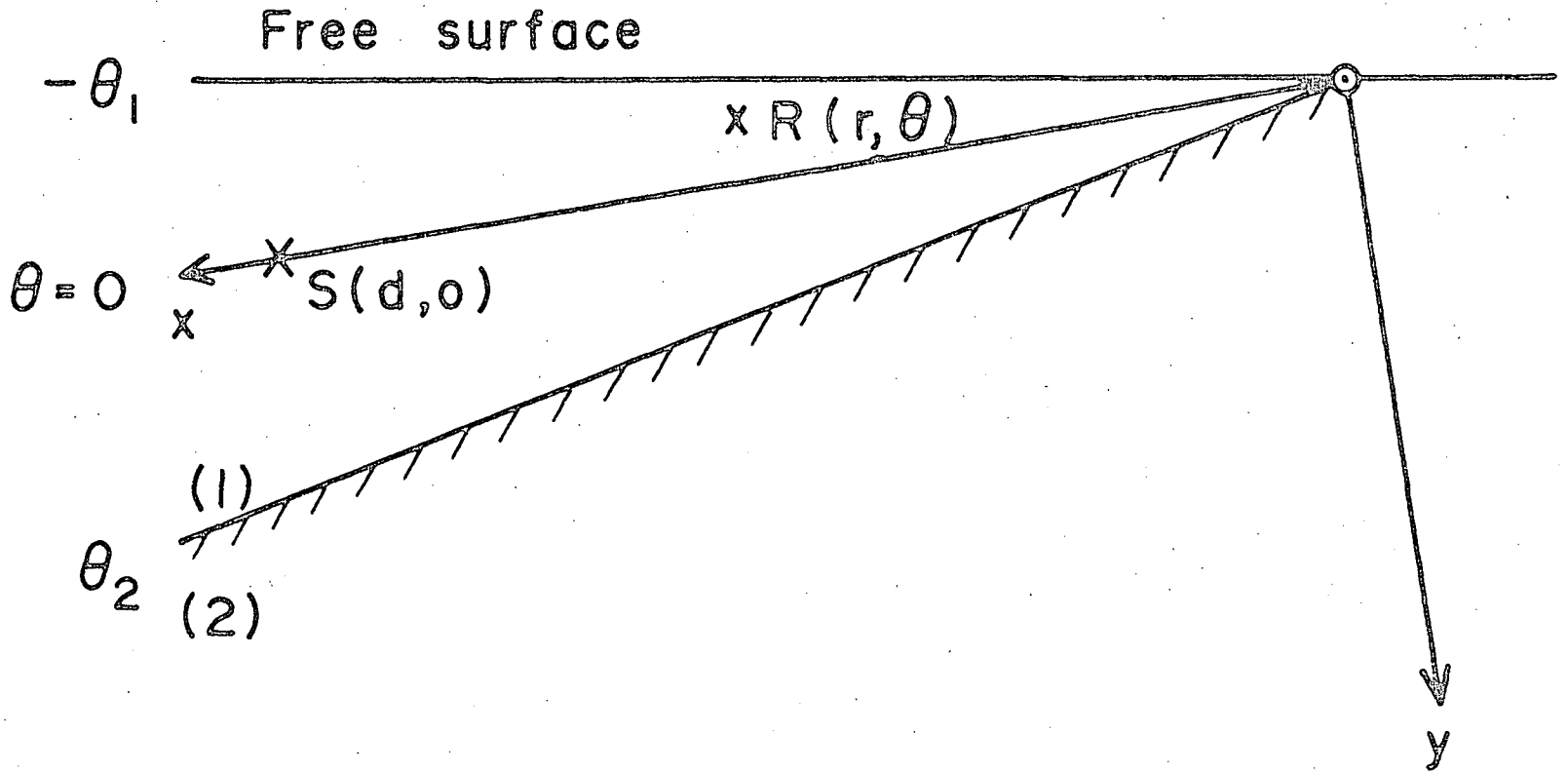

Fig. 4-1. Geometry of the problem: the line source (S) is located at (d,0) the receiver (R) at (r,θ) in the wedge bounded by the free surface $(\theta=-\theta_1)$ and the boundary $(\theta=\theta_2)$ between the two media.

The only non-zero component of stress is

$$(P_{z\theta})_i = \mu_i \frac{\partial u_i}{\partial \theta} \tag{4.3}$$

The boundary conditions then become

$$(P_{z\theta})_1 = 0 \qquad \text{at} \quad \theta = -\theta_1 \tag{4.4}$$

and

$$\begin{aligned} u_1 &= u_2 \\ (P_{z\theta})_1 &= (P_{z\theta})_2 \end{aligned} \qquad \text{at} \quad \theta = \theta_2 \tag{4.5}$$

To solve the line source problem, a plane wave solution satisfying the boundary conditions will first be obtained. The line source solution can then be obtained by integration of this solution with respect to the cylindrical angle.

4.3 Steady State Plane Wave Solution

The initial displacement due to a plane wave is expressed in the form

$$\begin{aligned} u_o' &= A_i \cdot e^{-ik_{b1}\{(d-x)\cos\alpha_i + |y|\sin\alpha_i\}} \\ &= A_i \cdot e^{ik_{b1} r\cos(\alpha_i + |\theta|) - ik_{b1} d\cos\alpha_i} \end{aligned} \tag{4.6}$$

where α_i is the angle between the x-axis and wave normal of the SH waves and may take on complex values in the evaluation of the effect due to a line source. For $\theta>0$, u_0' represents waves downgoing from the x-axis, while for $\theta<0$, u_0' represents waves upgoing from the x-axis. In those cases where the waves interact with the boundaries, the former collides with the dipping boundary first and the latter with the free surface first. In Chapter 2, the reflection and refraction of SH waves in a dipping layer has been investigated in detail. The solution by multiple reflection is obtained in the same manner.

For any observation point in the wedge, four expressions are required to express the motion depending on whether the initial direction of the wave is positive or negative and whether the final reflection is from the boundary (1) or the free surface (2). Using the same procedure as the derivation of (2.18) and (2.19), these expressions are

$$S_1^+(N)=A_i\sum_{n=1}^{N}\left(\prod_{k=1}^{n}A_k^+\right)e^{ik_{b1}r\cos(\alpha_i+2(n-1)\theta_1+2n\theta_2-\theta)-ik_{b1}d\cos\alpha_i} \tag{4.7}$$

$$S_2^+(N)=A_i\sum_{n=1}^{N}\left(\prod_{k=1}^{n}A_k^+\right)e^{ik_{b1}r\cos(\alpha_i+2n\theta_1+2n\theta_2+\theta)-ik_{b1}d\cos\alpha_i} \tag{4.8}$$

$$S_1^-(N')=A_i\sum_{n=1}^{N'}\left(\prod_{k=1}^{n}A_k^-\right)e^{ik_{b1}r\cos(\alpha_i+2n\theta_1+2n\theta_2-\theta)-ik_{b1}d\cos\alpha_i} \tag{4.9}$$

$$S_2^-(N')=A_i\sum_{n=1}^{N'}\left(\prod_{k=1}^{n}A_k^-\right)e^{ik_{b1}r\cos(\alpha_i+2(n+1)\theta_1+2n\theta_2+\theta)-ik_{b1}d\cos\alpha_i} \tag{4.10}$$

where the maximum numbers of reflections from the boundary N and N' are seen by examination of the phase in (4.7) to (4.10) to be determined by

$$\pi+\theta_2 \geqq 2(N-1)\theta_1+2N\theta_2 \geqq \pi-\theta_1 \tag{4.11}$$

or

$$\pi+\theta_1 \geqq 2N\theta_1+2N\theta_2 \geqq \pi-\theta_2 \tag{4.12}$$

and N' by

$$\pi+\theta_2 \geqq 2N'\theta_1+2N'\theta_2 \geqq \pi-\theta_1 \tag{4.13}$$

or

$$\pi+\theta_1 \geqq 2(N'+1)\theta_1+2N'\theta_2 \geqq \pi-\theta_2 \tag{4.14}$$

The expressions for the direct wave and the wave once reflected from the free surface are from (4.6)

$$S_o = A_i e^{ik_{b1}r\cos(\alpha_i+|\theta|)-ik_{b1}d\cos\alpha_i} \tag{4.15}$$

and

$$S_o^- = A_i e^{ik_{b1}r\cos(\alpha_i+2\theta_1+\theta)-ik_{b1}\cos\alpha_i} \tag{4.16}$$

The reflection coefficients for a wave which started as a downgoing wave with respect to the x-axis are similar to expression (2.20); namely

$$A_k^+ = \frac{\Delta \sin\{\theta_2 + 2(k-1)(\theta_1+\theta_2)+\alpha_i\} - \delta\sqrt{1-\Delta^2\cos^2\{\theta_2+2(k-1)(\theta_1+\theta_2)+\alpha_i\}}}{\Delta \sin\{\theta_2 + 2(k-1)(\theta_1+\theta_2)+\alpha_i\} + \delta\sqrt{1-\Delta^2\cos^2\{\theta_2+2(k-1)(\theta_1+\theta_2)+\alpha_i\}}} \tag{4.17}$$

and for a wave which started as an upgoing wave with respect to the x-axis is

$$A_k^- = \frac{\Delta \sin\{\theta_2 + 2k\theta_1 + 2(k-1)\theta_2+\alpha_i\} - \delta\sqrt{1-\Delta^2\cos^2\{\theta_2+2k\theta_1+2(k-1)\theta_2+\alpha_i\}}}{\Delta \sin\{\theta_2 + 2k\theta_1 + 2(k-1)\theta_2+\alpha_i\} + \delta\sqrt{1-\Delta^2\cos^2\{\theta_2+2k\theta_1+2(k-1)\theta_2+\alpha_i\}}} \tag{4.18}$$

Δ and δ are defined by $\Delta = C_{b2}/C_{b1}$ and $\delta = \mu_2/\mu_1$.

The solution u_1' on and close to the surface due to the initial disturbance and satisfying the boundary conditions (4.4) and (4.5) is, (using the same method as for the derivation of 2.25 and 2.26)

$$u_1' = S_0 + S_0^- + S_1^+(N-1) + S_2^+(N-1) + S_1^-(N'-1) + S_2^-(N'-1) \tag{4.19}$$

for conditions (4.11) and (4.13)

$$u_1' = S_0 + S_0^- + S_1^+(N-1) + S_2^+(N-1) + S_1^-(N') + S_2^-(N') \tag{4.20}$$

for conditions (4.11) and (4.14)

$$u_1' = S_0 + S_0^- + S_1^+(N) + S_2^+(N) + S_1^-(N'-1) + S_2^-(N'-1) \tag{4.21}$$

for conditions (4.12) and (4.13)

$$u_1' = S_0 + S_0^- + S_1^+(N) + S_2^+(N) + S_1^-(N') + S_2^-(N') \tag{4.22}$$

for conditions (4.12) and (4.14). It should be pointed out that these formal solutions are not a physical solution for an incident plane wave of a particular real angle. α_i but are the plane wave forms satisfying the boundary conditions from which the line source solution will be obtained.

The last terms of the series expressions (4.7)-(4.10) give rise to discontinuities in displacement and stress which serve as boundary conditions for the diffracted waves. These will be investigated in detail in a later section. Neglecting these last terms of the series,

$$u_1' = S_0 + S_0^- + S_1^+(N-1) + S_2^+(N-1) + S_1^-(N'-1) + S_2^-(N'-1)$$

is valid everywhere in medium 1.

For evaluation of the displacement due to a line source, it is convenient to express formulae (4.7)-(4.10) and (4.15) and (4.16) as

$$S_1^+(N) = A_i \sum_{n=1}^{N} \left(\prod_{k=1}^{n} A_k^+ \right) e^{-ik_{b1} R_{n1}^+ \cos(\alpha_i - \theta_{n1}^+)} \tag{4.23}$$

$$S_2^+(N) = A_i \sum_{n=1}^{N} \left(\prod_{k=1}^{n} A_k^+ \right) e^{-ik_{b1} R_{n2}^+ \cos(\alpha_i - \theta_{n2}^+)} \tag{4.24}$$

$$S_1^-(N') = A_i \sum_{n=1}^{N'} \left(\prod_{k=1}^{n} A_k^- \right) e^{-ik_{b1} R_{n1}^- \cos(\alpha_i - \theta_{n1}^-)} \tag{4.25}$$

$$S_2^-(N') = A_i \sum_{n=1}^{N'} \left(\prod_{k=1}^{n} A_k^- \right) e^{-ik_{b1} R_{n2}^- \cos(\alpha_i - \theta_{n2}^-)} \tag{4.26}$$

$$S_o = A_i e^{-ik_{b1} R_o \cos(\alpha_i - \theta_o)} \tag{4.27}$$

$$S_o^- = A_i e^{-ik_{b1} R_o^- \cos(\alpha_i - \theta_o^-)} \tag{4.28}$$

where

$$R_{n1}^+ = \sqrt{\{d - r\cos(2(n-1)\theta_1 + 2n\theta_2 - \theta)\}^2 + r^2 \sin^2(2(n-1)\theta_1 + 2n\theta_2 - \theta)}$$

$$\tan\theta_{n1}^+ = r\sin(2(n-1)\theta_1 + 2n\theta_2 - \theta) / \{d - r\cos(2(n-1)\theta_1 + 2n\theta_2 - \theta)\} \tag{4.29}$$

$$R^{+}_{n2} = \sqrt{\{d - r\cos(2n\theta_1 + 2n\theta_2 + \theta)\}^2 + r^2\sin^2(2n\theta_1 + 2n\theta_2 + \theta)}$$

$$\tan\theta^{+}_{n2} = r\sin(2n\theta_1 + 2n\theta_2 + \theta) / \{d - r\cos(2n\theta_1 + 2n\theta_2 + \theta)\} \quad (4.30)$$

$$R^{-}_{n1} = \sqrt{\{d - r\cos(2n\theta_1 + 2n\theta_2 - \theta)\}^2 + r^2\sin^2(2n\theta_1 + 2n\theta_2 - \theta)}$$

$$\tan\theta^{-}_{n1} = r\sin(2n\theta_1 + 2n\theta_2 - \theta) / \{d - r\cos(2n\theta_1 + 2n\theta_2 - \theta)\} \quad (4.31)$$

$$R^{-}_{n2} = \sqrt{\{d - r\cos(2(n+1)\theta_1 + 2n\theta_2 + \theta)\}^2 + r^2\sin^2(2(n+1)\theta_1 + 2n\theta_2 + \theta)}$$

$$\tan\theta^{-}_{n2} = r\sin(2(n+1)\theta_1 + 2n\theta_2 + \theta) / \{d - r\cos(2(n+1)\theta_1 + 2n\theta_2 + \theta)\} \quad (4.32)$$

$$R_o = \sqrt{\{d - r\cos|\theta|\}^2 + r^2\sin^2|\theta|}$$

$$\tan\theta_o = r\sin|\theta| / \{d - r\cos|\theta|\} \quad (4.33)$$

$$R^{-}_{o} = \sqrt{\{d - r\cos(2\theta_1 + \theta)\}^2 + r^2\sin^2(2\theta_1 + \theta)}$$

$$\tan\theta^{-}_{o} = r\sin(2\theta_1 + \theta) / \{d - r\cos(2\theta_1 + \theta)\} \quad (4.34)$$

4.4 Formal Steady State Solution for a Line Source

In order to generalize the results to the case of a line source, the operator

$$k_{b1}\int_{-i\infty}^{\pi+i\infty} \; d\alpha_i \tag{4.35}$$

is applied to the plane wave solution. In particular, the displacement u_0 due to the initial disturbance can be written using (4.6) as

$$\begin{aligned} u_0 &= k_{b1}\int_{-i\infty}^{\pi+i\infty} u_0' \, d\alpha_i \\ &= A_i k_{b1}\int_{-i\infty}^{\pi+i\infty} e^{-ik_{b1}\{(d-x)\cos\alpha_i + |y|\sin\alpha_i\}} \, d\alpha_i \\ &= A_i k_{b1}\pi H_0^{(2)}(k_{b1}R_0) \end{aligned} \tag{4.36}$$

Equation (4.36) can easily be derived from the results of Nakamura (1960). When $k_{b1}R_0$ is large, (4.36) can be approximated by the asymptotic formula,

$$u_0 = A_i\sqrt{\frac{2\pi k_{b1}}{R_0}}\, e^{-ik_{b1}R_0+\frac{\pi}{4}i} \tag{4.37}$$

which are the outgoing waves from the line source.

Using (4.19) to (4.22) and (4.23) to (4.28), the solution in the wedge corresponding to a line source (4.36) can be obtained as

$$u_1 = k_{b1} \int_{-i\infty}^{\pi+i\infty} u_1' \, d\alpha_i \tag{4.38}$$

4.5 Evaluation of the First Series Term of the Integral

In this section the integration of the terms which are produced by waves which are reflected once by the boundary between the media are evaluated. (As a guide to the evaluation of the higher order series terms, the contributions due to waves twice reflected from the boundary between the media are calculated in the Appendix III.) From (4.23)-(4.26) and (4.38), we see that they have the following forms:

$$I_{1\ell}^{m} = k_{b1} \int_{-i\infty}^{\pi+i\infty} A_1^m \cdot e^{-ik_{b1}R_{1\ell}^m \cos(\alpha_i - \theta_{1\ell}^m)} \, d\alpha_i \tag{4.39}$$

where

$$A_1^m = \frac{\Delta \sin(\phi_1^m + \alpha_i) - \delta\sqrt{1-\Delta^2\cos^2(\phi_1^m+\alpha_i)}}{\Delta \sin(\phi_1^m + \alpha_i) + \delta\sqrt{1-\Delta^2\cos^2(\phi_1^m+\alpha_i)}} \tag{4.40}$$

and $\ell = 1, 2$ and $m = +, -$. From the euqations (4.17) and (4.18), $\phi_1^+ = \theta_2$ and $\phi_1^- = 2\theta_1 + \theta_2$ and $R_{1\ell}^m$ and $\theta_{1\ell}^m$ are given by the equations (4.29) to (4.32).

For this integration, the original path L is taken in the plane for which $Re(\lambda_s) > 0$. The integrand of (4.39) contains the two-valued function $\lambda_s = \sqrt{1 - \Delta^2 \cos^2(\phi_1^m + \alpha_i)}$ and its branch points are given by the relation $\cos(\phi_1^m + \alpha_i) = \pm \frac{1}{\Delta}$ and are therefore located on the real axis of the α_i -plane at the points $B(\theta_B = \theta_0 - \phi_1^m), B'(\theta_{B'} = \pi - \theta_0 - \phi_1^m), \cdots$ (Figure 4-2) where $\cos\theta_0 = \frac{1}{\Delta} = n$, the refractive index. To facilitate evaluation, it is assumed that the medium is very slightly absorptive by setting $n = n_0 - i\varepsilon$ where ε is a very small positive quantity. (This assumption does not affect the final results which correspond to $\varepsilon \to 0$ but is only a technique to facilitate evaluation of the integrals.) The branch point B is then displaced by $\varepsilon / \sqrt{1 - n_0^2}$ parallel to the positive imaginary axis on the α_i-plane.

We choose the branch cut given by $Re(\lambda_s) = 0$ which is defined by:

$$\cos(x + \phi_1^m)\sin(x + \phi_1^m)\cosh y \sinh y = n_0 \varepsilon$$
$$\cos^2(x + \phi_1^m)\cosh^2 y - \sin^2(x + \phi_1^m)\sinh^2 y > n_0^2 \qquad (4.41)$$
$$\alpha_i = x + iy$$

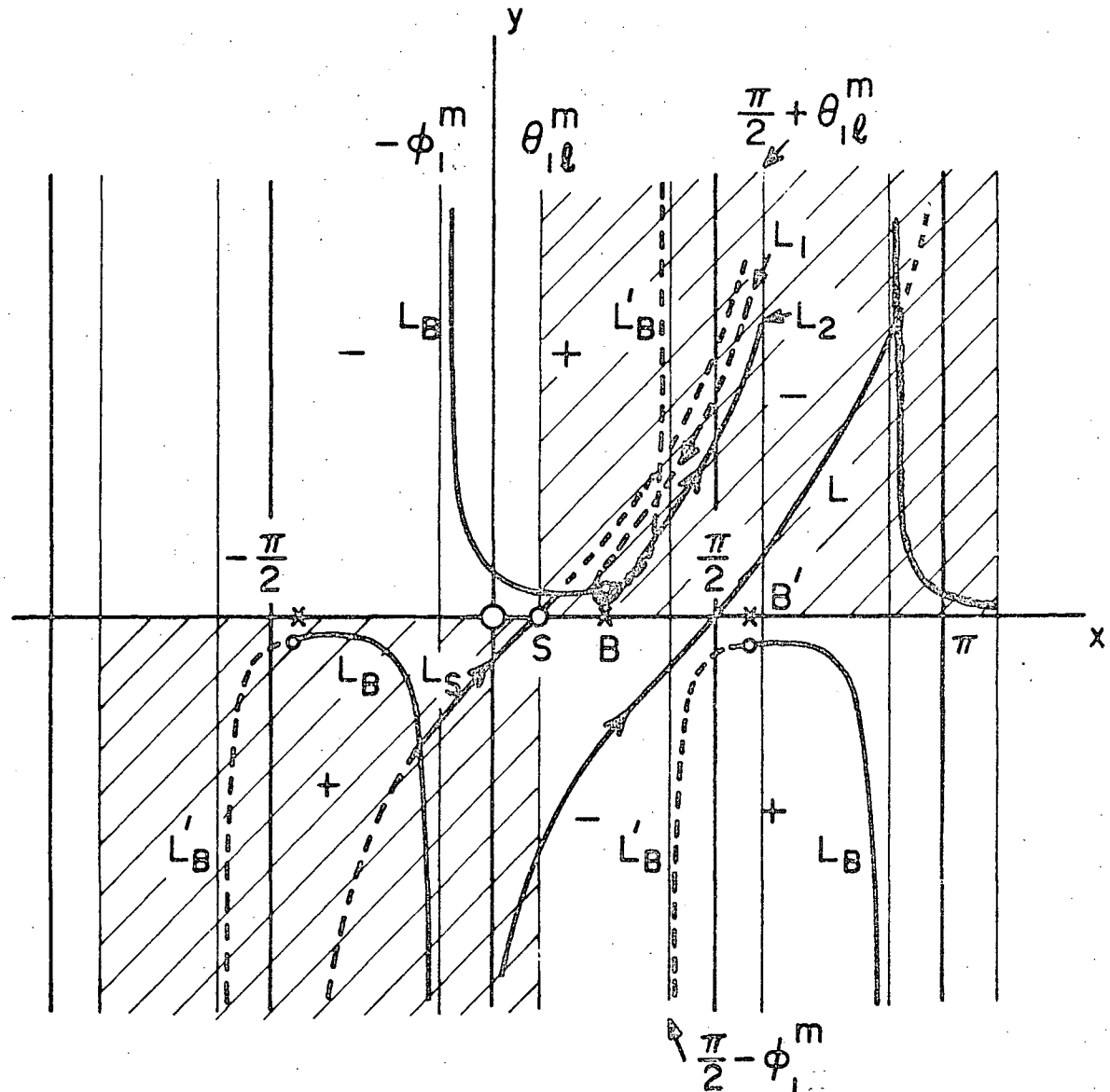

Fig. 4-2. The α -plane ($\alpha = x+iy$) on which $Re(\lambda_S)>0$ and the regions of positive and negative $Im(\lambda_S)$, separated by the curves L_B and L'_B, indicated. Notation: S-saddle-point; B,B′ - branch points; L - original path of integration; L_S- path of steepest descent through the saddle point; L_1,L_2- paths of branch line integral; L_B- branch cut $Re(\lambda_S)=0$; and L'_B - curve along which $Im(\lambda_S)=0$.

In Figure 4-2, L_B is $Re(\lambda_S)=0$, L'_B is $Im(\lambda_S)=0$ and the signs of $Im(\lambda_S)$ in the α_i-plane are indicated by plus and minus. When for large distances from the origin, $e^{-ik_{b1}R^m_{1\ell}\cos(\alpha_i-\theta^m_{1\ell})}$ vanishes along the path L, the path of integration can therefore be shifted on the Riemann surfaces. The region where $Im[\cos(\alpha_i-\theta^m_{1\ell})]<0$ or $e^{-ik_{b1}R^m_{1\ell}\cos(\alpha_i-\theta^m_{1\ell})}$ vanishes at a large distance from the origin is shown by hatching. The original path L, along which the relations $Im(\sin\alpha_i)<0$ and $Im(\lambda_S)<0$ hold, can be replaced by L_S and (L_1, L_2), where L_S passes through the saddle point S and (L_1, L_2) goes around the branch point B. The dotted lines denote that they are on the second Riemann sheet where $Re(\lambda_S)<0$. Each of them is drawn along the path of steepest descent,

$$\cos(x-\theta^m_{1\ell})\cosh y = 1 \tag{4.42}$$

and

$$\cos(x-\theta^m_{1\ell})\cosh y = \cos(\theta_B-\theta^m_{1\ell}) \tag{4.43}$$

respectively.

4.5.1 Contribution from the Saddle Point (Reflected Waves)

From (4.42), L_S makes an angle $\frac{\pi}{4}$ with the x-axis. In the neighbourhood of the saddle point the

following approximations are valid:

$$\alpha_i - \theta_{1\ell}^m = \rho\, e^{i\frac{\pi}{4}} \tag{4.44}$$

and

$$\cos(\alpha_i - \theta_{1\ell}^m) = 1 - i\rho^2/2 \tag{4.45}$$

The contour integral along L_S for (4.39) is then

$$u_S = A_i k_{b1} \int_{-\infty}^{\infty} A_1^m(\alpha_i)\, e^{\frac{\pi}{4}i - ik_{b1}R_{1\ell}^m - \frac{1}{2}k_{b1}R_{1\ell}^m \rho^2}\, d\rho \tag{4.46}$$

Expanding the term $A_1^m(\alpha_i)$ near the saddle point and using Watson's lemma (Jeffreys, 1956) we obtain

$$u_S = A_i \sqrt{\frac{2\pi k_{b1}}{R_{1\ell}^m}}\, A_1^m(\theta_{1\ell}^m)\, e^{-ik_{b1}R_{1\ell}^m + \frac{\pi}{4}i} \tag{4.47}$$

where, if $\theta_{1\ell}^m > \theta_B$,

$$A_1^m(\theta_{1\ell}^m) = \frac{\sin(\phi_1^m + \theta_{1\ell}^m) - \delta\sqrt{1/\Delta^2 - \cos^2(\phi_1^m + \theta_{1\ell}^m)}}{\sin(\phi_1^m + \theta_{1\ell}^m) + \delta\sqrt{1/\Delta^2 - \cos^2(\phi_1^m + \theta_{1\ell}^m)}} \tag{4.48}$$

and, if $\theta_{1\ell}^m < \theta_B$

$$A_1^m(\theta_{1\ell}^m) = \frac{\sin(\phi_1^m + \theta_{1\ell}^m) + i\delta\sqrt{\cos^2(\phi_1^m + \theta_{1\ell}^m) - 1/\Delta^2}}{\sin(\phi_1^m + \theta_{1\ell}^m) - i\delta\sqrt{\cos^2(\phi_1^m + \theta_{1\ell}^m) - 1/\Delta^2}} = e^{2i\varphi} \tag{4.49}$$

where

$$\tan\varphi = \frac{\delta\sqrt{\cos^2(\phi_1^m + \theta_{1\ell}^m) - 1/\Delta^2}}{\sin(\phi_1^m + \theta_{1\ell}^m)}$$

4.5.2 Contribution from the Branch Point (Head Waves)

Next the contribution from the integral along $L_1 L_2$ is considered. L_1 and L_2 are taken along the path of steepest descent around B and tend to $\frac{\pi}{2} + \theta_{1\ell}^m + i\infty$. Setting $\gamma = \sin(\phi_1^m + \alpha_i)$, we have from (4.39),

$$u_{L_1 L_2} = k_{b1} A_i \times$$

$$\int_{L_2} \left\{ \frac{\gamma - \delta\sqrt{1/\Delta^2 - 1 + \gamma^2}}{\gamma + \delta\sqrt{1/\Delta^2 - 1 + \gamma^2}} - \frac{\gamma + \delta\sqrt{1/\Delta^2 - 1 + \gamma^2}}{\gamma - \delta\sqrt{1/\Delta^2 - 1 + \gamma^2}} \right\} e^{-ik_{b1} R_{1\ell}^m \cos(\alpha_i - \theta_{1\ell}^m)} d\alpha_i$$

$$= -4\delta k_{b1} A_i \int_{L_2} \frac{\gamma\sqrt{1/\Delta^2 - 1 + \gamma^2}}{\gamma^2(1-\delta^2) + \delta^2(1 - 1/\Delta^2)} e^{-ik_{b1} R_{1\ell}^m \cos(\alpha_i - \theta_{1\ell}^m)} d\alpha_i \qquad (4.50)$$

It should be noted that along L_2 near B that $\mathrm{Re}(\lambda_s) > 0$ and $\mathrm{Im}(\lambda_s) > 0$. (4.51)

From (4.43) along L_2 we can write

$$\cos(\alpha_i - \theta_{1\ell}^m) = \cos(\theta_B - \theta_{1\ell}^m) - i\tau \qquad \tau > 0 \qquad (4.52)$$

therefore

$$d\alpha_i = i\, d\tau / \sin(\alpha_i - \theta_{1\ell}^m) \qquad (4.53)$$

along L_2 near B . Putting $\alpha_i = \theta_B + u + iv$ (4.54)

for very small u and v , we have approximately

$$(u+iv)\sin(\theta_B - \theta_{1\ell}^m) = i\tau \tag{4.55}$$

On the other hand, along L_2 we have

$$\begin{aligned}\sin(\alpha_i + \phi_1^m) &= \sin(\theta_0 + u + iv) \\ &= \sqrt{1-1/\Delta^2} + \frac{1}{\Delta}(u+iv)\end{aligned} \tag{4.56}$$

and from (4.55)

$$\sin(\alpha_i + \phi_1^m) - \sqrt{1-1/\Delta^2} = \frac{i\tau}{\Delta \sin(\theta_B - \theta_{1\ell}^m)} \tag{4.57}$$

Hence, in the limit when

$$\sin(\alpha_i + \phi_1^m) \to \sqrt{1-1/\Delta^2}$$

along L_2 , we have using (4.51)

$$\sqrt{\sin^2(\alpha_i+\phi_1^m) + 1/\Delta^2 - 1} = \frac{\sqrt{2}\,(1-1/\Delta^2)^{1/4}}{\sqrt{\Delta}\cdot\sqrt{\sin(\theta_B - \theta_{1\ell}^m)}}\sqrt{\tau}\cdot e^{i\frac{\pi}{4}} \tag{4.58}$$

As

$$\int_0^\infty \sqrt{\tau}\cdot e^{-ik_{b1}R_{1\ell}^m \tau}\, d\tau = \frac{\sqrt{\pi}}{2}\,\frac{1}{(k_{b1}R_{1\ell}^m)^{3/2}} \tag{4.59}$$

we have

$$u_{L_1L_2} \approx -A_i \cdot \frac{2\sqrt{2\pi}\,\delta}{\sqrt{\Delta}} \cdot \frac{1}{(k_{b1})^{1/2}(R_{1\ell}^m)^{3/2}} \times$$

$$\frac{1}{(1-1/\Delta^2)^{1/4}\{\sin(\theta_B-\theta_{1\ell}^m)\}^{3/2}} \cdot e^{-ik_{b1}R_{1\ell}^m \cos(\theta_B-\theta_{1\ell}^m)+\frac{3}{4}\pi i} \tag{4.60}$$

4.6 Aperiodic Solution

For computation of synthetic seismograms, it is convenient to choose a displacement of the form

$$\phi(t) = -\frac{A}{t^2+c^2} \qquad A>0\ ,\ c>0$$

Performing the operation

$$\frac{1}{\pi}\,\mathrm{Re}\int_0^\infty d\omega \int_{-\infty}^{\infty} \phi(\sigma) e^{-i\omega\sigma}\, d\sigma$$

on (4.37), (4.47) and (4.60) we obtain the following solutions

(1) Direct Waves

$$\bar{u}_1 = -A_i \frac{\pi}{\sqrt{2C_{b1}R_0}} \cdot \frac{A}{c^{5/2}} \cdot \frac{1}{\left\{1+\left(\frac{t-t_D}{c}\right)^2\right\}^{3/4}} \times$$

$$\cos\left\{\frac{3}{2}\tan^{-1}\frac{t-t_D}{c}+\frac{\pi}{4}\right\} \tag{4.61}$$

where

$$t_D = R_o / C_{b1}$$

(2) Waves reflected once from the interface

$$\bar{u}_S = -A_i \frac{\pi}{\sqrt{2 C_{b1} R_{1\ell}^m}} \frac{A}{C^{5/2}} \frac{A_1^m(\theta_{1\ell}^m)}{\left\{1+\left(\frac{t - {}_R t_{1\ell}^m}{C}\right)^2\right\}^{3/4}} \times \cos\left\{\frac{3}{2}\tan^{-1}\frac{t - {}_R t_{1\ell}^m}{C} + \frac{\pi}{4}\right\} \qquad (4.62)$$

for $\theta_{1\ell}^m > \theta_B$

$$\bar{u}_S = -A_i \frac{\pi}{\sqrt{2 C_{b1} R_{1\ell}^m}} \frac{A}{C^{5/2}} \frac{1}{\left\{1+\left(\frac{t - {}_R t_{1\ell}^m}{C}\right)^2\right\}^{3/4}} \times \cos\left\{\frac{3}{2}\tan^{-1}\frac{t - {}_R t_{1\ell}^m}{C} + \frac{\pi}{4} + 2\varphi\right\} \qquad (4.63)$$

for $\theta_{1\ell}^m < \theta_B$, where ${}_R t_{1\ell}^m = R_{1\ell}^m / C_{b1}$.

(3) Head Waves

$$\bar{u}_{L_1 L_2} = A_i \frac{2\sqrt{2}\,\pi \cdot \delta}{\sqrt{\Delta}\,(1-1/\Delta^2)^{1/4}} \frac{\sqrt{C_{b1}}}{(R_{1\ell}^m)^{3/2}} \frac{1}{\{\sin(\theta_B - \theta_{1\ell}^m)\}^{3/2}} \times \frac{A}{C^{3/2}} \frac{1}{\left\{1+\left(\frac{t - {}_H t_{1\ell}^m}{C}\right)^2\right\}^{1/4}} \cos\left\{\frac{1}{2}\tan^{-1}\frac{t - {}_H t_{1\ell}^m}{C} + \frac{3}{4}\pi\right\} \qquad (4.64)$$

where ${}_H t_{1\ell}^m = \dfrac{R_{1\ell}^m \cos(\theta_B - \theta_{1\ell}^m)}{C_{b1}}$

4.7 Interpretation of the Travel Time

In a study of wave propagation from a point source in a horizontal layer, Honda and Nakamura (1954) evaluated the contributions from branch points and a saddle point and associated the time factors of these contributions with head waves and reflected waves. Similarly, in this section we will determine the reflected and head wave travel times and find that they are given by ${}_Rt_{1\ell}^m$ and ${}_Ht_{1\ell}^m$, the time factors of the saddle point and branch point contributions.

Consider first the path $\overline{SAR}$ in Figure 4-3. Then

$$t_{SAR} = \frac{\overline{SA} + \overline{AR}}{C_{b1}} = \frac{\overline{S'R}}{C_{b1}}$$

$$= \frac{\sqrt{\{d\cos\theta_2 - r\cos(\theta_2 - \theta)\}^2 + \{d\sin\theta_2 + r\sin(\theta_2 - \theta)\}^2}}{C_{b1}}$$

$$= \frac{\sqrt{\{d - r\cos(2\theta_2 - \theta)\}^2 + r^2\sin^2(2\theta_2 - \theta)}}{C_{b1}} = \frac{R_{11}^+}{C_{b1}} = {}_Rt_{11}^+ \tag{4.65}$$

Also, the travel time along the path $\overline{SBCR}$ is given by

$$t_{SBCR} = \frac{\overline{SB}}{C_{b1}} + \frac{\overline{BC}}{C_{b2}} + \frac{\overline{CR}}{C_{b1}}$$

$$= \frac{d\sin\theta_2}{C_{b1}\sin(\theta_B + \theta_2)} + \frac{1}{C_{b2}}\left\{d\cos\theta_2 - r\cos(\theta_2 - \theta) - \frac{d\sin\theta_2 + r\sin(\theta_2 - \theta)}{\tan(\theta_B + \theta_2)}\right\} + \frac{r\sin(\theta_2 - \theta)}{C_{b1}\sin(\theta_B + \theta_2)} \tag{4.66}$$

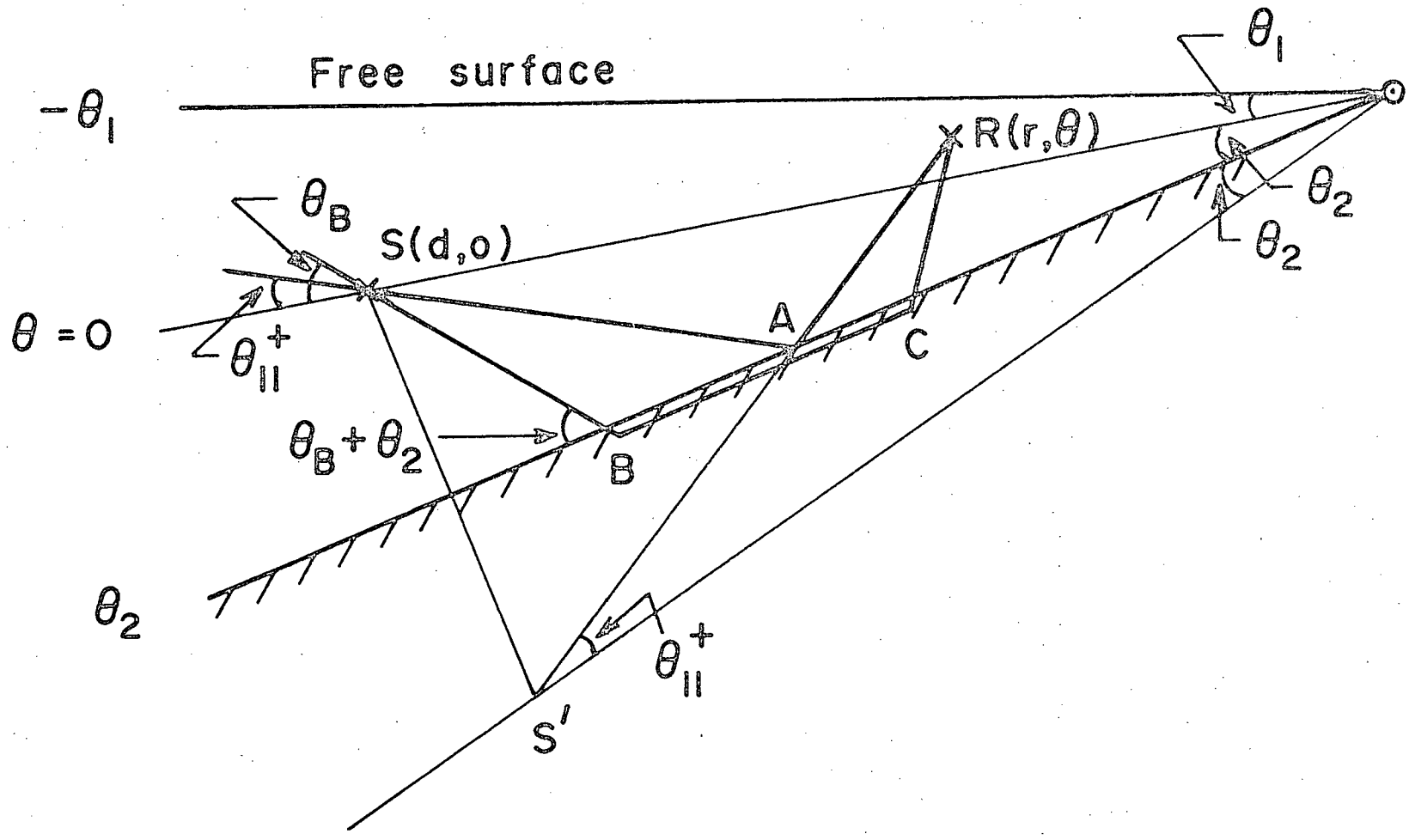

Fig. 4-3. Basic ray paths used in physical interpretation of contributions from branch and saddle points.

$$= \frac{1}{C_{b1}}\{(d\cos\theta_2 - r\cos(\theta_2-\theta))\cos(\theta_B+\theta_2) + (d\sin\theta_2 + r\sin(\theta_2-\theta))\sin(\theta_B+\theta_2)\} \quad (4.66)$$

$$= \frac{R_{11}^{+}}{C_{b1}}\cos(\theta_B - \theta_{11}^{+}) = {}_{H}t_{11}^{+}$$

since

$$\cos(\theta_B+\theta_2) = C_{b1}/C_{b2}$$

Hence we have verified the interpretation of ${}_{R}t_{1\ell}^{m}$ and ${}_{H}t_{1\ell}^{m}$ as the reflected and head wave respectively for $m=+$ and $\ell=1$. In a similar manner, ${}_{R}t_{1\ell}^{m}$ and ${}_{H}t_{1\ell}^{m}$ can be interpreted for different values of m and ℓ as shown in Figure 4-4. Obviously, for the observation point distant from the vertex, these waves arrive earlier than the diffracted waves which are produced by collisions of waves with the vertex. Hence this solution should adequately describe the early section of the seismogram.

4.8 Range of Existence of Head Waves

The range of existence of head waves can be determined by considering the process by which the integral (4.39) is evaluated. In Figure 4-2, when $\theta_B > \theta_{1\ell}^{m}$, we can form a closed contour which connects with the original path and which includes contributions of the saddle point and the branch point on application of Cauchy's theorem. On the other hand when $\theta_B < \theta_{1\ell}^{m}$, a closed contour cannot be

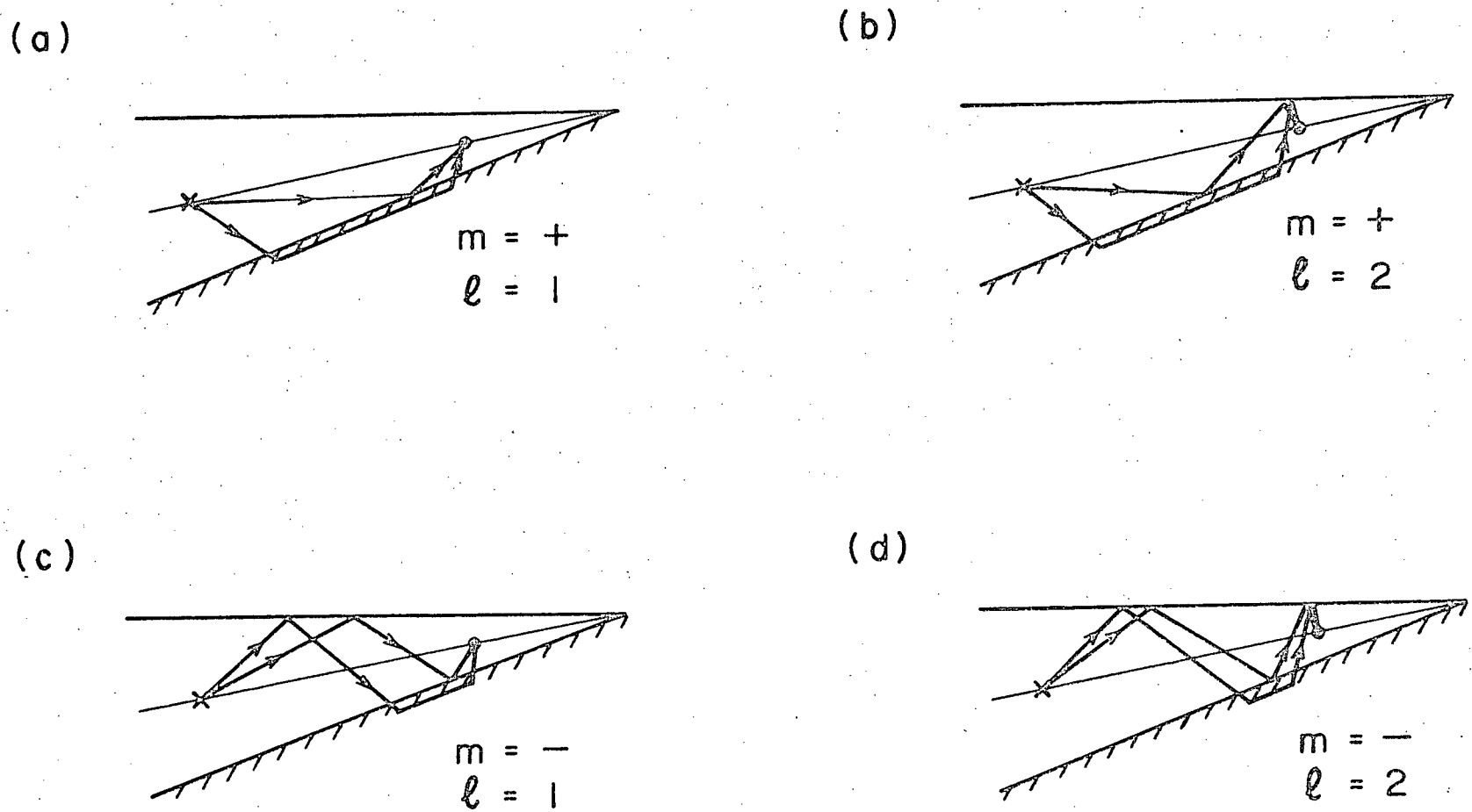

Fig. 4-4. Ray paths of the head and reflected waves expressed by the first series term of the integrals.

made without excluding the integral around the branch point. Therefore in the first case we have contributions from both the branch point (head waves) and saddle point (reflected waves) while in the second case there is only a saddle point contribution (reflected waves). It is clear that the critical condition to decide the existence of head waves is $\theta_B = \theta_{12}^m$. Obtaining θ_B and θ_{12}^m by the use of (4.17), (4.18) and (4.29), (4.30), (4.31), (4.32) respectively and using the critical condition we obtain the following transcendental equations:

$$\tan^{-1}\frac{r\sin(2\theta_2-\theta)}{d-r\cos(2\theta_2-\theta)} = \cos^{-1}\frac{1}{\Delta} - \theta_2 \qquad (4.67)$$

$$\tan^{-1}\frac{r\sin(2\theta_1+2\theta_2+\theta)}{d-r\cos(2\theta_1+2\theta_2+\theta)} = \cos^{-1}\frac{1}{\Delta} - \theta_2 \qquad (4.68)$$

$$\tan^{-1}\frac{r\sin(2\theta_1+2\theta_2-\theta)}{d-r\cos(2\theta_1+2\theta_2-\theta)} = \cos^{-1}\frac{1}{\Delta} - \theta_2 - 2\theta_1 \qquad (4.69)$$

$$\tan^{-1}\frac{r\sin(4\theta_1+2\theta_2+\theta)}{d-r\cos(4\theta_1+2\theta_2+\theta)} = \cos^{-1}\frac{1}{\Delta} - \theta_2 - 2\theta_1 \qquad (4.70)$$

In Figure 4-5, the range of existence of head waves whose paths are illustrated in Figure 4-4 is shown for $\theta_1 = 5^\circ$ and the observation point on the line $\theta = 0$. The abscissa is the ratio of source to observation point distances from the apex while the ordinate is the maximum θ_2 for which head waves exist. As expected from the small

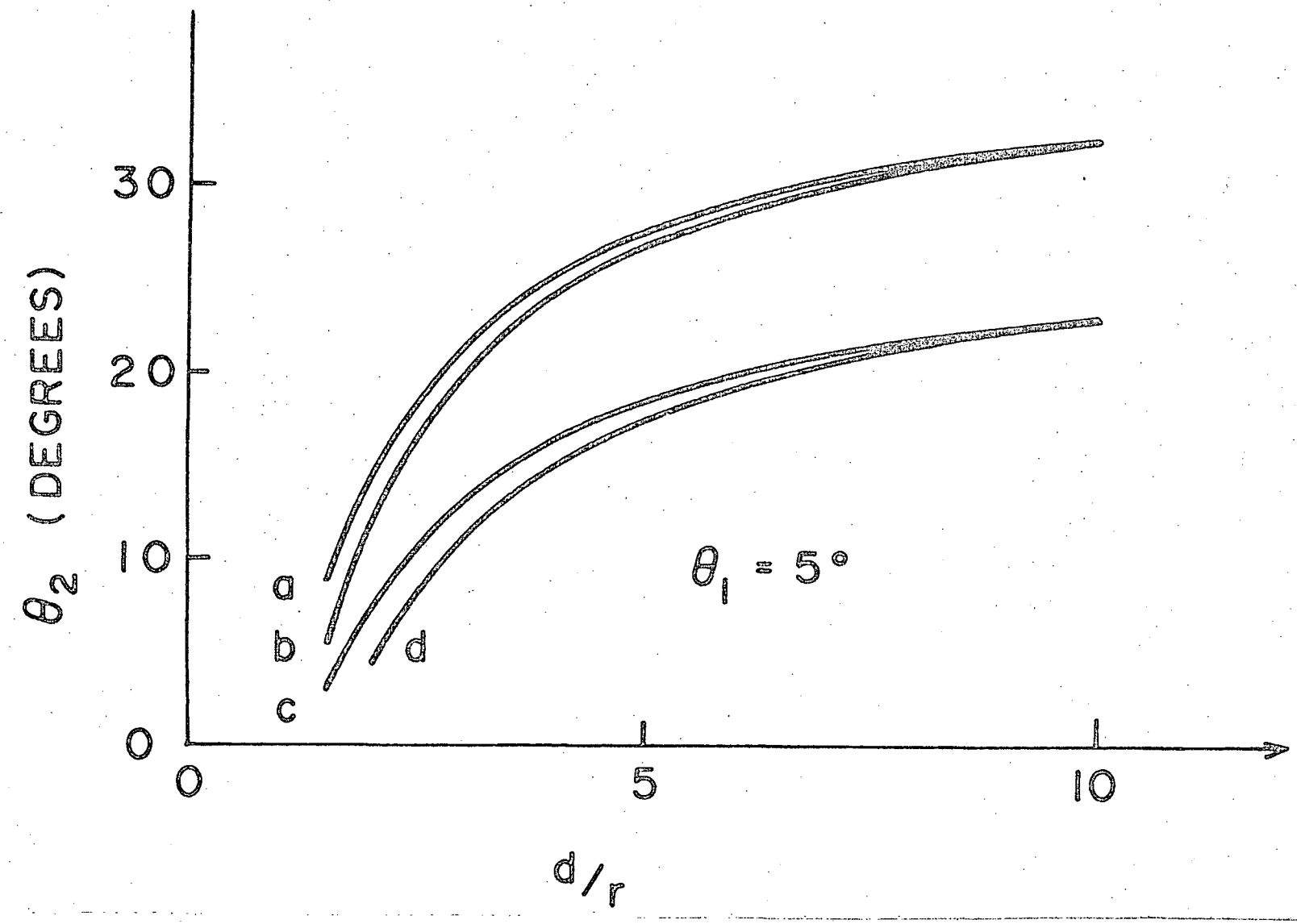

Fig. 4-5. Maximum value of θ_2 for which the head waves shown in Fig. 4-4. exist versus the ratio of source to observation distances. The observation and source points are 5° from the free surface.

path difference, the range of existence of (a) and (b) are close as are (c) and (d). The range of existence also decreases with increasing number of reflections and decreasing ratio d/r .

For an observation point at 5° from the free surface and a source-vertex to observation-vertex distance ratio of 10.0, Figure 4-6 shows the range of existence of head waves with changing θ_1 , which corresponds to a change of depth of the line source. It is noted that with increasing θ_1 , the dip angle for which the head waves (a) and (b) exist linearly increases while for head waves of type (c) and (d) it linearly decreases.

4.9 Discontinuities

Discontinuities in displacement and stress in medium (1) arise because the first collision of the wave with a boundary changes from the free surface to the boundary between the media as α_i passes through zero. This collision with the vertex results in a diffracted wave which is not considered in this solution. When both initially up-going and down-going waves and the interface of the last reflection are considered, we have four cases of the combination of the discontinuity as shown in Figure 4-7. The cross-hatched areas indicate the regions for which the

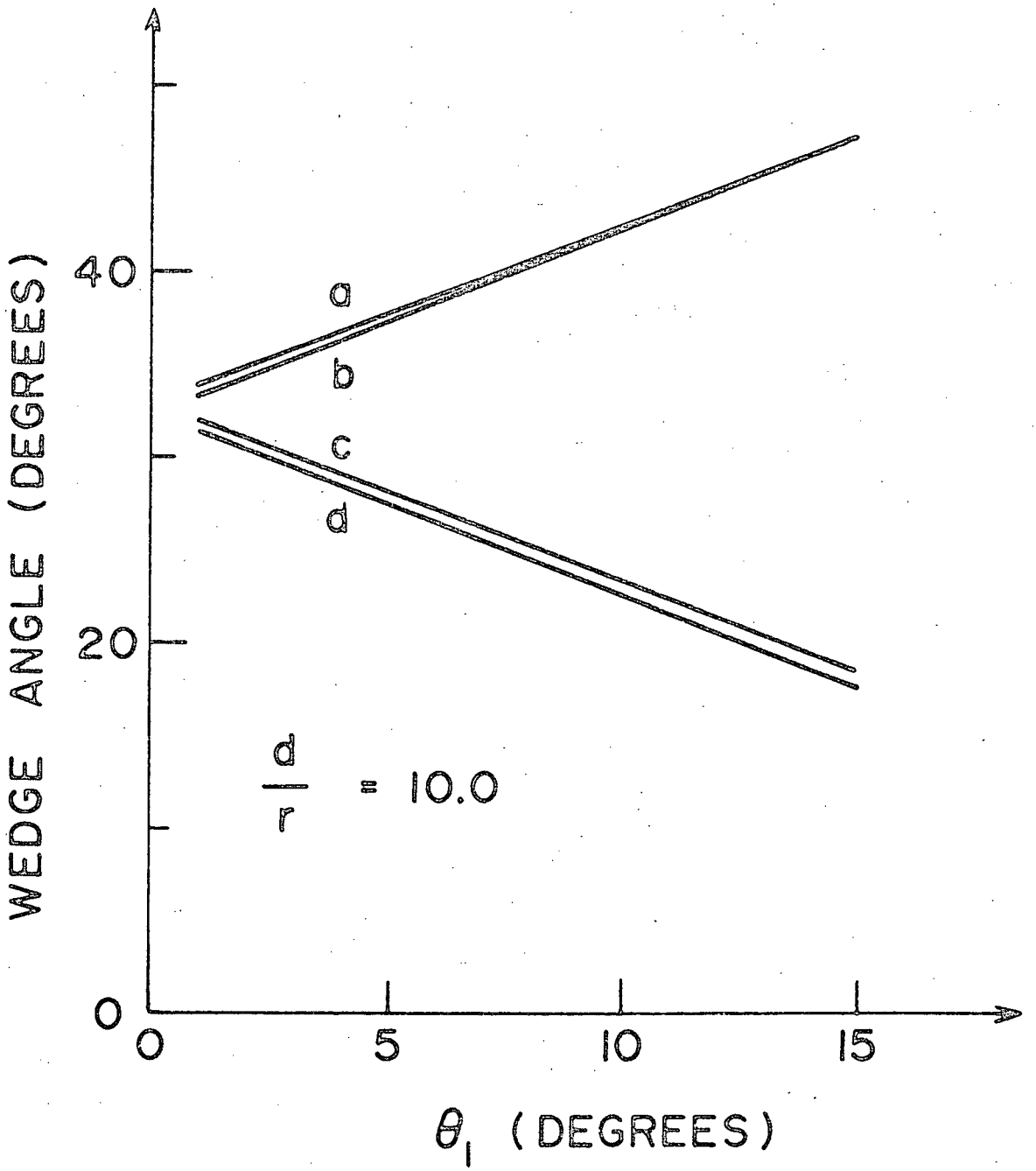

Fig. 4-6. Maximum value of the wedge angle $(\theta_1+\theta_2)$ for which the head waves of the types shown in Fig. 4-4. exist for an observation point at 5° from the free surface and d/r=10.0.

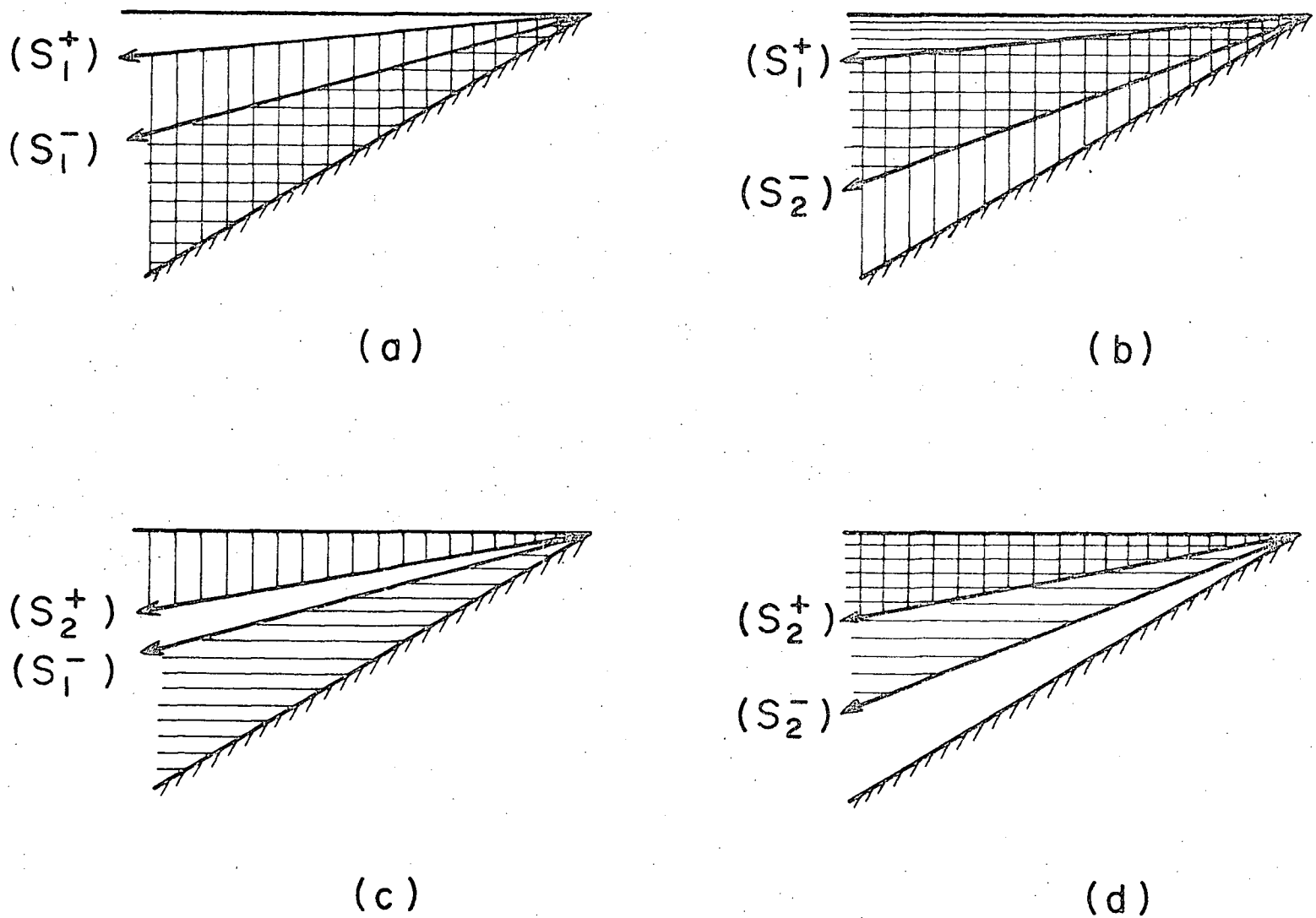

Fig. 4-7. Discontinuities in medium (1)due to interaction of the wave with the vertex. The lined areas indicate the regions for which the geometric wave from the last reflection exists with the term from which it arises indicated in brankets.

geometric wave from the last reflection exists. From equations (4.11)-(4.14) the equations of these lines of discontinuity are

(1) $S_1^+ : \theta = 2(N-1)\theta_1 + 2N\theta_2 - \pi$ (4.71)

(2) $S_2^+ : \theta = \pi - 2N\theta_1 - 2N\theta_2$ (4.72)

(3) $S_1^- : \theta = 2N'\theta_1 + 2N'\theta_2 - \pi$ (4.73)

(4) $S_2^- : \theta = \pi - 2(N'+1)\theta_1 - 2N'\theta_2$ (4.74)

The discontinuities indicate a discrepancy of my solution from the complete solution of the physical problem. In order to obtain a quantitative estimation of the displacement discontinuities, plane waves incident toward the vertex and propagating at very small angles upward (m=-) and downward (m=+) have been examined. The resulting discontinuities are shown in Figure 4-8.

For this geometry the reflected wave solution is a good approximation to the complete solution for $\theta_2 < 13^\circ$. However for $\theta_2 > 21^\circ$ the diffracted wave plays an important role. However, this formulation should adequately describe the early part of the seismogram as the diffracted waves from the vertex will arrive later than the initial phases.

It is seen that coincidence of the discontinuities in Figures 4-7b and 4-7c leads to at least partial cancellation of the discontinuities. Two special cases are of

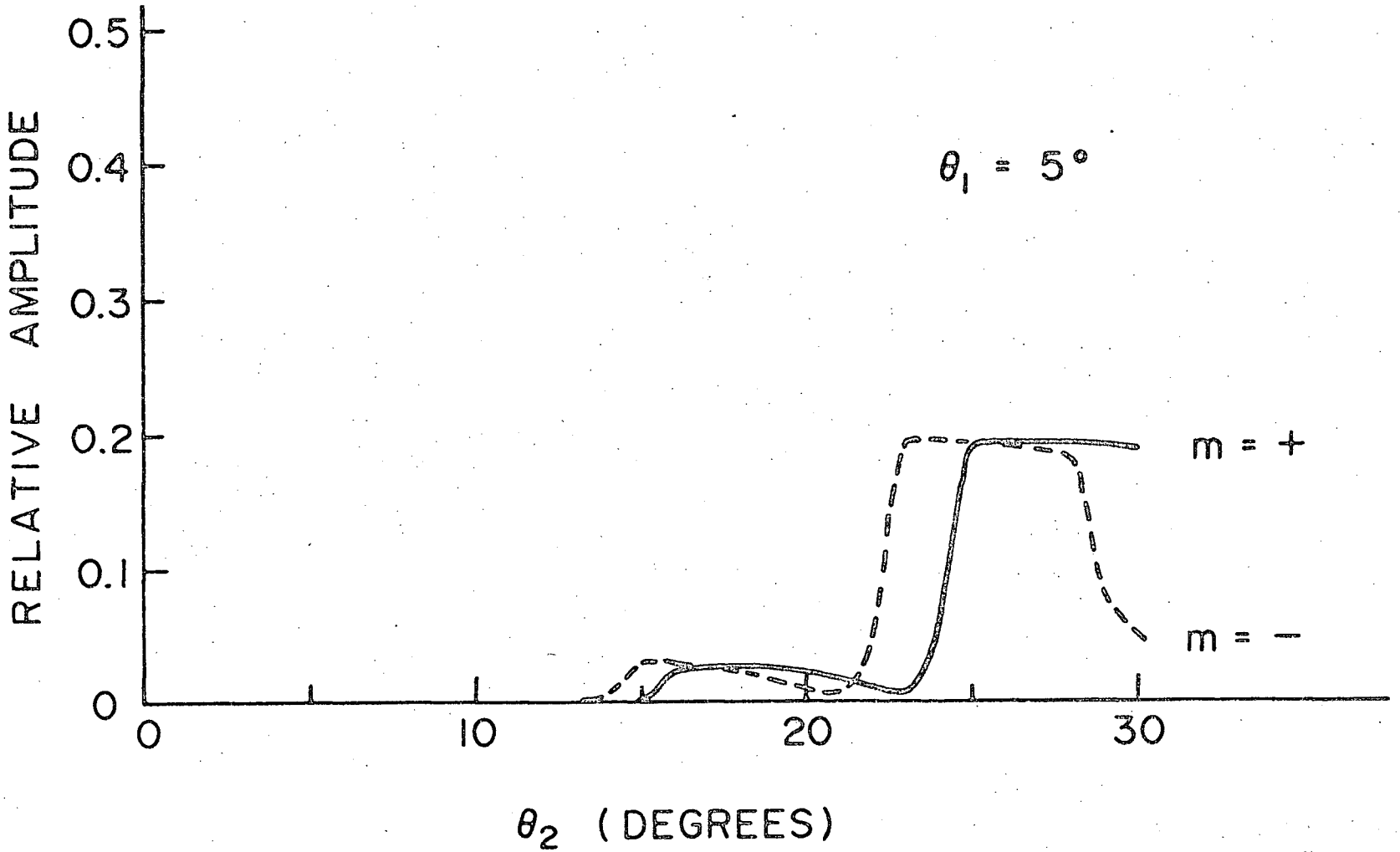

Fig. 4-8. Relative amplitudes of the displacement discontinuities due to a plane initial wave close to the x-axis for propagation upward (m=-) and downward (m=+).

interest as total cancellation results.

(1) Lower boundary free or rigid

When the lower boundary of the wedge is either free or rigid then A_k^+ and A_k^- are +1 or -1 respectively. The condition

$$\theta_1 + \theta_2 = \frac{\pi}{N+N'}$$

leads to (4.71) = (4.74) or (4.72) = (4.73) so that the two lines of the discontinuities are coincident and no discontinuities exist. Hence the solution is complete and no diffracted waves exist.

(2) Surface Source

If the line source is placed in the surface ($\theta_1 = 0$) then from (4.17) and (4.18) $A_k^+ = A_k^-$. For the particular situation

$$\theta_2 = \frac{\pi}{N+N'}$$

we have (4.71) = (4.74) or (4.72) = (4.73) and the two discontinuities coincide, hence in this case no discontinuities exist in medium (1).

In this discussion the discontinuities in medium (2) are again expected to be less important than those in medium (1).

4.10 Dispersion Equation for the Lower Boundary Free and Rigid

In this section the dispersion equation is derived for a dipping structure in the simple case where medium (2) is either air or rigid. When medium (2) is air or rigid, A_k^+ and A_k^- become +1 or -1 respectively.

For $2m(\theta_1+\theta_2) \ll 1$ we can write

$$\cos(\alpha_i+2m(\theta_1+\theta_2)) = \cos\alpha_i - 2m(\theta_1+\theta_2)\sin\alpha_i$$

In this case

$$S_1^+(N) = A_i e^{-ik_{b1}d\cos\alpha_i} \cdot \frac{1-(\pm 1)^m e^{-ik_{b1}r\{2(m-1)\theta_1+2m\theta_2\}\sin\alpha_i}}{1 \mp e^{-ik_{b1}r(2\theta_1+2\theta_2)\sin\alpha_i}}$$

$$\times\left\{e^{ik_{b1}r\cos(\alpha_i+2\theta_2-\theta)} + e^{ik_{b1}r\cos(\alpha_i+2m\theta_1+2(m+1)\theta_2-\theta)} + \cdots\right\} \qquad (4.75)$$

$$S_2^+(N) = A_i e^{-ik_{b1}d\cos\alpha_i} \frac{1-(\pm 1)^m e^{-ik_{b1}r(2m\theta_1+2m\theta_2)\sin\alpha_i}}{1 \mp e^{-ik_{b1}r(2\theta_1+2\theta_2)\sin\alpha_i}}$$

$$\times\left\{e^{ik_{b1}r\cos(\alpha_i+2\theta_1+2\theta_2+\theta)} + e^{ik_{b1}r\cos(\alpha_i+2(m+1)\theta_1+2(m+1)\theta_2+\theta)} + \cdots\right\} \qquad (4.76)$$

Similarly the expressions for $S_1^-(N)$ and $S_2^-(N)$ can be obtained. Operating with

$$k_{b1}\int_{-i\infty}^{\pi+i\infty} d\alpha_i$$

poles appear from the relation

$$1 \pm e^{-ik_{b1}r(2\theta_1+2\theta_2)\sin\alpha_i} = 0$$

which yields

$$\sin(k_{b1}r(\theta_1+\theta_2)\sin\alpha_i) = 0$$

$$\cos(k_{b1}r(\theta_1+\theta_2)\sin\alpha_i) = 0$$

For real α_i , we can then write

$$\frac{\omega}{C_n} r(\theta_1+\theta_2)\sqrt{\left(\frac{C_n}{C_{b1}}\right)^2 - 1} = \begin{cases} n\pi \\ (n-\frac{1}{2})\pi \end{cases} \qquad (4.77)$$

where C_n is the phase velocity as $\cos\alpha_i = C_{b1}/C_n$ ($0<\alpha_i<\pi$). This expression is the same as that obtained by Nagumo (1961) for a sloping rigid bottom. Further, if we put $r(\theta_1+\theta_2) = H$ (H is the depth in the case of a horizontal layer), the dispersion relation (4.77) coincides with that of the horizontally layered case. Nagumo (1961) has called C_n and $v_n = \frac{\partial\omega}{\partial k_n}$ the formal phase and group velocity to differentiate from the observed velocities.

4.11 The Horizontal Layer Solution

It is interesting to derive the solution for a horizontal layer using my method as the transition of the solution to the horizontal layer case may suggest a method for obtaining the surface wave solutions for the dipping layer. For the diffracted wave problem, it is useful to study this transition as the quantitative and qualitative behaviour of the discontinuities as they approach zero for zero dip angle may indicate the nature of the diffracted solution.

The same (x, y) coordinate system is used with the x-axis now being horizontal (Figure 4-9). The source is placed at $(d, 0)$ in the layer of thickness $H=H_1+H_2$. Employing the same procedure as for the dipping layer, we obtain the displacement for the time variations $e^{i\omega t}$,

$$
\begin{aligned}
u_1 = k_{b1}\int_{-i\infty}^{\pi+i\infty} A_i\Big[& e^{-ik_{b1}\{(d-x)\cos\alpha_i+|y|\sin\alpha_i\}} + e^{-ik_{b1}\{(d-x)\cos\alpha_i+(2H_1+y)\sin\alpha_i\}} \\
& + \sum_{n=1}^{\infty} A_1^n \Big\{ e^{-ik_{b1}\{(d-x)\cos\alpha_i+(2((n-1)H_1+nH_2)-y)\sin\alpha_i\}} \\
& \quad + e^{-ik_{b1}\{(d-x)\cos\alpha_i+(2(nH_1+nH_2)+y)\sin\alpha_i\}} \\
& \quad + e^{-ik_{b1}\{(d-x)\cos\alpha_i+(2(nH_1+nH_2)-y)\sin\alpha_i\}} \\
& \quad + e^{-ik_{b1}\{(d-x)\cos\alpha_i+(2((n+1)H_1+nH_2)+y)\sin\alpha_i\}} \Big\} \Big] d\alpha_i \\
= k_{b1}\int_{-i\infty}^{\pi+i\infty} A_i\Big[& e^{-ik_{b1}R_0\cos(\alpha_i-\theta_0)} + e^{-ik_{b1}R_0^-\cos(\alpha_i-\theta_0^-)}
\end{aligned}
\tag{4.78}
$$

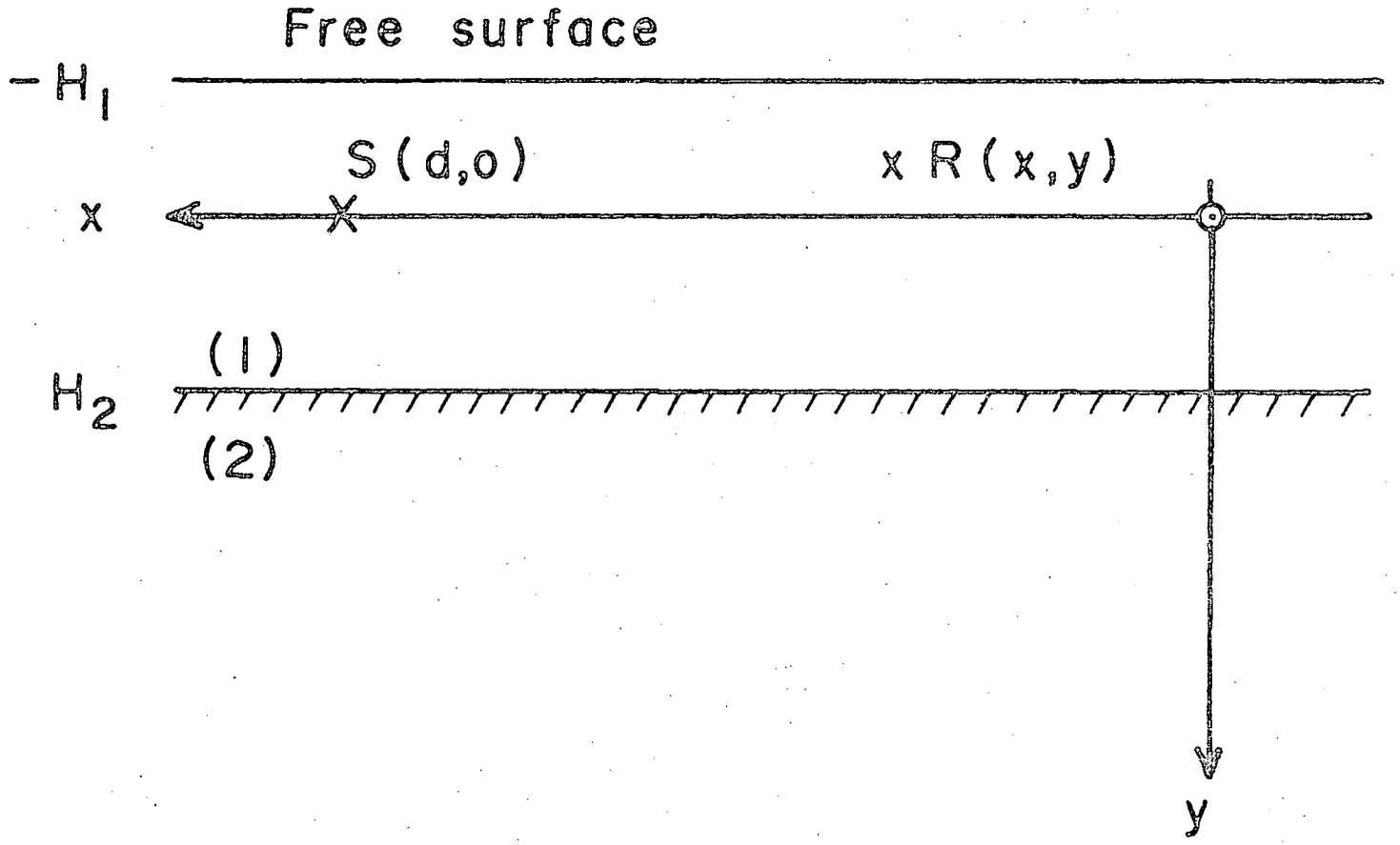

Fig. 4-9. Coordinate system for the horizontal layer case with the source (S) at (d,0) and the receiver (R) at (x,y).

$$+\sum_{n=1}^{\infty} A_1^n \left\{ e^{-ik_{b1}R_{n1}^{+}\cos(\alpha_i-\theta_{n1}^{+})} + e^{-ik_{b1}R_{n2}^{+}\cos(\alpha_i-\theta_{n2}^{+})} + e^{-ik_{b1}R_{n1}^{-}\cos(\alpha_i-\theta_{n1}^{-})} + e^{-ik_{b1}R_{n2}^{+}\cos(\alpha_i-\theta_{n2}^{-})} \right\} \Big] d\alpha_i \tag{4.78}$$

where

$$A_1 = \frac{\Delta \sin\alpha_i - \delta\sqrt{1-\Delta^2\cos^2\alpha_i}}{\Delta \sin\alpha_i + \delta\sqrt{1-\Delta^2\cos^2\alpha_i}} \tag{4.79}$$

$$R_o = \sqrt{(d-x)^2+y^2} \qquad \tan\theta_o = |y|/(d-x)$$

$$R_o^{-} = \sqrt{(d-x)^2+(2H_1+y)^2} \qquad \tan\theta_o^{-} = (2H_1+y)/(d-x)$$

$$R_{n1}^{+} = \sqrt{(d-x)^2+\{2(nH_1-H_1)-y\}^2} \qquad \tan\theta_{n1}^{+} = \{2(nH-H_1)-y\}/(d-x)$$

$$R_{n2}^{+} = \sqrt{(d-x)^2+(2nH+y)^2} \qquad \tan\theta_{n2}^{+} = (2nH+y)/(d-x)$$

$$R_{n1}^{-} = \sqrt{(d-x)^2+(2nH-y)^2} \qquad \tan\theta_{n1}^{-} = (2nH-y)/(d-x)$$

$$R_{n2}^{-} = \sqrt{(d-x)^2+\{2(nH+H_1)+y\}^2} \qquad \tan\theta_{n2}^{-} = \{2(nH+H_1)+y\}/(d-x) \tag{4.80}$$

As equation (4.78) is of the same form as (4.38), formulae (4.62) or (4.63) and (4.64) can be applied for the reflected and head waves respectively. Therefore the variations of the waveforms depend only on the values $R_{n\ell}^{m}$, $\theta_{n\ell}^{m}$ and θ_B. Equation (4.78) can also be derived from (4.38), the formal dipping layer solution, if we take the limit

$$r \to \infty, \quad \theta_1 \to 0, \quad \theta_2 \to 0$$

as

$$r\sin\theta_1 = H_1 \quad \text{and} \quad r\sin\theta_2 = H_2 \tag{4.81}$$

In the case of a horizontal layer, surface waves appear from contributions of poles. As our solution transforms to the horizontal layer solution, we could investigate surface waves in the case of a dipping layer if the finite series expression of our solution can be changed into a compact form which corresponds to a normal mode expression.

4.12 Computation of Displacement Seismograms

For the direct wave, head waves, and waves once reflected from the boundary, displacements have been calculated for the three cases shown in Figure 4-10. Elastic constants are again those employed by Haskell (1960). Ray paths of waves which contribute to the seismogram are shown in Figure 4-11.

The component waves are shown on the time-displacement plot of Figure 4-12 and the arrival times corresponding to the ray paths indicated by lettered arrows. A detailed feature is the small amplitude of the head waves compared to the direct and reflected waves. This is expected from inspection of equations (65) and (66) which show that the head waves decrease as $1/(R_{1\ell}^{m})^{3/2}$ and the reflected waves as $1/(R_{1\ell}^{m})^{1/2}$. Although the travel times changed significantly, the wave forms of the refracted and reflected waves do not undergo large changes for the three cases illustrated.

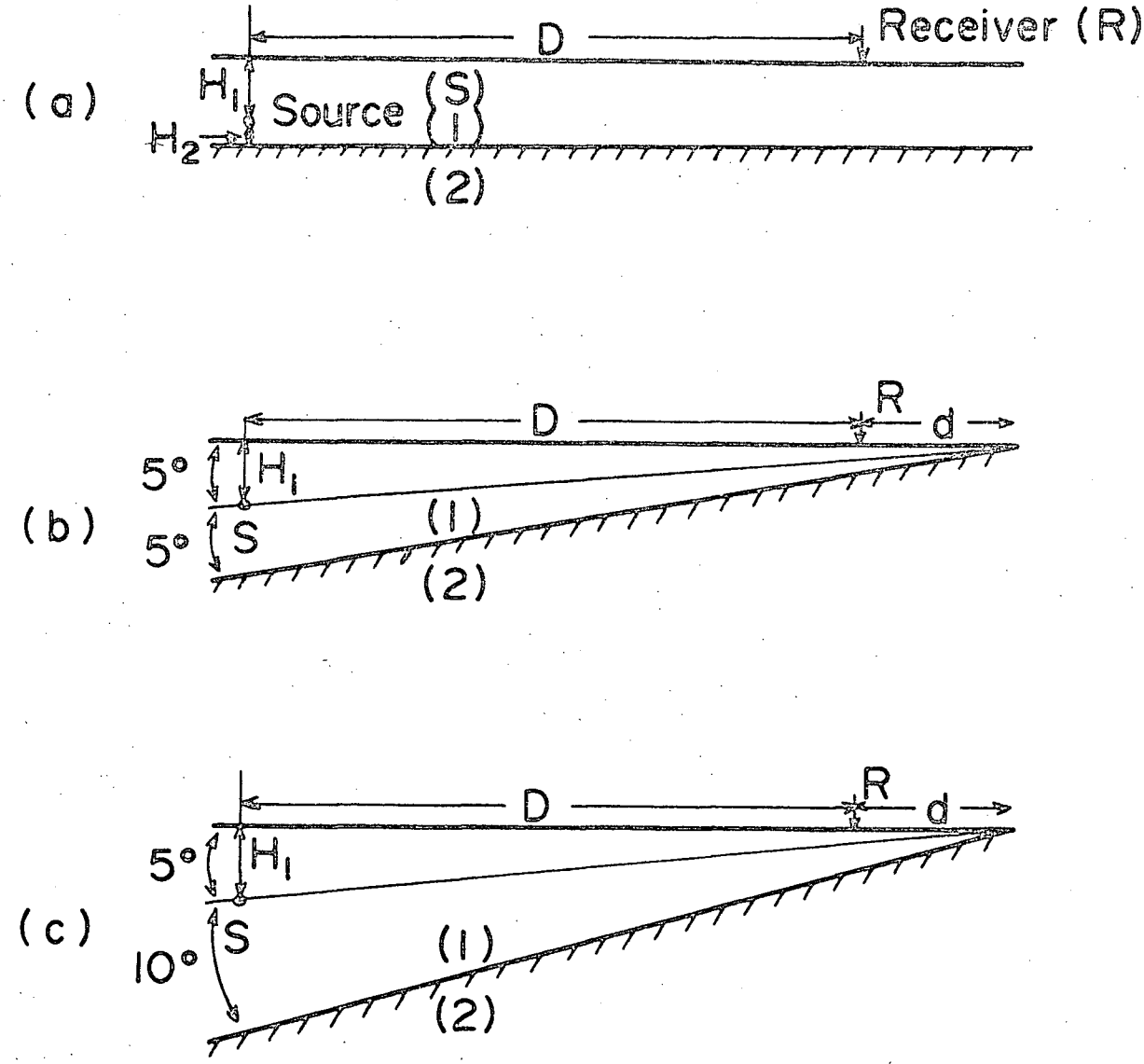

Fig. 4-10. Three cases for which theoretical seismograms were caluculated. The parameters used were: H_1= 9.59 km, H_2= 3.00 km, D= 99.6 km, d= 10.0 km, and the displacement parameter c= 0.05 sec.

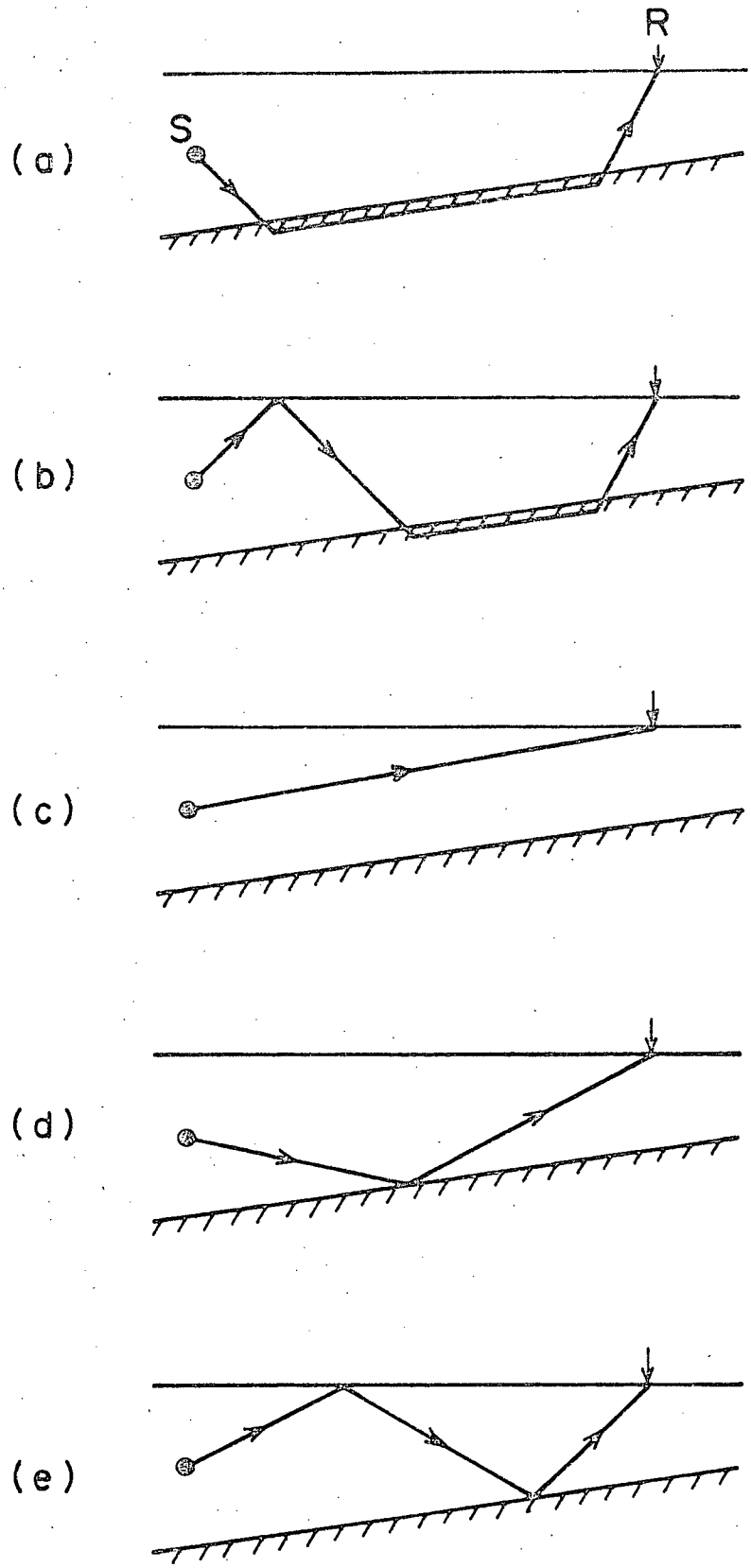

Fig. 4-11. Ray paths which contribute to the theoretical seismograms.

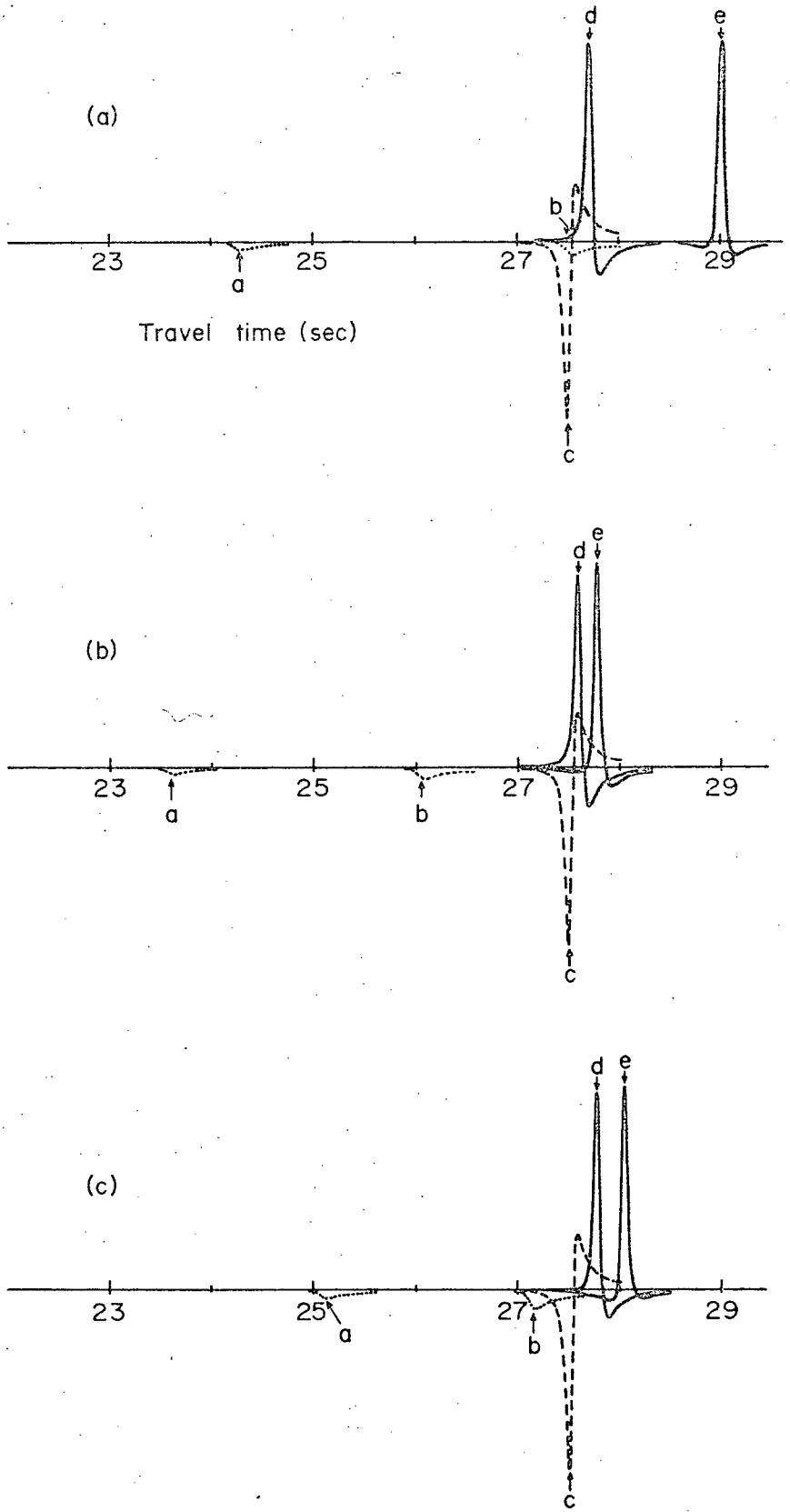

Fig. 4-12. Displacements of the component waves for the geometrics given in Figs. 4-10a, 4-10b, and 4-10c.

Figure 4-13 represents the seismograms synthesized from the components of Figure 4-12. The seismograms look very different. However, the different arrivals are all recognizable except for the head wave (b) is embedded in the wave forms of the direct wave (c) and the reflected wave (d) in the case of the horizontal layer. A very noticeable feature is the late arrival of the reflected wave (e) in the case of the horizontal layer. More multiply reflected waves will appear as later phases. As the distance between the observation point and the vertex is 10.0 km and the velocities of medium (1) and medium (2) are 3.64 km/sec and 4.62 km/sec respectively, the diffracted waves hardly contribute to the section of the seismogram shown here as the diffracted wave arriving 4 to 5 sec after the first arrival is due to a head wave of small amplitude interacting with the vertex.

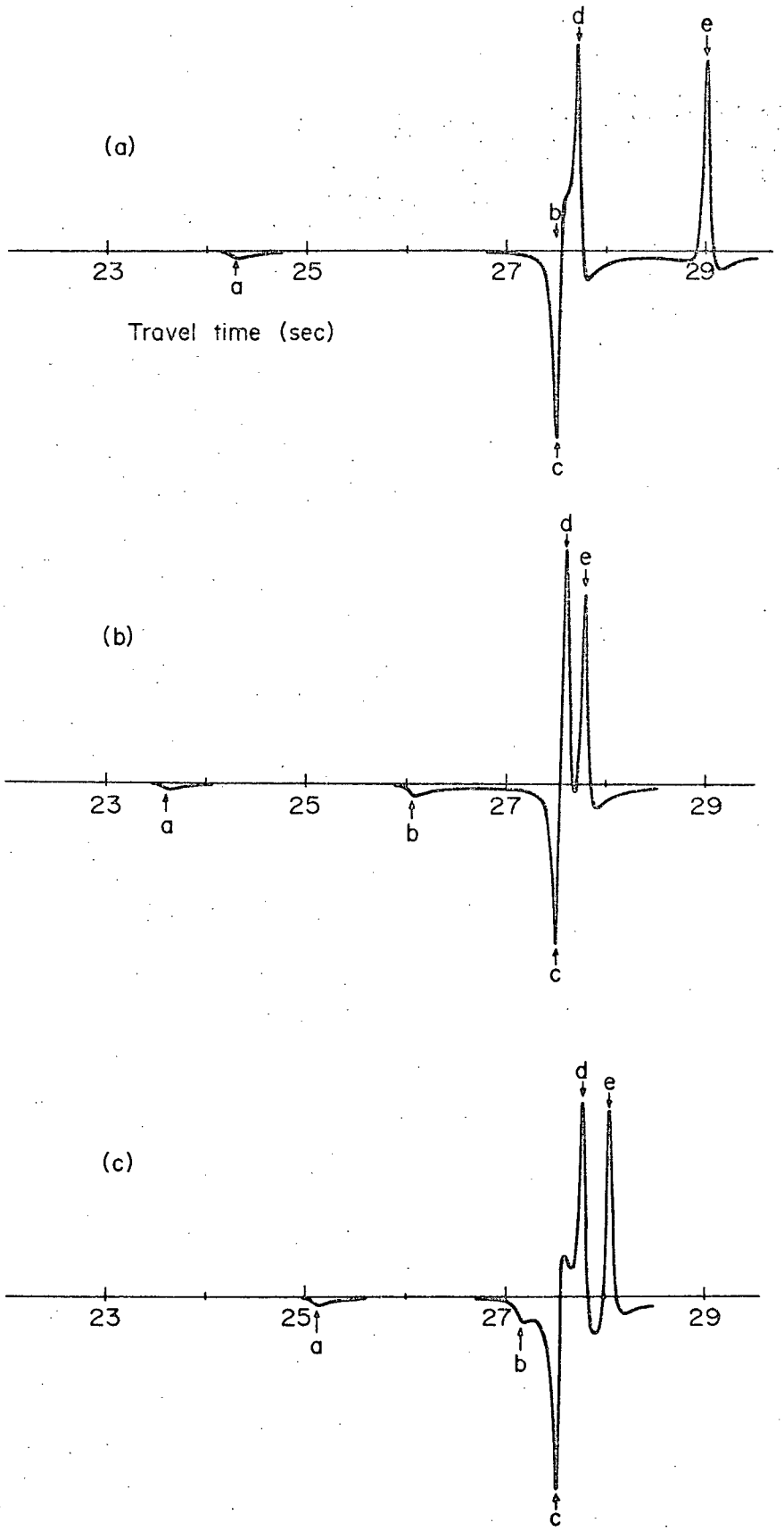

Fig. 4-13. Synthesized seismograms resulting from the displacements of Fig. 4-12.

CHAPTER 5

SUMMARY, CONCLUSIONS AND FURTHER STUDIES

5.1 Summary and Conclusions

In this paper, the behavior of elastic waves in a dipping layer overlying an elastic medium has been investigated in terms of body waves in order to expand the models available for the interpretation of crustal structure.

In Chapter 2, the reflected wave solution for a plane SH incident at the base of a dipping layer and perpendicular to strike has been developed and numerical examples presented. For waves propagating in the up-dip direction with angle of incidence in the range of that for teleseismic S waves ($45° < \alpha < 75°$), it is found that the reflected wave solution closely approximates the complete solution for small dip angles as the boundary conditions are approximately satisfied. However, for waves propagating in the down-dip direction, the displacement discontinuity along the edge of the final wave which does not collide with the interfaces becomes large. In this case the wave has reverberated only a very few times within the wedge and hence is still of significant amplitude. The size of this discontinuity has been determined and hence serves as a guide as to whether the ray solution

is applicable. For a transient input to the wedge, the reflected waves will arrive earlier than the diffracted waves and hence even for large discontinuities, this type of solution should apply to the composition of the initial section of a seismogram. The diffracted wave must provide continuity in displacement and stress along the edge of the final wave as well as those imposed at the surface and the boundary between the media.

In Chapter 3, the behaviour of P and SV waves incident at the base of a dipping layer and perpendicular to strike has been investigated by means of a reflected wave solution developed using a cylindrical coordinate system. Due to the complexity of this problem, a series solution is not presented as was done for the SH problem; however, a computational scheme is given by which the amplitudes and propagation directions of all the contributing waves are determined. In this way the displacement at any point in the wedge due to reflected waves may be found. Numerical examples of displacements and displacement ratios at the surface are presented for incident waves propagating in both up-dip ($\alpha, \beta = 60°$) and down-dip ($\alpha, \beta = 120°$) directions. It is found that the displacement ratios versus frequency curves for constant depth to interface become flat for incident P and SV waves propagating in the down-dip

direction for dip angles greater than 15°. This is very different from the case of up-dip direction. For the P wave propagating in the up-dip direction (α = 60°), the peaks are large for large dip angles and for dip angles greater than 10° the peaks shift to lower frequency and become narrower with decreasing dip. A feature of particular note is that the H/V displacement ratio curves for incident SV are much more sensitive to small changes of dip at small dip angles than are the V/H displacement ratio curves for incident P waves. It appears therefore that a study of SV waves would be more likely to yield information concerning dipping interfaces than would P waves. For waves propagating in the down-dip direction, it is found that the displacement discontinuity may be large even for small dip angles indicating that the diffracted wave is of significant amplitude. However, since the reflected waves will arrive earlier than the diffracted waves for a transient input to the wedge, the reflected wave solution should again apply to the composition of the initial section of the seismogram. The complex propagation direction used in this chapter has been interpreted in Appendix II using the example of a free Rayleigh wave to show that the real part of the angle indicates the propagation direction and the imaginary part gives the decrease of amplitude.

In Chapter 4, the propagation of SH waves from a

line source in a dipping layer overlying an elastic medium has been investigated using multiple reflection formulation. A formal solution which does not include diffracted waves has been obtained. The first two series terms of the integral have been evaluated using the method of steepest descent to obtain displacements for both a harmonic and an aperiodic time variation and contributions have been interpreted using ray paths in terms of head and reflected waves. If in the integral the branch points are smaller than the saddle points, head waves do not appear. Hence the range of existence of the various types of head waves may be determined. Using the same technique, the solution in the case of a horizontal layer has also been found and comparison made with the dipping layer through numerical examples. The wave forms of the arrivals do not differ greatly; however, the character of the synthetic seismogram markedly changes due to changes in arrival times. Discontinuities in displacement which are associated with the diffracted wave have been studied. For special cases it is found that the reflected wave solution is the complete solution. In the other cases, this solution can be applied to the initial section of the seismogram.

5.2 Suggestions for Further Studies

As a result of this study, the following lines of investigation are suggested:

(1) The calculation of a synthetic seismogram at a station in a wedge with an elastic base for an incident plane wave pulse.

(2) The calculation of the amplitude characteristics of a multiple reflection in the case of both dipping and horizontal layers by a combination of the technique developed in this thesis and Haskell's method (Haskell, 1953).

(3) The problem of P and SV line sources in a wedge overlying an elastic medium in terms of head and reflected waves neglecting the diffracted waves.

(4) The exact solution in terms of multiply reflected waves and multi-reflected head waves in the case of a line source in a dipping layer with an elastic base for transient time variations using the method of Cagniard (1962).

(5) An investigation of surface wave propagation in the presence of a dipping layer overlying an elastic medium. In the case of a horizontal layer, surface waves appear from a contribution of poles. When the dip angle approaches zero, the solution found in Chapter 4 reduces

to the case of a horizontal layer. Hence surface waves in the presence of a dipping layer could be investigated if the finite series solution can be written in a compact form which corresponds to a normal mode expression.

(6) An attack on the problem of diffracted waves using the multiple reflection wave solution and the discontinuities found in this solution which are related to the diffracted waves.

BIBLIOGRAPHY

Cagniard, L., 1962. Reflection and refraction of progressive seismic waves, McGraw-Hill, New York.

Clowes, R. M., Kanasewich, E. R., and Cumming, G. L., 1968. Deep crustal seismic reflections at near-vertical incidence, *Geophysics*, 33, 441-451.

Ellis, R. M. and Basham, P. W., 1968. Crustal characteristics from short-period P waves, *Bull. Seism. Soc. Amer.*, 58, 1681-1700.

Emura, K., 1960. Propagation of the disturbances in the medium consisting of semi-infinite liquid and solid, Sci. Rep. Tohoku Univ., Ser. 5, Geophysics, 12, 63-100.

Ewing, W. M., W. S. Jardetzky, and F. Press, 1957. Elastic waves in layered media, McGraw-Hill, New York.

Fernandez, L. M. and Careaga, J., 1968. The thickness of the crust in central United States and La Paz, Bolivia, from the spectrum of longitudinal seismic waves, *Bull. Seism. Soc. Amer.*, 58, 711-741.

Fuchs, K., 1966. Synthetic seismograms of P waves propagating in solid wedges with free boundaries, *Geophysics*, 31, 524-535.

Haskell, N. A., 1953. The dispersion of surface waves in multilayered media, *Bull. Seism. Soc. Amer.*, 43, 17-34.

Haskell, N. A., 1960. Crustal reflection of plane SH waves, *J. Geophys. Res.*, 65, 4147-4150.

Haskell, N. A. 1962. Crustal reflection of plane P and SV waves, *J. Geophys. Res.*, 67, 4751-4767.

Honda, H. and Nakamura, K., 1954. On the reflection and refraction of the explosive sounds at the ocean bottom II, Sci. Rep. Tohoku Univ., Ser. 5, Geophysics, 6, 70-84.

Hudson, J. A., 1963. SH waves in a wedge-shaped medium, *Geophys. J. R.A.S.*, 7, 517-546.

Hudson, J. A. and Knopoff, L., 1964. Transmission and reflection of surface waves at a corner 2, Rayleigh waves, *J. Geophys. Res.*, 69, 281-289.

Ibrahim, A. B., 1969. Determination of crustal thickness from spectral behavior of SH waves, *Bull. Seism. Soc. Amer.*, 59, 1247-1258.

Jeffreys, H. and Jeffreys, B. S., 1956. Methods of mathematical physics, Cambridge Univ. Press, Cambridge, England.

Kane, J. and Spence, J., 1963. Rayleigh waves transmission on elastic wedges, *Geophysics*, 28, 715-723.

Kane, J., 1966. Teleseismic response of a uniform dipping crust (Part I of a series on crustal equalization of seismic arrays), *Bull. Seism. Soc. Amer.*, 56, 841-859.

Keller, J. B., 1962. Geometrical theory of diffraction, *J. Acoust. Soc. Am.*, 52, 116-130.

Lapwood, E. R., 1961. The transmission of a Rayleigh pulse round a corner, *Geophys. J. R. Astr. Soc.*, 4, 174-196.

McGarr, A. and Alsop, L. E., 1967. Transmission and reflection of Rayleigh waves at vertical boundaries, *J. Geophys. Res.*, 72, 2169-2180.

Nagumo, S., 1961. Elastic wave propagation in a liquid layer overlying a sloping rigid bottom, *J. Seism. Soc. Japan*, 14, 189-197.

Nakamura, K., 1960. Normal mode waves in an elastic plate (1), Sci. Rep. Tohoku Univ., Ser. 5, Geophysics, 12, 44-62.

Phinney, R. A., 1964. Structure of the earth's crust from spectral behavior of long period body waves, *J. Geophys. Res.*, 69, 2997-3017.

Sato, R., 1963. Diffraction of SH waves at an obtuse-angled corner, *J. Phys. Earth*, 11, 1-17.

APPENDIX I

ENERGY RELATIONS

As a check on the amplitude relations derived in the text, the method used by Ewing et al (1957) has been used to derive expressions for energy partition between the incident, reflected and refracted waves.

To calculate kinetic energies, we note that the velocities $\bar{u}$ are related to the displacements u by $\bar{u} = i\omega u$ and hence may be obtained directly from equations (3.17) and (3.18). The energy flux for the waves can then be obtained by multiplying the kinetic energy per unit volume, $\frac{1}{2}\rho(\bar{u}_r^2 + \bar{u}_\theta^2)$ by the velocity of propagation and the area of wavefront involved. For a P wave incident on the surface, its energy flux per unit area must be equal to the sum of the energies in the reflected and refracted waves. We have

$$\begin{aligned}
&\frac{1}{2}\rho_2 C_{a2}^2 C_{in} C_{a2} \left|\sin(\alpha_i - \theta_d)\right| \\
&= \frac{1}{2}\rho_2 C_{a2}^2 C_{r\ell}^2 C_{a2} \left|\sin(\alpha_{r\ell} - \theta_d)\right| \\
&+ 2\rho_2 C_{b2}^2 D_{r\ell}^2 C_{b2} \left|\sin(\beta_{r\ell} - \theta_d)\right| \\
&+ \frac{1}{2}\rho_1 C_{a1}^2 A_{rf}^2 C_{a1} \left|\sin(\alpha_{rf} - \theta_d)\right| \\
&+ 2\rho_1 C_{b1}^2 B_{rf}^2 C_{b1} \left|\sin(\beta_{rf} - \theta_d)\right|
\end{aligned} \qquad \text{(A-1.1)}$$

A following computationally more useful form is obtained

using (3.28)

$$1=\left(\frac{C_{rl}}{C_{in}}\right)^2+4\left(\frac{V_{b2}}{V_{a2}}\right)^3\left(\frac{D_{rl}}{C_{in}}\right)^2\frac{\sqrt{1-(V_{b2}/V_{a2})^2\cos^2(\theta_d-\alpha)}}{|\sin(\theta_d-\alpha)|}$$
$$+\frac{1}{\delta}\left(\frac{1}{V_{a2}}\right)^3\left(\frac{A_{rs}}{C_{in}}\right)^2\frac{\sqrt{1-(1/V_{a2})^2\cos^2(\theta_d-\alpha)}}{|\sin(\theta_d-\alpha)|} \qquad \text{(A-1.2)}$$
$$+\frac{4}{\delta}\left(\frac{V_{b1}}{V_{a2}}\right)^3\left(\frac{B_{rs}}{C_{in}}\right)^2\frac{\sqrt{1-(V_{b1}/V_{a2})^2\cos^2(\theta_d-\alpha)}}{|\sin(\theta_d-\alpha)|}$$

The corresponding equation for S waves is

$$1=\left(\frac{D_{rl}}{D_{in}}\right)^2+\frac{1}{4}\left(\frac{V_{a2}}{V_{b2}}\right)^3\left(\frac{C_{rl}}{D_{in}}\right)^2\frac{\sqrt{1-(V_{a2}/V_{b2})^2\cos^2(\theta_d-\beta)}}{|\sin(\theta_d-\beta)|}$$
$$+\frac{1}{\delta}\left(\frac{V_{b1}}{V_{b2}}\right)^3\left(\frac{B_{rs}}{D_{in}}\right)^2\frac{\sqrt{1-(V_{b1}/V_{b2})^2\cos^2(\theta_d-\beta)}}{|\sin(\theta_d-\beta)|} \qquad \text{(A-1.3)}$$
$$+\frac{1}{4\delta}\left(\frac{1}{V_{b2}}\right)^3\left(\frac{A_{rs}}{D_{in}}\right)^2\frac{\sqrt{1-(1/V_{b2})^2\cos^2(\theta_d-\beta)}}{|\sin(\theta_d-\beta)|}$$

For P and SV waves incident on the boundary from medium (1), the relations are respectively

$$1=\left(\frac{A_{rl}}{A_{in}}\right)^2+4\nu_{b1}^3\left(\frac{B_{rl}}{A_{in}}\right)^2\frac{\sqrt{1-\nu_{b1}^2\cos^2(\theta_d-\alpha)}}{|\sin(\theta_d-\alpha)|}$$

$$+\delta\nu_{a2}^3\left(\frac{C_{rf}}{A_{in}}\right)^2\frac{\sqrt{1-\nu_{a2}^2\cos^2(\theta_d-\alpha)}}{|\sin(\theta_d-\alpha)|} \qquad \text{(A-1.4)}$$

$$+4\delta\nu_{b2}^3\left(\frac{D_{rf}}{A_{in}}\right)^2\frac{\sqrt{1-\nu_{b2}^2\cos^2(\theta_d-\alpha)}}{|\sin(\theta_d-\alpha)|}$$

$$1=\left(\frac{B_{rl}}{B_{in}}\right)^2+\frac{1}{4}\frac{1}{\nu_{b1}^3}\left(\frac{A_{rl}}{B_{in}}\right)^2\frac{\sqrt{1-(1/\nu_{b1})^2\cos^2(\theta_d-\beta)}}{|\sin(\theta_d-\beta)|}$$

$$+\frac{1}{4}\delta\left(\frac{\nu_{a2}}{\nu_{b1}}\right)^3\left(\frac{C_{rf}}{B_{in}}\right)^2\frac{\sqrt{1-(\nu_{a2}/\nu_{b1})^2\cos^2(\theta_d-\beta)}}{|\sin(\theta_d-\beta)|} \qquad \text{(A-1.5)}$$

$$+\delta\left(\frac{\nu_{b2}}{\nu_{b1}}\right)^3\left(\frac{D_{rf}}{B_{in}}\right)^2\frac{\sqrt{1-(\nu_{b2}/\nu_{b1})^2\cos^2(\theta_d-\beta)}}{|\sin(\theta_d-\beta)|}$$

APPENDIX II

EXPRESSION OF A FREE RAYLEIGH WAVE USING COMPLEX ANGLES

In the calculation of the displacements, complex angles have been used in order that the cases of total reflection and incident angles greater than the critical are involved in the results. Although Rayleigh waves are not produced in this problem, the expression of Rayleigh waves in terms of complex angles is of interest. Consider an elastic half-space with free surface $\theta = 0$ (Figure A-1) The solution in the medium can be written as

$$\Theta_R = A_R \cdot e^{ik_{a1} r \cos(\theta - \alpha_R)}$$
$$\tilde{\omega}_R = B_R \cdot e^{ik_{b1} r \cos(\theta - \beta_R)} \qquad \text{(A-2.1)}$$

The boundary conditions at $\theta = 0$ are

$$\widehat{\theta\theta} = 0$$
$$\widehat{r\theta} = 0 \qquad \text{(A-2.2)}$$

Substituting (A-2.1) into the boundary conditions using (3.15) and (3.16), we have

$$(1 - 2\nu_{b1}^2 \cos^2\alpha_R) A_R + 4\nu_{b1}^2 B_R \sin\beta_R \cos\beta_R = 0$$
$$-A_R \sin\alpha_R \cos\alpha_R + (1 - 2\cos^2\beta_R) B_R = 0 \qquad \text{(A-2.3)}$$

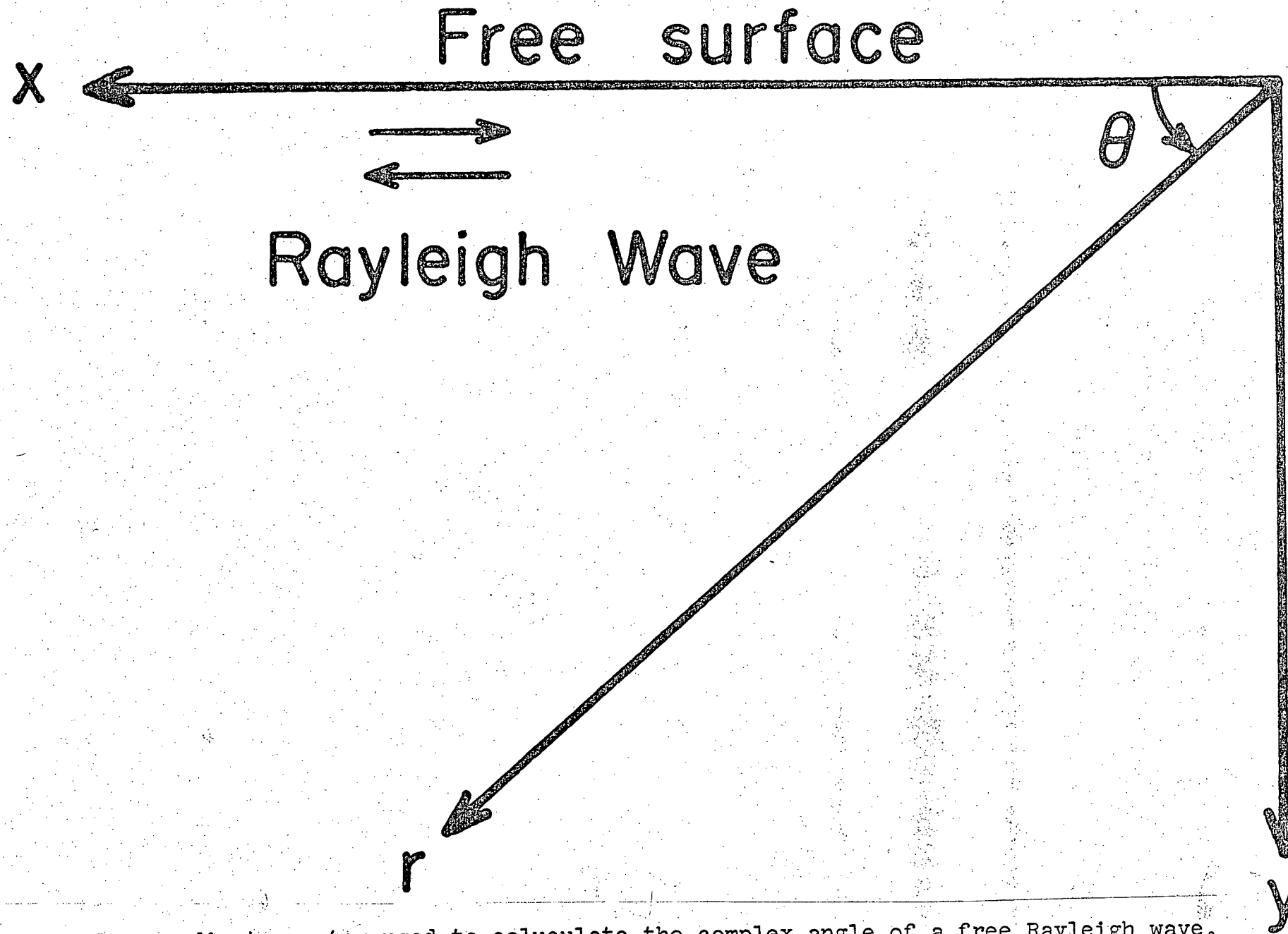

Fig. A-1. Coordinate system used to caluculate the complex angle of a free Rayleigh wave.

and

$$\nu_{b1}\cos\alpha_R = \cos\beta_R \tag{A-2.4}$$

From (A-2.3), we have

$$(1-2\nu_{b1}^2\cos^2\alpha_R)(1-2\cos^2\beta_R) - 4\nu_{b1}^2\sin\alpha_R\cos\alpha_R\sin\beta_R\cos\beta_R = 0 \tag{A-2.5}$$

Substituting (A-2.4), and writing $\chi=\cos^2\alpha_R$ and $\nu=\nu_{b1}^2$ gives

$$16(1-\nu)\chi^3+\left(16-\frac{24}{\nu}\right)\chi^2+\frac{8}{\nu^2}\chi-\frac{1}{\nu^3}=0 \tag{A-2.6}$$

Assuming Poisson's relation, $\lambda=\mu$, yields

$$\frac{32}{3}\chi^3-56\chi^2+72\chi-27=0 \tag{A-2.7}$$

The real root of this equation is $\chi=3.549$ which corresponds to $\cos\alpha_R=\pm 1.884$ and using (A-2.4), $\cos\beta_R=\pm 1.088$. Recalling the relations

$$\arccos(-z)=\pi-\arccos z$$

$$\arccos p = i\,\mathrm{arccosh}\,p \qquad (p=\text{real}>1)$$

we obtain

$$\alpha_R = 1.247\,i \quad \text{or} \quad \pi-1.247\,i$$

$$\beta_R = 0.4068\,i \quad \text{or} \quad \pi-0.4068\,i \tag{A-2.8}$$

If in equations (A-2.1), we use

$$\cos(p \pm iq) = \cos p \cosh q \mp i \sin p \sinh q$$

$$\sin(p \pm iq) = \sin p \cosh q \mp i \cos p \sinh q$$

we have

$$\Theta_R = A_R e^{\pm i k_{a1} r (1.884 \cos\theta \pm i 1.597 \sin\theta)}$$

$$= A_R e^{\pm i \frac{\omega}{0.9194 c_{b1}} x - \frac{0.9218}{c_{b1}} \omega y} \qquad \text{(A-2.9)}$$

$$\tilde{\omega}_R = B_R e^{\pm i k_{b1} r (1.088 \cos\theta \pm i 0.4278 \sin\theta)}$$

$$= B_R e^{\pm i \frac{\omega}{0.9194 c_{b1}} x - \frac{0.4278}{c_{b1}} \omega y} \qquad \text{(A-2.10)}$$

We see that the dilatation and rotation propagate with the velocity $0.9194 c_{b1}$ which coincides with the velocity of the free Rayleigh wave. As a result we see that for a Rayleigh wave written in terms of complex angles, the real part of the angle indicates the propagation direction and the imaginary part gives the decrease of amplitude with the two solutions of (A-2.8) representing waves propagating in opposite directions (0 and π).

APPENDIX III

EVALUATION OF THE SECOND SERIES TERMS OF THE INTEGRAL

As a guide to computation of higher order terms in the series, a summary of the evaluation procedures and results for the contributions by waves twice reflected from the boundary between the elastic media are evaluated here. The second terms of the series have the form

$$I_{2\ell}^{m} = k_{b1}\int_{-i\infty}^{\pi+i\infty} A_1^m \cdot A_2^m \cdot e^{-ik_{b1}R_{2\ell}^m \cos(\alpha_i - \theta_{2\ell}^m)}\, d\alpha_i \qquad \text{(A-3.1)}$$

where

$$A_1^m = \frac{\Delta\sin(\phi_1^m+\alpha_i) - \delta\sqrt{1-\Delta^2\cos^2(\phi_1^m+\alpha_i)}}{\Delta\sin(\phi_1^m+\alpha_i) + \delta\sqrt{1-\Delta^2\cos^2(\phi_1^m+\alpha_i)}} \qquad \text{(A-3.2)}$$

$$A_2^m = \frac{\Delta\sin(\phi_2^m+\alpha_i) - \delta\sqrt{1-\Delta^2\cos^2(\phi_2^m+\alpha_i)}}{\Delta\sin(\phi_2^m+\alpha_i) + \delta\sqrt{1-\Delta^2\cos^2(\phi_2+\alpha_i)}}$$

and $\ell = 1, 2$ and $m = +, -$.

From equations (4.17) and (4.18)

$$\phi_1^+ = \theta_2 \quad , \quad \phi_1^- = 2\theta_1 + \theta_2 \qquad \text{(A-3.3)}$$

$$\phi_2^+ = 2\theta_1 + 3\theta_2 \quad , \quad \phi_2^- = 4\theta_1 + 3\theta_2 \, .$$

$R_{2\ell}^m$ and $\theta_{2\ell}^m$ have been given by equations (4.29) to (4.32).

As the integrands of (A-3.1) contain the expressions

$$\lambda_{s1}=\sqrt{1-\Delta^2\cos^2(\phi_1^m+\alpha_i)}$$
and
$$\lambda_{s2}=\sqrt{1-\Delta^2\cos^2(\phi_2^m+\alpha_i)} \qquad \text{(A-3.4)}$$

which are both two-valued, a four-sheeted Riemann surface is required for their representation. The branch cuts, along which the four sheets coalesce are defined by $Re(\lambda_{s1})=0$ and $Re(\lambda_{s2})=0$. For evaluation purposes the medium is assumed to be very slightly absorptive as before. The sheets I, II, III and IV are defined corresponding to the combinations (A-3.5)

$$(Re(\lambda_{s1})<0, Re(\lambda_{s2})>0), \quad (Re(\lambda_{s1})>0, Re(\lambda_{s2})>0),$$
$$(Re(\lambda_{s1})>0, Re(\lambda_{s2})<0), \quad (Re(\lambda_{s1})<0, Re(\lambda_{s2})<0).$$

respectively. The original path of integration can be shifted on any sheet of the Riemann surface for the factor $e^{-ik_{b1}R_{2\ell}^m\cos(\alpha_i-\theta_{2\ell}^m)}$ vanishing along the path at a large distance from the origin. The original path L is taken on sheet II where the relations $Im(\sin\alpha_i)<0$, $Im(\lambda_{s1})<0$ and $Im(\lambda_{s2})<0$ hold along L.

As an example, when $\theta_B>\theta_c>\theta_s$

where

$$\theta_B = \theta_o - \phi_1^m$$

$$\theta_c = \theta_o - \phi_2^m \qquad \text{(A-3.6)}$$

$$\theta_o = \text{Arccos}(1/\Delta)$$

$$\theta_S = \theta_{2\ell}^m$$

the original path can be shifted to L_S , (L_3, L_4) and (L_1, L_2) as shown in Figure A-2. L_S passes through the saddle point S , and the contours (L_3, L_4) and (L_1, L_2) go around the branch points C and B respectively, each one of them being drawn along the path of steepest descent given by

$$\cos(x - \theta_{2\ell}^m)\cosh y = 1 \qquad \text{(A-3.7)}$$

$$\cos(x - \theta_{2\ell}^m)\cosh y = \cos(\theta_c - \theta_{2\ell}^m) \qquad \text{(A-3.8)}$$

and

$$\cos(x - \theta_{2\ell}^m)\cosh y = \cos(\theta_B - \theta_{2\ell}^m) \qquad \text{(A-3.9)}$$

where

$$\alpha_i = x + iy$$

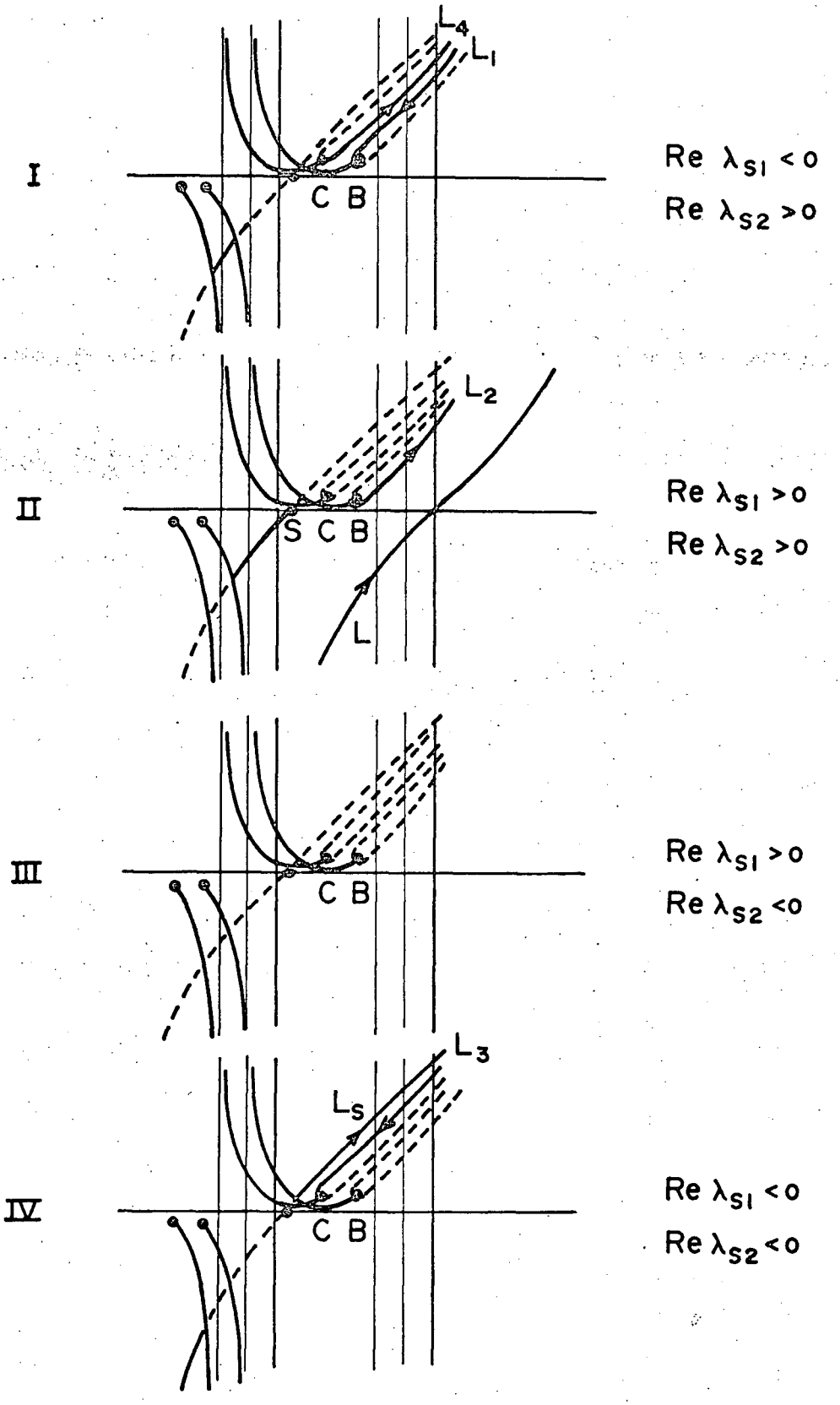

Fig. A-2. The α_i-plane showing branch cuts and integral paths for evaluation of the second series term of the integrals. Notation: B,C - branch points; S - saddle point; L - original path of integration; L_S - path of steepest descent through saddle point; and L_i (i= 1,2 ...) - paths of branch line integral.

Integral Around C

The contour integrals along (L_3, L_4) can be evaluated by the same procedure as before. By noting the relations

$$\mathrm{Re}(\lambda_{s1})<0 \ , \ \mathrm{Im}(\lambda_{s1})<0 \ , \qquad \text{(A-3.10)}$$
$$\mathrm{Re}(\lambda_{s2})>0 \ , \ \mathrm{Im}(\lambda_{s2})>0 \ .$$

for the path L_4 near C on sheet I, for a harmonic time variation the contribution to the displacement is found to be

$$u_{L_3L_4} = -A_i \frac{2\sqrt{2\pi}\cdot\delta}{\sqrt{\Delta}} \cdot \frac{1}{(k_{b1})^{1/2}(R^m_{2\ell})^{3/2}} \times \qquad \text{(A-3.11)}$$
$$\frac{1}{(1-1/\Delta^2)^{1/4}\{\sin(\theta_c-\theta^m_{2\ell})\}^{3/2}} \cdot e^{-ik_{b1}R^m_{2\ell}\cos(\theta_c-\theta^m_{2\ell})+2i\varphi_4+\frac{3}{4}\pi i}$$

where

$$\tan\varphi_4 = \frac{\delta\sqrt{\Delta^2\cos^2(\phi_1^m+\theta_c)-1}}{\Delta\sin(\phi_1^m+\theta_c)} \qquad \text{(A-3.12)}$$

Integral Around B

The contour integrals along (L_1, L_2) can also be evaluated by the same procedure as before. By noting the

relations

$$\mathrm{Re}(\lambda_{s1})>0\ ,\ \mathrm{Im}(\lambda_{s1})>0,$$
$$\mathrm{Re}(\lambda_{s2})>0\ ,\ \mathrm{Im}(\lambda_{s2})>0. \qquad \text{(A-3.13)}$$

for the path L_2 near B lying on sheet II, for a harmonic time variation the contribution to the displacement is found to be

$$u_{L_1L_2}=-A_i\frac{2\sqrt{2\pi}\cdot\delta}{\sqrt{\Delta}}\cdot\frac{1}{(k_{b1})^{1/2}(R_{2\ell}^m)^{3/2}}\cdot\frac{1}{(1-1/\Delta^2)^{1/4}\{\sin(\theta_B-\theta_{2\ell}^m)\}^{3/2}}\times$$
$$\frac{\Delta\sin(\phi_2^m+\theta_B)-\delta\sqrt{1-\Delta^2\cos^2(\phi_2^m+\theta_B)}}{\Delta\sin(\phi_2^m+\theta_B)+\delta\sqrt{1-\Delta^2\cos^2(\phi_2^m+\theta_B)}}\cdot e^{-ik_{b1}R_{2\ell}^m\cos(\theta_B-\theta_{2\ell}^m)+\frac{3}{4}\pi i} \qquad \text{(A-3.14)}$$

Integral through S

The contour integral along L_S can also be evaluated by the same procedure as before. For a harmonic time variation the contribution to the displacement is found to be

$$u_S=A_i\sqrt{\frac{2\pi k_{b1}}{R_{2\ell}^m}}\,A_1^m(\theta_{2\ell}^m)\cdot A_2^m(\theta_{2\ell}^m)\cdot e^{-ik_{b1}R_{2\ell}^m+\frac{\pi}{4}i} \qquad \text{(A-3.15)}$$

where for $\theta_{2\ell}^m > \theta_B > \theta_C$

$$A_1^m(\theta_{2\ell}^m) = \frac{\Delta \sin(\phi_1^m + \theta_{2\ell}^m) - \delta\sqrt{1-\Delta^2\cos^2(\phi_1^m+\theta_{2\ell}^m)}}{\Delta \sin(\phi_1^m + \theta_{2\ell}^m) + \delta\sqrt{1-\Delta^2\cos^2(\phi_1^m+\theta_{2\ell}^m)}}$$

$$A_2^m(\theta_{2\ell}^m) = \frac{\Delta \sin(\phi_2^m + \theta_{2\ell}^m) - \delta\sqrt{1-\Delta^2\cos^2(\phi_2^m+\theta_{2\ell}^m)}}{\Delta \sin(\phi_2^m + \theta_{2\ell}^m) + \delta\sqrt{1-\Delta^2\cos^2(\phi_2^m+\theta_{2\ell}^m)}} \qquad \text{(A-3.16)}$$

if $\theta_B > \theta_{2\ell}^m > \theta_C$

$$A_1^m(\theta_{2\ell}^m) = e^{2i\varphi_1} \qquad \text{(A-3.17)}$$

$A_2^m(\theta_{2\ell}^m)$ = same as (A-3.16)

$$\tan\varphi_1 = \frac{\delta\sqrt{\Delta^2\cos^2(\phi_1^m+\theta_{2\ell}^m)-1}}{\Delta\sin(\phi_1^m+\theta_{2\ell}^m)} \qquad \text{(A-3.18)}$$

if $\theta_B > \theta_C > \theta_{2\ell}^m$

$$A_1^m(\theta_{2\ell}^m) = e^{2i\varphi_1}$$

$$A_2^m(\theta_{2\ell}^m) = e^{2i\varphi_2} \qquad \text{(A-3.19)}$$

$$\tan\varphi_2 = \frac{\delta\sqrt{\Delta^2\cos^2(\phi_2^m+\theta_{2\ell}^m)-1}}{\Delta\sin(\phi_2^m+\theta_{2\ell}^m)} \qquad \text{(A-3.20)}$$

Aperiodic Solution

When the motions are aperiodic and vary as

$$\phi(t) = -\frac{A}{t^2 + C^2} \qquad A > 0 \ , \ C > 0$$

the operation

$$\frac{1}{\pi} Re \int_0^\infty d\omega \int_{-\infty}^{\infty} \phi(\sigma) e^{-i\omega\sigma} d\sigma$$

applied to (A-3.11), (A-3.14) and (A-3.15) yields the following solutions:

Head waves,

$$\bar{u}_{L_3L_4} = A_i \frac{2\sqrt{2}\pi\delta}{\sqrt{\Delta}(1-1/\Delta^2)^{1/4}} \frac{\sqrt{C_{b1}}}{(R_{2\ell}^m)^{3/2}} \frac{1}{\{\sin(\theta_c - \theta_{2\ell}^m)\}^{3/2}} \frac{A}{C^{3/2}} \times$$

(A-3.21)

$$\frac{1}{\left\{1+\left(\frac{t - {}_{H_c}t_{2\ell}^m}{C}\right)^2\right\}^{1/4}} \times \cos\left\{\frac{1}{2}\tan^{-1}\frac{t - {}_{H_c}t_{2\ell}^m}{C} + 2\varphi_4 + \frac{3}{4}\pi\right\}$$

where $${}_{H_c}t_{2\ell}^m = \frac{R_{2\ell}^m \cos(\theta_c - \theta_{2\ell}^m)}{C_{b1}}$$ (A-3.22)

$$\bar{u}_{L_1L_2} = A_i \frac{2\sqrt{2}\pi\delta}{\sqrt{\Delta}(1-1/\Delta^2)^{1/4}} \frac{\sqrt{C_{b1}}}{(R_{2\ell}^m)^{3/2}} \frac{1}{\{\sin(\theta_B - \theta_{2\ell})\}^{3/2}} \frac{A}{C^{3/2}} \times$$

$$\frac{1}{\left\{1+\left(\frac{t - {}_{H_B}t_{2\ell}^m}{C}\right)^2\right\}^{1/4}} \times \frac{\Delta\sin(\phi_2^m + \theta_B) - \delta\sqrt{1-\Delta^2\cos^2(\phi_2^m + \theta_B)}}{\Delta\sin(\phi_2^m + \theta_B) + \delta\sqrt{1-\Delta^2\cos^2(\phi_2^m + \theta_B)}}$$

(A-3.23)

$$\times \cos\left\{\frac{1}{2}\tan^{-1}\frac{t-{}_{H_B}t^m_{2\ell}}{C}+\frac{3}{4}\pi\right\} \qquad \text{(A-3.23)}$$

where $${}_{H_B}t^m_{2\ell}=\frac{R^m_{2\ell}\cos(\theta_B-\theta^m_{2\ell})}{C_{b1}} \qquad \text{(A-3.24)}$$

Reflected waves,

$$\bar{u}_s=-A_i\frac{\pi}{\sqrt{2C_{b1}R^m_{2\ell}}}\cdot\frac{A}{C^{5/2}}\cdot\frac{A^m_1(\theta^m_{2\ell})\cdot A^m_2(\theta^m_{2\ell})}{\left\{1+\left(\frac{t-{}_Rt^m_{2\ell}}{C}\right)^2\right\}^{3/4}}\times$$

$$\cos\left\{\frac{3}{2}\tan^{-1}\frac{t-{}_Rt^m_{2\ell}}{C}+\frac{\pi}{4}\right\}$$

for $\theta^m_{2\ell}>\theta_B>\theta_c$ (A-3.25)

$$\bar{u}_s=-A_i\frac{\pi}{\sqrt{2C_{b1}R^m_{2\ell}}}\cdot\frac{A}{C^{5/2}}\cdot\frac{A^m_2(\theta^m_{2\ell})}{\left\{1+\left(\frac{t-{}_Rt^m_{2\ell}}{C}\right)^2\right\}^{3/4}}\times$$

$$\cos\left\{\frac{3}{2}\tan^{-1}\frac{t-{}_Rt^m_{2\ell}}{C}+2\varphi_1+\frac{\pi}{4}\right\}$$

for $\theta_B>\theta^m_{2\ell}>\theta_c$ (A-3.26)

$$\bar{u}_s=-A_i\frac{\pi}{\sqrt{2C_{b1}R^m_{2\ell}}}\cdot\frac{A}{C^{5/2}}\cdot\frac{1}{\left\{1+\left(\frac{t-{}_Rt^m_{2\ell}}{C}\right)^2\right\}^{3/4}}\times$$

$$\cos\left\{\frac{3}{2}\tan^{-1}\frac{t-{}_Rt^m_{2\ell}}{C}+2\varphi_1+2\varphi_2+\frac{\pi}{4}\right\} \qquad \text{(A-3.27)}$$

for $\theta_B > \theta_c > \theta_{2\ell}^m$

where ${}_R t_{2\ell}^m = R_{2\ell}^m / c_{b1}$ (A-3.28)

If the branch points are smaller than the saddle points head waves do not appear. The ray paths for arrivals which travel along part of the path as head waves are shown in Figure A-3.

Hence, except for diffracted waves, we can formally obtain a complete synthetic seismogram in the case of a dipping layer by applying this procedure to the third and higher order series terms of the formal integral solution.

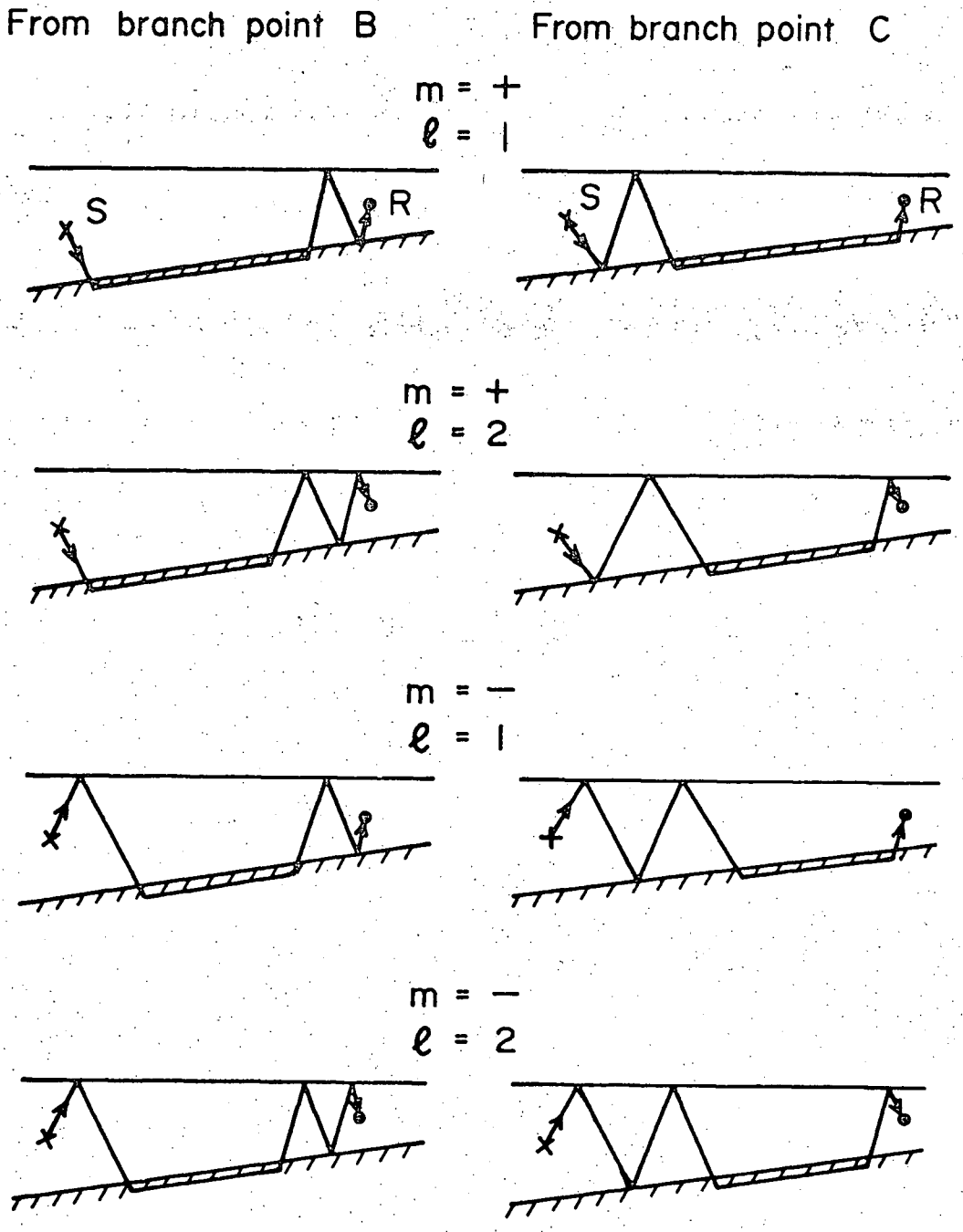

Fig. A-3. Ray paths of the head waves expressed by the second term of the integrals with the four conbinations of m(+,-) and $\ell(1,2)$ corresponding to the four second series terms of the integral $I^{m}_{2\ell}$ in (A-3.1).

PUBLICATIONS

Nakamura, K. and Ishii, H., 1965. Refraction of explosive sound waves from a line source in air into water, Sci. Rep. Tohoku Univ., Ser. 5, Geophysics, 16, 90-107.

Tohoku Univ. Aftershocks Observation Group, 1966. Observation of aftershocks of an earthquake happened off Oga-Peninsula on 7th, May, 1964, Tohoku Disaster Prevention Research Group Report, 85-101.

Ishii, H. and Takagi, A., 1967. Theoretical study on the crustal movements, Part I. The influence of surface topography (Two-dimensional SH torque source), Sci. Rep. Tohoku Univ., Ser. 5, Geophysics, 19, 77-94.

Ishii, H. and Takagi, A., 1967. Theoretical study on the crustal movements, Part II. The influence of horizontal discontinuity, Sci. Rep. Tohoku Univ., Ser. 5, Geophysics, 19, 95-106.

Ishii, H. and Ellis, R. M., Multiple reflection of plane SH waves by a dipping layer, Bull. Seism. Soc. Amer. (accepted for publication).